An Examination of Plasma Contactor Performance through a Comparison of Theory, Numerical Results, and Data

by

Marilyn Rose Oberhardt

S.B. Aeronautical and Astronautical Engineering, Massachusetts Institute of Technology, 1986

SUBMITTED TO THE DEPARTMENT OF
AERONAUTICS AND ASTRONAUTICS
IN PARTIAL FULFILLMENT OF THE
REQUIREMENTS FOR THE DEGREE OF
Master of Science
in
Aeronautics and Astronautics
at the
Massachusetts Institute of Technology

July 1989

Signature of Author _____
Department of Aeronautics and Astronautics
July 1989

Certified by _____
Professor Daniel E. Hastings
Thesis Supervisor
Class of 1956 Career Development
Associate Professor of Aeronautics and Astronautics

Accepted by _____
Professor Harold Y. Wachman
Chairman, Department Graduate Committee

An Examination of Plasma Contactor Performance through a Comparison of Theory, Numerical Results, and Data

by

Marilyn Rose Oberhardt

Submitted to the Department of Aeronautics and Astronautics, July 5,1989, in partial fulfillment of the requirements for the degree of
Master of Science

Abstract

To maintain current flow through an electrodynamic tether system in space, a current closure path must be completed within the ionosphere. A number of methods have been suggested to attain such closure, among them the concept of the plasma contactor. The use of plasma contactors in space has been proposed as a means to probe or control spacecraft environments, in particular those of tethered space systems. In fact, efficient plasma contactors may hold the key to safe and reliable use of electrodynamic tether systems.

A plasma contactor is a device that expels plasma, thereby providing electrical contact between a space vehicle and the medium through which it is travelling. Such a device is capable of either emitting electrons to or collecting electrons from the ambient space plasma. The contactor ensures electrical contact by providing a plasma region in which ambient electrons may be emitted or collected and by providing a means to ionize neutral gas in that region.

This thesis focusses on the plasma contactor as a current collection device. There have been several theories developed to predict the behavior of current collection through plasma contactor clouds. These theories offer markedly different predictions regarding the current amplification properties of these clouds. The key features of each theory and the points of disagreement between these theories are addressed. The various treatments of the distinct plasma regions composing the plasma contactor cloud are discussed. A new theory is presented that combines two of these distinct plasma regions. The goal of

Acknowledgements

I would like to offer my very special thanks to my advisor, Prof. Daniel Hastings, for his unwavering support of this endeavor. Without his patience and forebearance, this degree would not have been possible. When I was scattered unto the four winds, he remained supportive in the face of it all. I have learned a great deal from him and will always be extremely grateful for his guidance and encouragement. Also, I am indebted to Prof. Manuel Martinez-Sanchez for his faith in me and what I have set out to accomplish in my stay as a graduate student at MIT. It has been both an honor and an inspiration to work with both of them.

Also, I would like to thank all of my fellow graduate students who have helped me throughout the past two years in many ways. In particular, I would like to thank Nick Gatsonis, Rodger Biasca, Sean Tavares, Georgia Denktsis and (Prof.) Mark Lewis.

I am indebted to my colleagues in the plasma physics community for numerous valuable discussions and insights, particularly Dr. Luciano Iess, Prof. Paul Wilbur, Dr. Victoria Davis, and John Williams. I am especially grateful to Dr. Michael Gerver who provided many suggestions that helped to form this work.

My colleagues at the Geophysics Laboratory deserve special mention for affording me the opportunity to pursue this degree. I cannot adequately express my thanks to Mr. Gary Mullen, Dr. M. Susan Gussenhoven, and Dr. David A. Hardy for all their support. Thanks to Lts Bob Redus and Kevin Kerns and Ms. Kristina Lynch for providing numerous sanity checks!

Without Junko Nagano, I probably would have starved to death, been attacked by giant dust balls, or overcome by enormous stacks of the Boston Globe. Thanks for being a great friend!

I wish to thank my parents and brother Matthew for all of the hours invested in buoying me when things looked bleak and sharing my joy when things looked bright. Without their love and prayers, I would not be where I am today.

Finally, special thanks must go to my fiancé, Dr. Frederick G. Barker, who has kept me going through these especially trying two years of graduate school. His love and support have meant everything to me. I would not have succeeded without him.

Thanks, I.M.!

Contents

List of Figures

List of Tables

Chapter 1
Introduction

1.1 The Concept of Electrodynamic Tethers

The development of tethers for use in space is primarily due to the efforts of Giuseppe Colombo and Mario Grossi in the early 1970's. Grossi [32] first proposed to NASA in 1972 that a tether of $\sim 20 - 100km$ in length be deployed from the Space Shuttle for use as an antenna. Grossi consulted Colombo on this idea, the former seeking the latter's expertise in long flexible members. Their collaborative efforts yielded insight into the many potential uses of tethers in space, such as generation of thrust, generation of power, augmentation of communications, and exploration of the space plasma environment. Beyond the engineering applications of tethers, there have opened up new scientific opportunities for the investigation of ionospheric properties. For example, the energy associated with the electrical circuit of an electrodynamic tether system can be used to explore the effects of numerous disturbances on the ionosphere, given the system's predicted ability to produce large amplitude plasma and electrodynamic waves within the ambient plasma. Clearly, the electrodynamic tether has invited an extraordinary merger of scientific and engineering interests in its development and in the implementation of the TSS-1 program.

The electrodynamic tether can be considered a power conversion system that either yields electrical energy from orbital potential energy or changes electrical energy into orbital kinetic energy. The electrodynamic tether is a long conductive wire deployed from a spacecraft while in orbit. The tether interacts with the earth's magnetic field and ambient space plasma to permit a number of technological advancements.

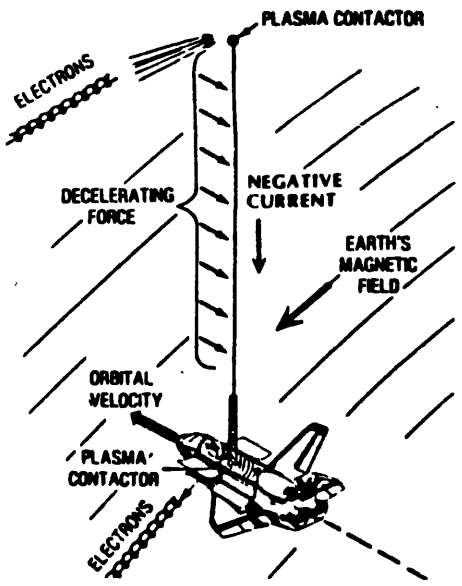

Figure 1.1: Electrodynamic Tether as a High Power Generator [63]

The tether system is shown in the power generation configuration in Figure 1.1. If electrons are collected at the satellite end of the system and ejected at the Orbiter end, a current can flow in the tether. In such a configuration, the subsatellite acts as a large electrode when immersed in the ionospheric plasma. At the Orbiter end, electron guns or an electrically neutral plasma source, *e.g.* hollow cathode plasma contactor, may be used to return electrons to the ambient plasma. As a point of reference, it was noted in the NASA Atmospheres, Magnetospheres, and Plasmas in Space (AMPS) Science Definition Study of 1974 [7] that a conductive, gravity–gradient–stabilized tether connecting a conductive subsatellite and the Orbiter would experience an *emf* of $0.1 - 0.2\,V/m$ as the tether passed across the earth's magnetic field lines.

An electric field set up by the $\vec{v} \times \vec{B}$, where $\vec{v}$ is the orbital velocity and $\vec{B}$ is the vector of the earth's geomagnetic field, induces a potential difference along the tether length, $\vec{l}$. In this system, the subsatellite is considered an anode and a source of electron emission to act as a cathode is then required onboard the Orbiter. Without a source of electron emission, there could be no current

flow in the tether since there would be no mechanism to dissipate that current onboard the Orbiter, resulting in excessive charging of the Orbiter. The potential difference is given by the expression $V_{tether} = (\vec{v} \times \vec{B}) \cdot \vec{l}$, and represents the voltage which would exist across the two ends of an ideal tether that had no line losses. It is assumed that the present state of tether technology is such that adequate electrical insulation of the tether can be provided to prevent current collection from or current emission to the ambient plasma. With these assumptions in mind, and using the AMPS estimate as an example, a $20km$ tether would then induce a potential drop on the order of $2 - 4kV$.

If a current I is allowed to flow in the tether, orbital energy is converted into electrical energy at a rate $P = IV_{tether}$, where P equals the power converted. Note that not all of the total power will appear across the load, but that some of the power will be lost due to inefficiencies and will appear as heat. To maintain this current flow without extreme charging of the Orbiter, a closure path must exist between the tethered system and the ionosphere. Completion of this closure path requires that electrical "contact" be made between the tethered satellite system and the ionosphere. This contact can be achieved with a number of devices. The scope of this work centers upon the use of plasma "contactors", devices that eject a plasma into the ambient space plasma surrounding a spacecraft in order to maintain charge equilibrium.

If the tethered system is used in the power generation mode, a drag penalty must be taken into account. Drag upon the satellite is caused by the Lorentz force associated with the $\vec{I} \times \vec{B}$ interaction when there is current flow in the tether. Consequently, there is some interest in comparing the tether power system efficiency with that of other competing power systems. The major competition for space tethers in the arena of power generation comes from batteries, fuel cells, and regenerative fuel cells. The major difference between the tethered power system and the fuel cell systems is that the fuel cell makes use of only the chemical energy in the fuel while the tethered system uses both the chemical energy and the kinetic energy of the fuel. According to calculations performed by NASA Lewis Research Center (LeRC) [72], the drag penalty incurred is relatively small. As an example, consider a space station operating with an open

Table 1.1 Comparative Efficiency of Tether Power Generator

- Hydrogen-Oxygen consumption to overcome electrical and aerodynamic drag of the tether power generator equal to $0.16\,kg/kWH$.
- Hydrogen-Oxygen reactant consumption for 73% efficient fuel cell equal to $0.39\,kg/kWH$.
- Total tether power generator drag ($\sim 1.36\,kg$) can be offset by controlled ejection of waste products.

loop life support system. If the expellant waste products and water of such a system are aimed in the right direction, the resultant thrust produces a break-even kinetic energy balance for the tethered power system. Table 1.1 shows the comparative efficiency of a tether power generator [72].

A number of studies have indicated that the use of tethers as power generators is a promising concept. Martinez-Sanchez and Hastings [52] obtained results indicating that tether power systems offer large fuel savings over electrochemical generators. The use of tethers as replacements for batteries in solar array energy storage is not quite as effective, but tethers may serve to partially replace batteries in other circumstances with some positive returns.

For a tether system operating in power generation mode, orbital energy can be converted into primarily electrical energy at a rate equal to the product of the open circuit voltage and the current in the circuit $P = IV_{tether}$. If one accounts for actual physical constraints in an operational electrodynamic tether, the effective voltage drop across the load is significantly reduced from the open circuit tether voltage. This is due to tether impedance and the corresponding voltage drops of the elements comprising the tether system, such as the tether reel mechanism which acts as a large variable inductor. Notably, there will be a voltage drop ΔV_t due to the tether wire itself, the anode and cathode at each end (ΔV_a and ΔV_c), and a drop due to the impedance of the ionosphere ΔV_{ion}.

In terms of the electrical power available from the tether system to a spacecraft load and the power gleaned from the orbital kinetic energy, an expression of efficiency can be obtained:

$$\eta = V_{Load}/V_{tether} \tag{1.1}$$

alternatively expressed as,

$$\eta = \frac{V_{Load}}{V_{Load} + \Delta V_t + \Delta V_a + \Delta V_c + \Delta V_{ion}} \tag{1.2}$$

The ionospheric plasma ΔV_{ion} is typically smaller than that of the other electrodynamic tether system elements [40]. It will also be the most variable of the voltage drops, highly dependent upon the altitude and inclination of the spacecraft's orbit.

The voltage drop of the tether itself is a function of the present state of tether technology. This is because its impedance depends not only on the wire size and material, but also upon how well it is protected from the ambient environment through which it must pass as well as the amount of tether wound up on the system's reel mechanism. The tether must maintain its structural integrity in spite of mass demands of the system, atomic oxygen degradation, and debris strikes. To meet all of these demands, the TSS-1 tether is a structure comprised of five layers as shown in Figure 1.2.

The result of most tether concept designs is to yield a lower bound on tether impedance, thereby also lowering ΔV_t. System efficiency is then driven by the engineer's ability to reduce the voltage drops associated with the system's anode and cathode. Therefore, the goal of the engineer developing a plasma contactor is then to produce a contactor that operates at low voltages, has a low mass, and offers reliability and maintainability.

The relation of the various voltage drops associated with a tether system is depicted graphically in Figure 1.3. In this figure the magnetic field vector $\vec{B}$ is oriented into the page and the orbital velocity vector $\vec{v}$ is directed to the right. The electric field vector $\vec{E}$, in the reference frame of the tether, and the Lorentz force induced current $\vec{I}$ will then point upwards for the generator in Figure 1.3 a), and downwards for the thruster in Figure 1.3 b). The thruster figure

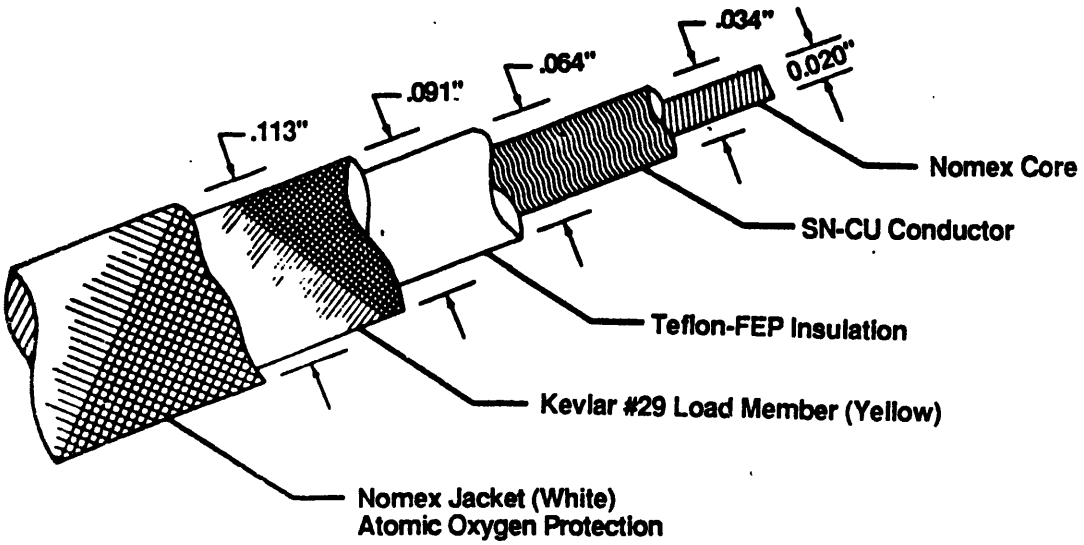

Figure 1.2: TSS-1 Conducting Tether [63]

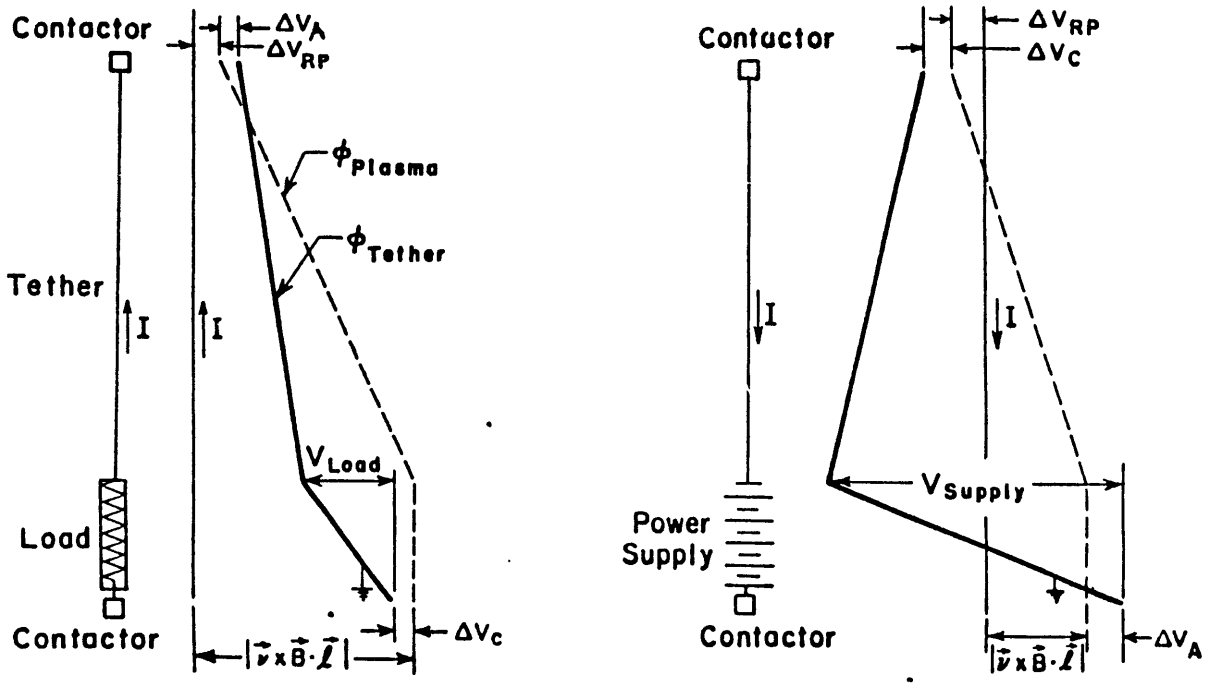

Figure 1.3: Potential Diagram for Tether as a) Generator and b) Thruster [52]

is presented to contrast the circuits for power generation and for propulsive systems.

The ionospheric current density naturally available is relatively low. Consequently, there must be an enhancement of the effective electron collection area of the subsatellite anode with some current amplification device to achieve high levels of collection current. The object of this present work is to examine plasma contactors for use as such an amplification device. The plasma contactor can provide a net gain to the system in two ways. The contactor emits a plasma cloud that surrounds the vehicle and thereby effectively increases its radius, allowing greater collection of ambient current. Secondly, the ionization of neutrals within the plasma cloud surrounding the spacecraft offers enhancement of electron current collection. This second approach only comes into play, however, at higher electron temperatures and large hollow cathode currents since it is only under these conditions that ionization of neutrals within the core cloud

will occur.

Plasma contactors are worthy of investigation since they offer a very attractive dual identity not afforded by electron guns used as "contactors"; that is, they can function as both anodes and as cathodes to augment power production as well as thrust generation. The electron gun can serve only to emit electrons in the tethered system power production mode and cannot function as an electron collector, a mode equally important to the power production process.

1.2 Development of Present Work

This research has focussed on the theory and results pertaining to the use of plasma contactors as current collectors. Theoretical work on plasma contactors as current collectors has fallen into primarily two categories, collisionless space-charge-limited double layer theory and collisional quasineutral theory. Experiments utilizing plasma contactors at low current in ground-based plasma chambers can be modelled by the collisionless theory [83] to a certain extent. The collisionless model does not apply, however, when symmetrical double layer structure breaks down followed by ionization within the resultant asymmetrical double layer structure. Also note that very high anode potentials are needed to draw a substantial ambient electron current across the magnetic field in the absence of collisions or effective collisions due to turbulence. It has been stated (Section 1.1) that such a high potential drop is undesirable. The collisionless theory, then, has limited applicability to power generation by electrodynamic tethers in space. Isotropic quasineutral models of contactor clouds, extending over a region where the effective collision frequency ν_e exceeds the electron cyclotron frequency ω_{ce} [34,36,37], have the low contactor anode potentials desirable for efficient contactor operation. The drawback with the low anode potentials in the isotropic quasineutral theories is that collected electron current is also quite low, thereby limiting the contactor's performance as an electron collector.

In an effort to combine the advantages of the space-charge-limited models and the isotropic quasineutral models, a new model has been developed. This

combination model is an anisotropic contactor cloud oriented along the magnetic field, with $\nu_e < \omega_{ce}$ [29]. The electron motion along the magnetic field is modelled as a collisionless space-charge-limited double layer, while across the magnetic field the electrons are assumed to diffuse collisionally and the potential profile is modelled as quasineutral. Using a simplified expression for ν_e, the collision frequency due to ion acoustic turbulence, an analytic solution has been found for this model, which should be applicable to current collection in space [29]. The contactor anode potential is low, in conjunction with a collected electron current that can be much greater than the emitted ion current, in turn yielding an improved gain. The overall system gain is enhanced since there is a substantial reduction in the impedance of the electron current collection from the ionosphere.

The plasma contactors studied in this work used an anode to collect electrons from either the ambient ionospheric plasma or an "ambient" plasma source in a chamber experiment. A contactor acting as an electron collector acts also as an ion emitter. Consequently, the figures of merit for such a contactor are its potential with respect to the ambient plasma, ϕ_0, the fraction of neutral gas ionized within the core cloud region, χ_i, and the gain ξ. The core cloud is the inner plasma region over which electrons can be collected to the contactor anode. The system gain is defined as

$$\xi = I/I_i(r_{anode}) \tag{1.3}$$

where $I = I_i + I_e$ is the total current of emitted ions and collected electrons at the contactor anode, $r = r_{anode}$. The potential of the anode with respect to the ambient plasma determines the maximum power that can be generated by a tethered space system with a contactor, given the nature of the system's electrical circuit (Section 1.1). The power is greatest when the contactor impedance is lowest. The gain is a critical parameter since it sets the rate at which the contactor's neutral gas supply must be used to produce ions for a given total current level. A high gain system results in less neutral gas being used to collect a given current while a low gain system requires a greater degree of ionization to collect the same current.

Both the impedance and the gain will depend on the total current. In order

to achieve an efficient and reliable system, a tradeoff must be undertaken. At very low current, both high gain and low impedance are possible, but the power is too low. At high current, high gain can be obtained only at the cost of a very large ϕ_0, which results in a low power to the load. The highly desirable low ϕ_0 and high power combination is feasible only with a low gain plasma contacting system.

In previous work [38,73], the description of the plasma contactor cloud has consisted of several different regions. In close proximity to the contactor orifice, there is an inner plasma core. This core cloud was considered to be isotropic because the two major directions of anistropy, the earth's magnetic field and the direction of motion of the source, would be excluded by the dense plasma from the contactor source. There are then two outer regions in which the two directions of anisotropy are manifested. Earlier work in quasineutral theory had assumed that a significant current of ambient electrons could be collected from infinity along only those field lines that passed through the core cloud [36,38]. In Chapter 3, the anisotropic contactor model presented indicates that, for conditions in low earth orbit (LEO), it is possible to collect a significant electron current from the contactor's plasma transition region, where the anisotropy due to the magnetic field is important.

This thesis is intended to expand the understanding of plasma contactor performance through the careful examination of theory, experiments, and analysis performed by the community to date and the extension of the collisionless space-charge-limited flow model to space conditions. The results presented in that extension are based on both a one-dimensional computational model which solved Poisson's equation for a spherically symmetric double layer for the collisionless space-charge-limited case and an anisotropic model that combines the space-charge-limited collisionless double layer with a quasineutral plasma core profile. Varying the operating parameters of the hollow cathode within the computational model was done to allow comparison with laboratory data from NASA Lewis Research Center (LeRC), Colorado State University (CSU), University of California at Los Angeles (UCLA) and Instituto di Fisica dello Spazio Interplanetario (IFSI), Frascati, Italy. The three primary figures of merit men-

tioned earlier are used in the comparison of the models to experimental contactor performance.

In Chapter 2, the research to date on the topic of plasma contactors is discussed. This includes examination of quasineutral models, space-charge-limited models, laboratory data, spaceflight experiments, and correlation of the modelling efforts and the laboratory results to space conditions. Chapter 2 describes a collisional quasineutral theory, related to the models of Dobrowolny and Iess [25,42] and Hastings and Blandino [10,36], which is more applicable to contactors emitting a large ion current, either in space or in ground based experiments, than the collisionless models. The Dobrowolny and Iess model is a fluid model that neglects magnetic field effects but includes anomalous friction arising from plasma instabilities. The Hastings and Blandino model assumes that ambient electrons can only be collected over the cross-section of the isotropic inner core region, where the effective collision frequency is greater than the electron gyroradius. With this restriction, the model predicts that very little ambient electron current can be collected in space. The collisionless space-charge-limited model is built upon the seminal work of Wei and Wilbur [83]; this model describes the process of electron collection in the absence of a magnetic field and contactor velocity effects. There is an examination of the development of the Katz, et. al. modelling effort that had a quasineutral starting point that was then merged with double layer theory. In addition to the IFSI, CSU, and NASA LeRC chamber experiments performed to validate the theories of the experimenters involved, the ground-based experimental work of Stenzel and Urrutia of UCLA is also covered. They perform experiments examining the space-time evolution of a current carrying system that has great bearing in the plasma contactor arena.

In Chapter 3 a collisionless double layer theory, similar to the models of Wei and Wilbur [83] and of Parks and Katz [58], is extended to include the effects of the magnetic field on the electrons and the effect of finite anode radius. If the electrons are taken to be strictly collisionless in space, then they will be collected by the contactor anode only if they travel from infinity along magnetic field lines contained within the flux tube that intersects the area of the anode. This in

turn places a limit on current collected by the contactor. The collisionless model presented by Wei and Wilbur [83] lacks consideration of angular momentum effects on the paths taken by the electrons. The Parker-Murphy condition [57] has been used in this study to account for angular momentum considerations within the framework of a collisionless space-charge-limited spherical double layer model. This approach is shown in Chaper 3. An additional consideration in this approach is that of the finite anode. This alters the formation of the double layer for certain conditions since the inner edge, r_{inner}, of the double layer, has its position determined by the collected current and the anode potential when the current is space-charge-limited and cannot be less than the contactor anode radius if physically realistic conditions are to be described by the model.

The collisionless double layer model outlined above gives a reasonable approximation of some of the results of ground-based plasma contactor experiments. The applicable laboratory experiments are those which have contactor clouds of radius less than or comparable to an ambient electron gyroradius, and double layers with r_{inner} greater than or equal to the contactor anode, r_{anode}, and have $\lambda_D \leq r_{d.l.}$, where λ_D is the plasma Debye length and $r_{d.l.}$ is the width of the double layer. However, to effectively achieve power generation with electrodynamic tethers in space, the contactor radius required to collect significant currents is much greater than an ambient electron gyroradius. The Parker-Murphy criterion and the finite anode size then imply that the double layer impedance is extremely high, so it is impossible to obtain high power operating a plasma contactor in this manner in space. If the emitted ion current is low enough, roughly less than 1 mA for the case of an Argon plasma contactor in LEO conditions, a double layer can be formed satisfying the equations of Wei and Wilbur [83], with r_{inner} greater than or equal to the anode radius, with anode potential great enough to draw the required electron current across the magnetic field, but less than the total tether potential, V_{tether}. In the event of such a formation, the collisionless double layer model will be self-consistent, and the result is that it is not possible to generate high power with plasma contactors in space.

At higher ion currents emitted from the plasma contactor, a region will exist in which the electrons cannot go straight to the anode, but where ambient

electrons will be trapped, keeping the plasma quasineutral [23]. The electrons that become trapped remain trapped much longer than it takes an unmagnetized electron to traverse the double layer to the anode. Presumably, these trapped orbits are filled with secondary and scattered electrons. If there are effective collisions due to instabilities, some of these trapped electrons may be able to diffuse to the anode, and the collected electron current may be much greater than that calculated with the collisionless model [29]. In Chapter 3, then, work on a model of the outer core region is detailed, in which the motion along the magnetic field is collisionless, forming a double layer, but the motion across the magnetic field is collisional and quasineutral is detailed [29]. This model is expected to be highly applicable to contactors in space and indicates that significant current may be collected from the outer core region, while exhibiting low contactor anode potential. The plume and spot modes of contactors operating as collectors are examined. The plume mode is that operating state in which there is high-voltage, low-current plasma discharge and spot mode is that mode in which there is high-current, low voltage plasma discharge. Spot mode is alternatively known as ignited mode since there is a region of glowing discharge associated with it. A summary and conclusions of the reviews and numerical results is presented in Chapter 4.

Chapter 2
Examination of Plasma Contactor Studies to Date

2.1 Introduction

There has been much debate about the size of the inner plasma core region over which electrons can be collected to a plasma contactor. One estimate is obtained by matching the cloud density to the ambient density[59],

$$n_{cloud}(r_{core}) \approx n_{ea} \tag{2.1}$$

while another comes from taking magnetic field effects into account[34],

$$\nu_e(r_{core}) \approx \omega_{ce}. \tag{2.2}$$

Here ν_e is the radially dependent electron collision frequency, including effective "collisions" due to turbulence, and ω_{ce} is the electron gyrofrequency. A third estimate is obtained by requiring regularity of the self-consistent potential[25,42],

$$\frac{\partial \phi}{\partial r}\Big|_{r_{core}} \approx 0. \tag{2.3}$$

Finally, a fourth estimate comes by requiring a consistent space charge limited flow inside the core[83] and includes pressure balance,

$$m_i n_i u_i^2|_{r_{core}} \approx m_e n_e u_e^2|_{r_{core}}. \tag{2.4}$$

In Eq. 2.4, u_i is the outgoing ion flow velocity and u_e is the incoming electron flow velocity. These diverse theories yield a wide range of current enhancement factors for the plasma cloud. Such discrepancies in system gain strongly suggest that determining the size of the core region is critical to the understanding of the current collection.

Assuming a spherical core cloud of radius r_{core}, one obtains from continuity of current,

$$I = I_i(r_0) + I_e(r_0) = I_i(r_{core}) + I_e(r_{core}), \tag{2.5}$$

with an overall system gain, ξ, of

$$\xi = \frac{I_e(r_{core})}{I_i(r_0)} + \frac{I_i(r_{core}) - I_i(r_0)}{I_i(r_0)} + 1. \tag{2.6}$$

Plasma contactor clouds enhance or produce electron current flow through two possible paths as described in Section 1.1. They can serve as virtual anodes through which electrons can be drawn from infinity and collected to the real anode at the center of the plasma core cloud. This path is taken into account in the first term on the right hand side of Eq. 2.6. Secondly, the neutral gas within the cloud surrounding the contactor can become ionized, creating electron-ion pairs. These electrons will be collected to the anode and the ions will be repelled. This current collection is included in the second term on the right hand side of Eq. 2.6.

For use in space with an electrodynamic tether, however, ionization of contactor neutrals external to the contactor is not considered an efficient use of neutral gas. This point is demonstrated by modelling presented in Section 3.1.5. If this ionization of neutrals were the only means by which the collection current could be enhanced, then the same neutral gas can be used more efficiently by ionizing it internally in an ion source. Plasma contactors will be most useful and efficient if the ionosphere is the primary source of electron current for collection. The two sources of electrons in the ionosphere are the ionospheric plasma and the ionospheric neutrals. Note, though, that the mean free path for ionization of the ionospheric neutral gas is on the order of kilometers so that ionization of this gas on the length scale of the plasma contactor cloud is highly improbable. Consequently, it is assumed that all ionization associated with the plasma contactor is ionization of contactor, and not ionospheric, neutral gas. Therefore, plasma contactors will be advantageous to an electrodynamic tether system only if they enhance current by collecting ambient electrons from the ionosphere.

The collected electron current, $I_e(r_{core})$, will generally be the saturation cur-

rent times the area of the core cloud, $4\pi r_{core}^2$, but if the contactor is collecting electrons only along magnetic field lines intersecting the core cloud, then $I_e(r_{core})$ will be the saturation current times $2\pi r_{core}^2$. As a result, the r_{core} dimension is a critical measure of the effectiveness of plasma contactors as electron collectors in space. Within the Wilbur et. al. model, r_{core} is taken to be the inner radius, r_i, of the space-charge-limited collisionless double layer. This core collection region is not explicitly set in the Dobrowolny and Iess model but is found when calculating a self-consistent plasma potential profile from the contactor anode out to infinity. The Hastings et. al. model uses a collisionality condition to determine r_{core}. The efforts of Katz et. al. have centered upon the use of density matching to obtain the core cloud dimension. The following sections explore these limits and compare and contrast them. This comparison and contrast is also made with laboratory data sets and spaceborne contactor data sets. Limitations in the existing data sets are examined and recommendations for future experiments presented.

2.2 Space Charge Limited Models and Results

2.2.1 The Wilbur, et. al. Model

The model presented by Wei and Wilbur [83] , describing the plasma contactor electron collection process, is based upon a space-charge-limited theory and is often referred to as the double diode model. The approach taken is to develop an understanding of the near-field plasma contacting process. The near-field consideration results from the fact that the model is based upon experimental observations where the magnetic field is excluded and the plasma contactor is stationary with respect to the ambient plasma. Three separate regions are associated with the plasma contacting process,

1. High Density Plume Region
2. Double-sheath Region
3. Ambient Plasma

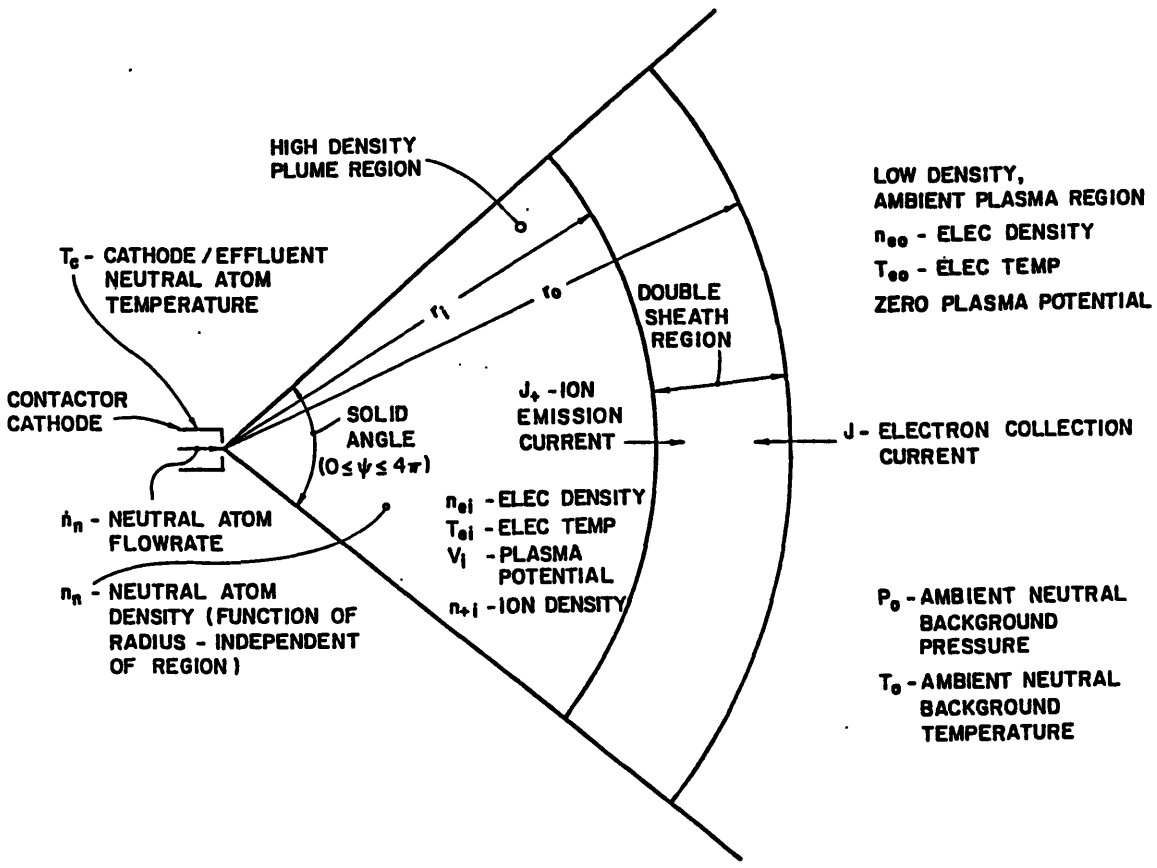

Figure 2.1: Double Sheath Conceptual View of Plasma Contacting Process [85]

This model represents the electron collection process as having electron current flow from the ambient plasma to the positively biased high density plume region, illustrated in Fig. 2.1 with flow through a spherical segment ψ. The high density plume region denotes that area just outside of the hollow cathode orifice where ionization processes occur, resulting in a plasma density exceeding the ambient plasma density. Separating this high density region from the ambient plasma is an area designated as the double-sheath. (Note that the terms double-sheath and double layer may be used interchangeably and that this usage varies from author to author.) In the double-sheath, the current flow is assumed to be space-charge-limited and a voltage drop is maintained.

In Figure 2.2 , the basic components of the spherically symmetric double-sheath problem are shown. The Wei and Wilbur solution presented is the first published for this problem [83] . The inner spherical surface r_i is at the potential V_i and is a uniform source of positively charged ions. The outer surface r_o is a uniform source of oppositely charged particles and its potential is $V_o = 0$. It is assumed that this outer radius collects a fixed current from the ambient plasma and is determined solely by the ambient plasma conditions [85] . Velocities attained by the charged particles at the spherical surfaces are determined by the potential drop, ΔV, between the inner and outer radii, r_i and r_o. Ions of mass m_i are accelerated from a zero initial velocity radially toward r_o, producing the ion current flow. The same condition holds for the electrons, with mass m_e, except that the current flows radially inward from r_o. With this initial boundary condition for the velocities, they are given by

$$u_i = \sqrt{\frac{2e}{m_i}(V_i - V)} \tag{2.7}$$

$$u_o = \sqrt{\frac{2e}{m_o}V} \tag{2.8}$$

Total current flowing in this model is given by $J_i + J_o = J_{tot}$. Assuming no ionization or recombination occurs between the two surfaces, the ion and electron currents, respectively, are given by,

$$J_i = 4\pi r^2 n_i e u_i \tag{2.9}$$

$$J_o = 4\pi r^2 n_o e u_o \tag{2.10}$$

Poisson's equation for this potential drop between the spherical surfaces is

$$\nabla^2 V = \frac{-e}{\epsilon_o}(n_i - n_o) \tag{2.11}$$

With the spherical symmetry integral to the model, Eq. 2.11 becomes

$$\frac{1}{r^2}\frac{d}{dr}\left(r^2\frac{dV}{dr}\right) = \frac{-e}{\epsilon_o}(n_i - n_o) \tag{2.12}$$

In order to nondimensionalize the simplified Poisson's equation, the following variables were introduced:

$$\phi = \frac{V}{V_i} \tag{2.13}$$

$$\rho = \ln\left(\frac{r}{r_o}\right) \tag{2.14}$$

$$j_o = (J_o/4\pi\epsilon_o V_i^{3/2})\sqrt{m_o/2e} \tag{2.15}$$

$$\alpha = (J_o/J_i)\sqrt{m_o/m_i} \tag{2.16}$$

The nondimensionalized Poisson equation now obtained is

$$\frac{d^2\phi}{d\rho^2} + \frac{d\phi}{d\rho} = j_o\left(\frac{1}{\sqrt{\phi}} - \frac{1}{\alpha\sqrt{1-\phi}}\right) \tag{2.17}$$

The boundary conditions accompanying Eq. 2.17 are

$$\phi = 1, \quad @ \quad \rho = \rho_i = \ln\left(\frac{r_i}{r_o}\right) \tag{2.18}$$

$$\phi = 0, \quad @ \quad \rho = 0 = \ln\left(\frac{r_o}{r_o}\right) \tag{2.19}$$

Eq. 2.17 and the accompanying boundary conditions in Eqs. 2.18 and 2.19 describe a non-linear problem, exhibiting singularities at the two spherical boundaries. These singularities are the result of the particle densities approaching infinity at their respective source surfaces in order to satisfy the current condition from each surface at zero initial velocity. Consequently, no analytical solution has been found and the problem has been solved numerically. The problem is solved with a relaxation technique to compute the values of j_o and α, as well as $\Delta V(r)$ as a function of the spherical surfaces' radius ratio (r_i/r_o), appropriate to the solution of interest, the space-charge-limited case. The space-charge-limited spherical double sheath currents are determined by the radius ratio, r_i/r_o, not the magnitude of those radii.

To obtain the solution of interest to Eq. 2.17, *i.e.* the space-charged-limited solution, j_o and α must be selected to satisfy two additional boundary conditions:

$$\frac{d\phi}{d\rho} = 0, \quad at \quad \rho = \rho_i \tag{2.20}$$

$$\frac{d\phi}{d\rho} = 0, \quad at \quad \rho = 0. \tag{2.21}$$

A numerical procedure was then employed to solve Eq. 2.17 meeting the conditions imposed by Eqs. 2.18, 2.19, 2.20 and 2.21. In order to simplify their

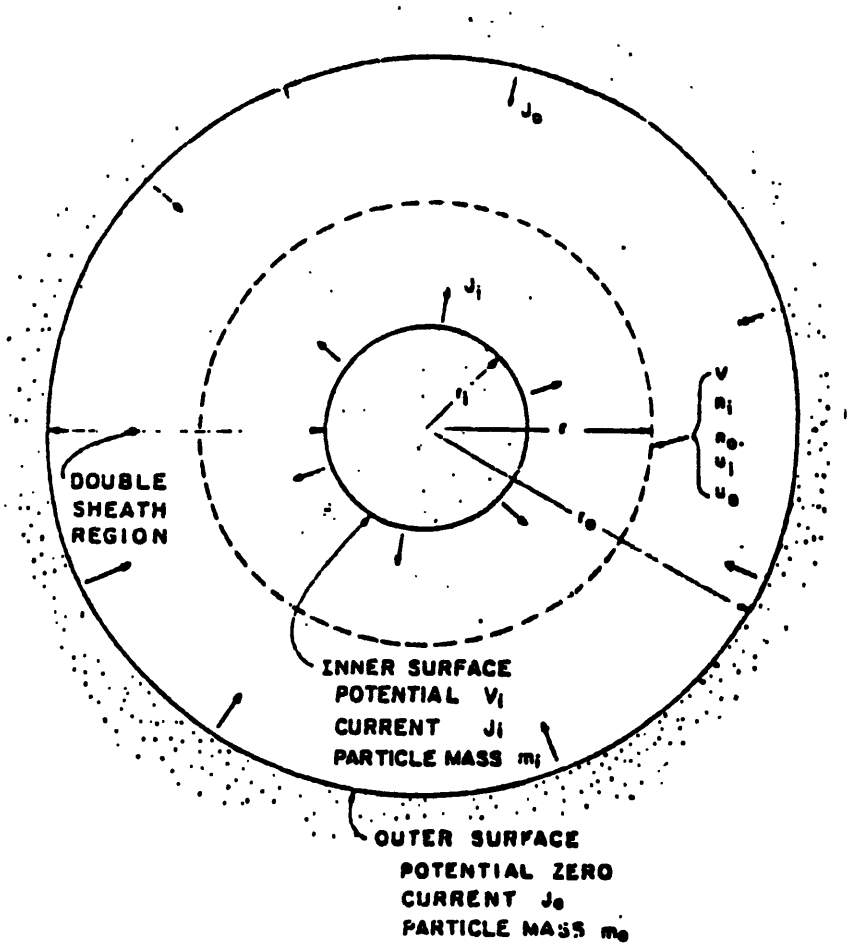

Figure 2.2: Spherical Double Sheath Model of Space-Charge-Limited Current Flow [83]

procedure Wei and Wilbur obtained an expression relating j_o and α,

$$\frac{1}{\alpha} = 1 - \frac{1}{2j_o}\int_0^{\rho_i}\left(\frac{d\phi}{d\rho}\right)^2 d\rho. \tag{2.22}$$

The relaxation technique employed by Wei and Wilbur used Eq. 2.22 to obtain the variations of j_o and α with r_i/r_o as shown in Figs. 2.3 and 2.4. The current enhancement α is given below

$$\frac{J_o}{J_i} = \alpha\sqrt{\frac{m_i}{m_o}} \tag{2.23}$$

Wei and Wilbur found that their potential profiles and space-charge-limited current densities agreed with the analytical results obtained by Langmuir [47] to within 2%. While the potential profiles and potential gradient profiles are valuable results, it is the magnitude of the counterflowing currents that is of the greatest interest. The parameters j_o and α were uniquely determined for the entire range of double layer widths, $0 \leq r_r \leq 1$, where r_r is the radius ratio r_i/r_o. Figure 2.3 shows that the normalized current drawn into the double layer decreases with double layer thickness and approaches infinity as the radius ratio approaches unity. As $r_r \rightarrow 1$, the current ratio α is seen to also approach unity in Figure 2.4. The unity value of r_r corresponds to a planar sheath case and a comparison with Langmuir's analytical results [47] can again be made. For this planar case, Langmuir obtained $\alpha = 1$.

Based upon their problem formulation and numerical solution, Wei and Wilbur concluded that space-charge-limited spherical double layer currents are determined by the radius ratio, r_r, of the two plasma surfaces that form but remain independent of the magnitudes of the radii of these two surfaces. In addition, the current drawn from the outer surface to that drawn from the inner surface varies inversely with the square root of the mass ratio of the particle species carrying the two opposing currents. The enhancement factor in the current ratio formula, Eq. 2.23, is dependent upon the radius ratio of the spherical double layer and lies within the range $\sim 0.01 - 1.0$.

Further work has been done by Williams [89] to extend the Wei and Wilbur double sheath model to the cylindrical case. Success of such an effort represents

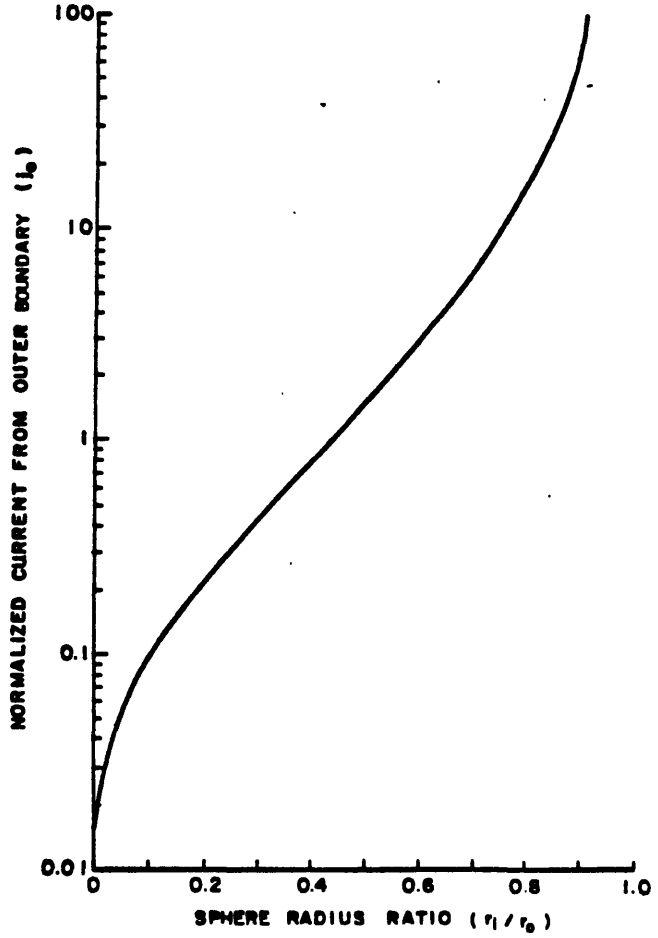

Figure 2.3: Normalized Electron Current vs. Double-Sheath Radius Ratio, Wei and Wilbur Numerical Results [83]

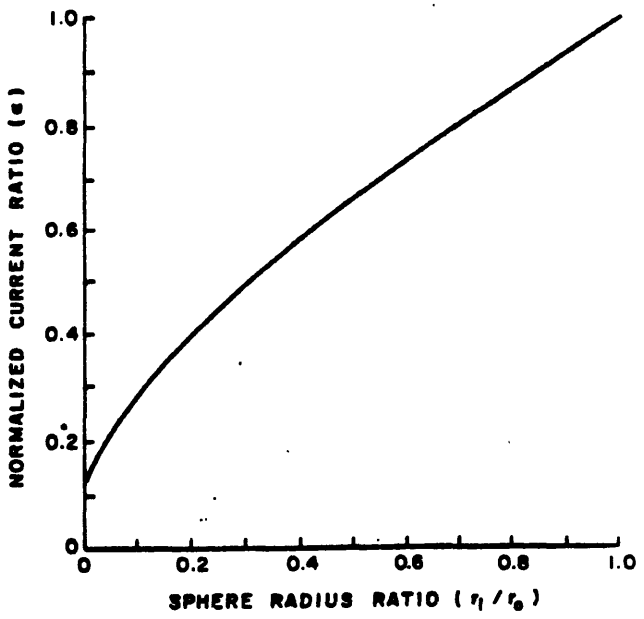

Figure 2.4: Current Enhancement Factor vs. Double-Sheath Radius Ratio Wei and Wilbur Numerical Results [83]

significant progress since the contactor cloud cloud is thought to pass from a spherical to a cylindrical sheath when a number of plasma parameters are varied in the operation of the contactor. Williams has developed a set of equations that one use to may solve the cylindrical space-charge-limited case as well as a Green's function approach to the solution of the Poisson equation. Figure 2.5 represents a possible plasma configuration for the transition from a spherical sheath to a cylindrical sheath. As is underscored when the experimental data is presented in Section 2.6, successful development of this combination of spherical and cylindrical segments is vital to the application of the space-charge-limited modelling effort to actual experiments.

2.2.2 Derivation of the Collisionless Space-Charge-Limited Unmagnetized Spherical Double Sheath Model

The theoretical calculations of the currents limited by space charge must incorporate the cases of parallel planes, coaxial cylinders, and concentric spheres [48]. To facilitate development of the theories of the current flows for these systems, it

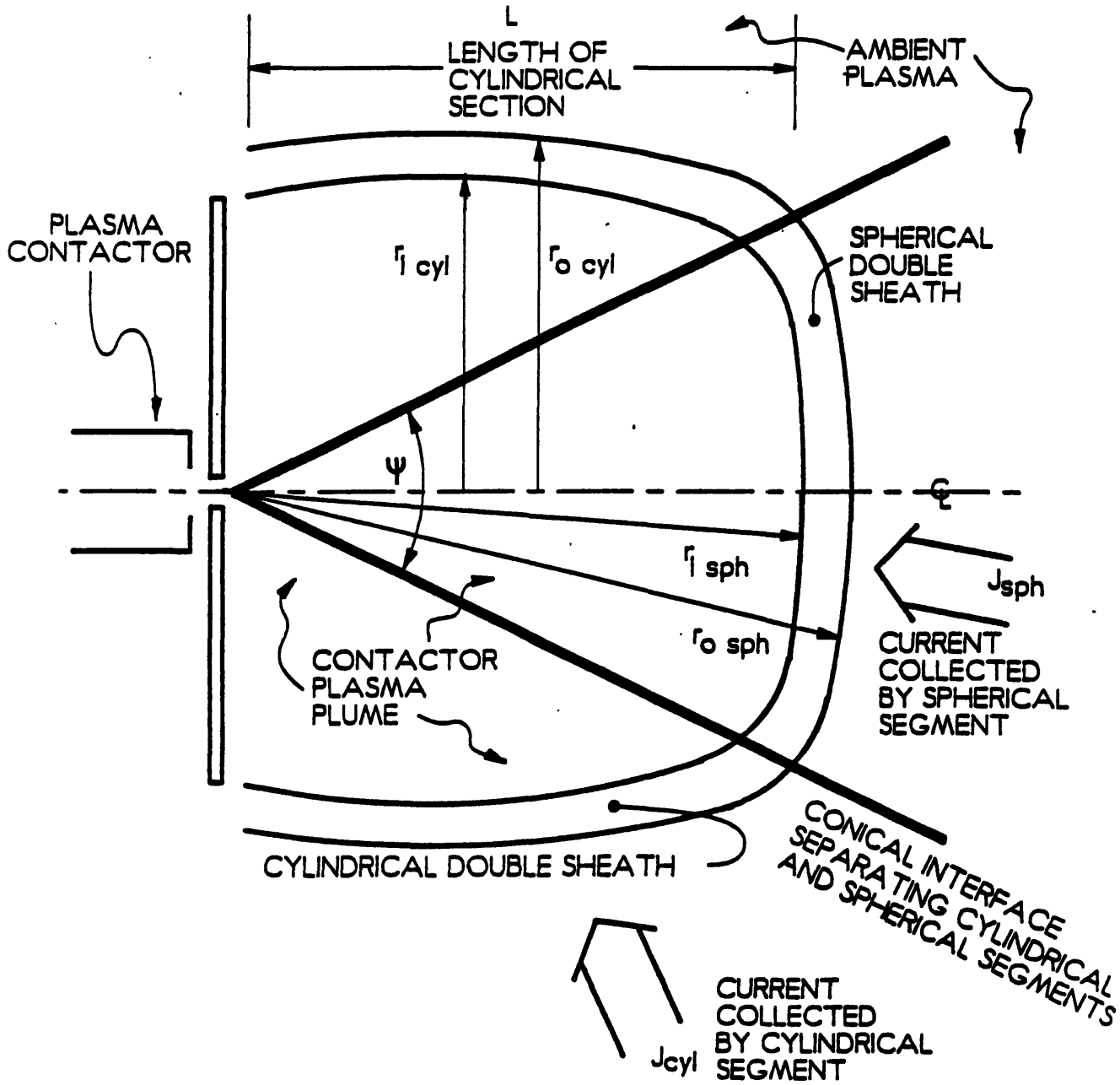

Figure 2.5: Schematic of Cylindrical/Spherical Double Sheath [89]

is extremely useful to note that, in the case of electron current flow, the lines of force and the electron paths coincide. Over the years, the space-charge-limiting effect has been examined rigorously. Child and Langmuir [21,47,48] obtained analytic solutions to the planar single sheath problem, the planar double sheath problem, and the spherical double sheath problem. To this author's knowledge, there has been no complete analytic treatment of the collisionless, unmagnetized, space-charge-limited spherical double sheath model. To date, only the numerical solutions, such as those of Wei and Wilbur [83] presented in this work, have answered the question of how space-charge-limited currents flow in a spherical double sheath.

However, recent work has built upon the Wei and Wilbur model given in Section 2.2.1 [29] to provide a more complete model of the plasma contacting process. Assuming the presence of two components of plasma, an ambient component and a contactor component, a collisionless space-charge-limited unmagnetized model is derived as follows.

The ambient ions and electrons are Maxwellian at a radial distance, r, far from the double layer's outer edge, r_o. T_{ia} and T_{ea} are the ion and electron temperatures and the ambient plasma density is n_{∞}. The contactor plasma component has Maxwellian electrons at temperature T_{ec}. Cold ions stream radially out from the plasma in the vicinity of the anode with an ion current I_i. The potential drop ϕ_0 between the anode, $r = r_{anode}$, and the ambient plasma, present as $r \rightarrow \infty$, is assumed to be much greater than any of the other temperatures. The width of the double layer, $r_{d.l.}$, is considered to be much greater than a Debye length. With these assumptions, the plasma is quasineutral everywhere except inside the double layer, $r_i < r < r_o$. Note that r_o is the same radius as that called r_{core} in the Section 2.1, the radius at which the ambient electron saturation current is collected.

No ambient ions can get inside the contactor core cloud, the region $r < r_i$. The density of ambient electrons, which have been accelerated through the double layer to the core cloud region, is much less than the density of contactor electrons. Quasineutrality within the core cloud then requires $n_{ec}(r) = n_{ic}(r)$. The densities of contactor electrons and ions are related to the plasma potential

ϕ, defined with respect to the ambient plasma at $r = \infty$, by

$$n_{ec} = n_{anode} e^{[(\phi - \phi_0)/T_{ec}]} \tag{2.24}$$

$$n_{ic} = n_{anode}(r_{anode}/r)^2[1 + (\phi_0 - \phi)/T_{ec}]^{-1/2}. \tag{2.25}$$

Here it is assumed that ions are leaving the contactor plasma at the sound speed $(T_{ce}/m_i)^{1/2}$, due to their acceleration in a Bohm presheath. Any ionization or recombination occurring at $r > r_{anode}$ has been neglected.

Setting the right hand sides of Eqs. 2.24 and 2.25 equal to each other gives a transcendental equation for $\phi(r)$ [29]. It is evident that for $r \gg r_{anode}$,

$$\phi(r) \approx \phi_0 - 2T_{ec} \ln(r/r_{anode}). \tag{2.26}$$

The potential then drops by only a few factors of T_{ec} inside the contactor cloud; this drop is much less than the total potential drop. The density at the contactor orifice n_{anode} is related to the ion current I_i by

$$I_i = 4\pi r_{anode}^2 e n_{anode}(T_{ce}/m_i)^{1/2}. \tag{2.27}$$

Outside the double layer, the region $r > r_o$, the ambient electron density decreases from n_∞ as r decreases because no electrons are able to exit from the double layer into the ambient plasma. Assume that there are no sources of electrons or collisions producing electrons that can fill in the resulting empty region of velocity space. From quasineutrality, the ambient ion density must also decrease as r decreases. This occurs even if the density of contactor ions accelerated in the double layer is small compared to the ambient ion density. Then the potential must rise by an amount on the order of T_{ia}. If T_{ia} is much less than T_{ea}, the ambient electron density is not affected by the potential. This assumes that the current being drawn from the outer radius of the double layer is conducted primarily by the electrons and that its flow into the inner plasma core region is through the spherical solid angle segment depicted in Figure 2.1. The geometric factor influencing the current flow is included in the following expression in which the ambient electron density is reduced from n_∞ as r decreases,

$$n_{ea}(r) = \frac{1}{2} n_\infty [1 + (1 - r_o^2/r^2)^{1/2}]. \tag{2.28}$$

The potential is given by,

$$\phi(r) = T_{ia} \ln(n_\infty / n_{ea}). \tag{2.29}$$

The potential drop from r_o to ∞ is just $T_{ia} \ln 2$, much less than the total potential drop. Most of the potential drop must therefore occur in the double layer.

Within the double layer, $r_i < r < r_o$, the plasma is not quasineutral. Poisson's equation must be solved to determine the potential profile across the double layer. Poisson's equation, as given in Eq. 2.12, is modified and given below as

$$\frac{1}{r^2}\frac{d}{dr}r^2\frac{d\phi}{dr} = 4\pi(n_e - n_i). \tag{2.30}$$

Eq. 2.30 must be satisfied subject to the boundary conditions given in Eqs. 2.18 and 2.19. To obtain the unique space-charge-limited solution to Eq. 2.30, Eqs. 2.20 and 2.21 must also be invoked.

Since the bulk of the potential drop occurs in the double layer, a good approximation of the boundary condition Eq. 2.18 is,

$$\phi(r_i) = \phi_0 - 2T_{ec} \ln(r_i / r_{anode}). \tag{2.31}$$

The ambient ion density drops much more quickly than the ambient electron density as the potential starts to rise, in travel toward the contactor from infinity, if $T_{ia} \ll T_{ea}$. Consequently, one may neglect the ambient ion density, n_{ia}, in the total ion density term, n_i, in Eq. 2.30. Similarly, since the energy of the contactor ions is greater than T_{ec} at r_i, even if only by a logarithmic factor, the contactor electron density drops much more quickly than the contactor ion density in travelling from r_i to infinity. Then it is a reasonable approximation to neglect the contactor electron density in the double layer. In the double layer, one can solve Poisson's equation, Eq. 2.30, with

$$n_e = \frac{n_\infty}{2}\frac{r_o^2}{r^2}e^{(\phi/T_{ea})}[1 - erf(\sqrt{\phi/T_{ea}})] \tag{2.32}$$

$$n_i = n_{anode}\frac{r_{anode}^2}{r^2}\left(\frac{\phi_0 - \phi(r)}{T_{ec}}\right)^{-1/2} \tag{2.33}$$

An approximate analytic solution is derived for the case when the double layer is thin, *i.e.* $r_o - r_i \ll r_i$. Then, in the vicinity of r_i, for $\lambda_D \ll r - r_i \ll r_o - r_i$, the potential approximates a Child-Langmuir sheath, with negligible n_e

$$\phi(r_i) - \phi(r) \approx 3^{4/3} T_{ec} \ln(r_i/r_{anode}) \left(\frac{r - r_i}{\lambda_{Di,i}} \right)^{4/3} \tag{2.34}$$

where

$$\lambda_{Di,i}^2 = \frac{T_{ec} \ln(r_i/r_{anode})}{2\pi e^2 n_{anode}} (r_i/r_{anode})^2 \tag{2.35}$$

is the ion Debye length at r_i. In the vicinity of r_o, for $\lambda_D \ll r_o - r \ll r_o - r_i$, the potential approximates an inverted Child-Langmuir sheath, with negligible n_i

$$\phi(r) \approx \frac{3^{4/3}}{2} T_{ea} \left(\frac{r_o - r}{\lambda_{De,o}} \right)^{4/3} \tag{2.36}$$

where

$$\lambda_{De,o}^2 = \frac{T_{ea}}{2\pi e^2 n_\infty} \tag{2.37}$$

is the electron Debye length at r_o. The transition from Eq. 2.34 to Eq. 2.36 occurs when $n_e \approx n_i$, at the point where the two expressions for $\phi(r)$, Eq. 2.34 and Eq. 2.36, have second derivatives that are equal in magnitude but have opposite signs. At this point, the two expressions for $\phi(r)$ must have the same first derivative. This means that the transition from Eq. 2.34 and Eq. 2.36 must occur half way between r_i and r_o, with $\phi(r)$ antisymmetric about this point, and the coefficients in front of the two expressions for $\phi(r)$ must be equal,

$$2T_{ec} \ln(r_i/r_{anode}) \lambda_{Di,i}^{-4/3} = T_{ea} \lambda_{De,o}^{-4/3}. \tag{2.38}$$

The double layer stability condition [13], alternatively referred to as the Langmuir condition, follows from Eq. 2.38,

$$I_e/I_i = (m_i/m_e)^{1/2} \tag{2.39}$$

with $I_e = 2\pi r_o^2 J_e^\infty$, and $J_e^\infty = e n_\infty (2\pi T_{ea}/m_e)^{1/2}$, the ambient electron saturation current. In other words, the contactor cloud will expand freely until the ion current density $I_i/4\pi r^2$ is equal to the ambient electron saturation current times $(m_e/m_i)^{1/2}$. If $T_{ea} \approx T_{ec}$, then this will occur when the density of the contactor plasma is comparable to the density of the ambient plasma, given Eqs. 2.35 and

2.37, in which the Debye lengths' dependence on plasma density is expressed. Note that, if the inner radius of the double is equal to the contactor anode radius, this approximate analytic solution does not hold since the ion Debye length would be set equal to zero.

From Eqs. 2.34, 2.36, and 2.38, the width of the double layer, $r_{d.l.}$, is related to the potential drop $\Delta\phi = \phi(r_i) - \phi(r_o)$ by

$$r_o - r_i = \frac{2}{3}\lambda_{De,o}\left(\frac{\Delta\phi}{T_{ea}}\right)^{3/4}. \tag{2.40}$$

The results of this two component analytic collisionless space-charge-limited double layer model are valid only if the width given by Eq. 2.40 is much less than r_i. This requires that the pressure balance be such that the thin double layer has been pushed out a significant distance from the anode, yielding a reasonably large core cloud region attached at the inner edge of the double layer. Otherwise if this condition is not satisfied, Poisson's equation must be solved numerically, as has been done by Wei and Wilbur [83], Williams [90], and this author. Those solutions then encompass both the thick double layer with r_i constrained only by $r_i \geq r_{anode}$ with widely ranging core cloud radius and the thin double layer developed at significant distance from the origin of the source plasma at the contactor anode. In both of these cases, I_e/I_i will be smaller than $(m_i/m_e)^{1/2}$.

It is important to note that the effect of these electrons in neutralizing the ion space charge cannot in and of itself cause the contactor ion current, I_i, to increase [47]. Instead, the effect is manifested in the change in the thickness of the double layer to accomodate the required potential drop. As the temperature of a cathode rises in a plasma containing current flow between an anode and a cathode, the electron current density increases and equals the cathode's electron emission until $\alpha = 1$. At that point, the electron current can no longer increase in value and becomes space-charge-limited, regardless of any increase in the contactor ion current. Under low pressure space conditions, consider the ambient source plasma to act as a cathode emitting electrons that then flow into a double layer through the presheath towards a plasma contactor. This analogy can be made since the presheath will cause the electrons entering the double layer to be supersonic and, obviously, their temperature to be high. It

was seen in Langmuir's experiments [47] that no matter how hot the source electrons became, the double sheath was formed in low pressure conditions. See Section 2.7.1 for further discussion of the need for supersonic electrons to make the double layer model applicable in space.

2.3 Quasineutral Models and Results

2.3.1 The Dobrowolny and Iess Model

Dobrowolny and Iess [25,42] model the plasma contacting process in the ionosphere by expanding the contactor plasma one-dimensionally into the surrounding ambient plasma. In this model, the hollow cathode plasma source is taken to be polarized suprathermally with respect to the ambient plasma surrounding it. The Dobrowolny and Iess model is a fluid model including anomalous friction due to the presence of plasma instabilities. An analytic solution is obtained from which potential profiles and current enhancement factors are calculated numerically. These calculations do not account for the presence of the magnetic field and the core region of plasma surrounding the hollow cathode is considered to be highly diamagnetic. Their analytic and numerical results indicate rather large overall system gains relevant to the operation of a plasma contactor in a low density ambient plasma. In modelling the radial expansion of the contactor cloud, they calculated a sizable core cloud, in keeping with their assumption of a highly diamagnetic core region surrounding the plasma contactor.

The plasma contactor is taken to be biased positively with respect to the ambient plasma at ϕ_o, causing ions produced by the hollow cathode to move away to infinity and electrons escaping the device's orifice to be collected. Those electrons are therefore not permitted to connect with the ambient plasma. Using the Dobrowolny and Iess notation, *i.e.* indices 1 and 2 indicate the source plasma and the ionospheric plasma respectively, Poisson's equation is given for

a spherically symmetric case and nondimensionally as,

$$\frac{1}{\hat{r}^2}\frac{d}{\hat{r}}\left(\hat{r}^2\frac{d\hat{\phi}}{d\hat{r}}\right) = A\left[\frac{n_{i1}}{n_2} + \frac{n_{i2}}{n_1} - \frac{n_{e2}}{n_1}\right]. \tag{2.41}$$

This nondimensionalization of the problem is accomplished with the following two equations,

$$\hat{r} = \frac{r}{r_o} \tag{2.42}$$

$$\hat{\phi} = \frac{\phi}{\phi_o} \tag{2.43}$$

where r_o is taken to be the distance from the contactor source where spherical symmetry of the source plasma can be assumed valid. (Note that this use of r_o differs from its use throughout the rest of this thesis.) The constant A is given by,

$$A = -\left(\frac{r_o}{\lambda_{De2}}\right)^2 \frac{1}{\tilde{\phi}_o}\frac{n_1}{n_2} \tag{2.44}$$

with,

$$\tilde{\phi}_o = \frac{e\phi}{kT_{e2}} \tag{2.45}$$

Note that λ_{De2} is the Debye length as calculated with the ionospheric electrons.

In order to obtain self-consistent results within their model and given $A \gg 1$, Dobrowolny and Iess impose quasineutrality in the region exterior to the hollow cathode plasma source,

$$n_{e2} = n_{i1} + n_{i2}. \tag{2.46}$$

Dobrowolny and Iess use this approximation in their numerical calculations of the plasma potential profiles and find that it differs insignificantly from the complete solution to the problem as they have posed it.

The ions emitted from the hollow cathode are considered collisionless, thereby conserving energy, yielding,

$$\frac{v_{i1}}{v_o} = \left[1 + 2\frac{c_{s2}^2}{v_o^2}\tilde{\phi}_o(1-\hat{\phi})\right]^{1/2}. \tag{2.47}$$

Conservation of mass in the plasma flow gives,

$$\frac{n_{i1}}{n_1} = \frac{1}{\hat{r}^2}\frac{v_o}{v_{i1}} \tag{2.48}$$

The velocity of the ions at the orifice of the device is v_o while c_{s2} is the sound speed of the ions calculated using T_{e2}. Eqs. 2.47 and 2.48 allow the explicit determination of n_{i1} as a function of the plasma potential, ϕ. In order to match the potential profile smoothly from the contactor plasma to the ambient plasma at ∞, the ions are repelled from the interaction region according to the following equation,

$$n_{i2} = n_2 e^{-e\phi/kT_{e2}}. \tag{2.49}$$

As mentioned in Section 2.2.2, and is further discussed in Section 2.7.1, the polarization of the plasma source with respect to the surrounding plasma results in supersonic motion of the particles. Dobrowolny and Iess account for this phenomenon by including an anomalous friction term in the calculation of mass conservation for electrons. Two friction terms are used, one referenced to the counterstreaming motion of the electrons with respect to the source ions and the other with respect to the ionospheric ions. This is done assuming that the ionospheric ions are at rest. These frictional terms become critical only when an ion acoustic instability is triggered. The collision frequency for this instability once triggered is taken to be,

$$\nu^*_{acoustic} = \omega_{pe}\frac{\sqrt{\pi}}{32}\left(\frac{n_{i1,2}}{n_2}\frac{n_2}{n_{e2}}\right)^2. \tag{2.50}$$

The electron plasma frequency in the ambient plasma is given by ω_{pe}.

By then combining their expression for electron momentum with the quasineutrality condition imposed in Eq. 2.46 and the mass conservation equations, Dobrowolny and Iess are able to to obtain a first order equation for $\hat{\phi}$ from the following expression,

$$-\frac{1}{\hat{r}^2}(1+\psi_s) = B\left(\frac{n_{e2}}{n_1}\right)^{1/2}\left\{\hat{\phi}' - \frac{1}{\tilde{\phi}_o}\left[\frac{d}{d\hat{r}}\ln n_{e2} + \frac{d}{d\hat{r}}\left(\frac{v_{e2}}{v_{the}}\right)^2\right]\right\}. \tag{2.51}$$

where

$$B = \frac{32}{\sqrt{\pi}}\frac{\lambda_{De2}}{r_o}\frac{v_{the}}{v_o}\left(\frac{n_2}{n_1}\right)^{1/2}\tilde{\phi}_o. \tag{2.52}$$

The following boundary conditions are imposed to secure a smooth and self-consistent solution to the first order form of Eq. 2.51,

$$\hat{\phi}(\hat{r}=1) = 1 \tag{2.53}$$

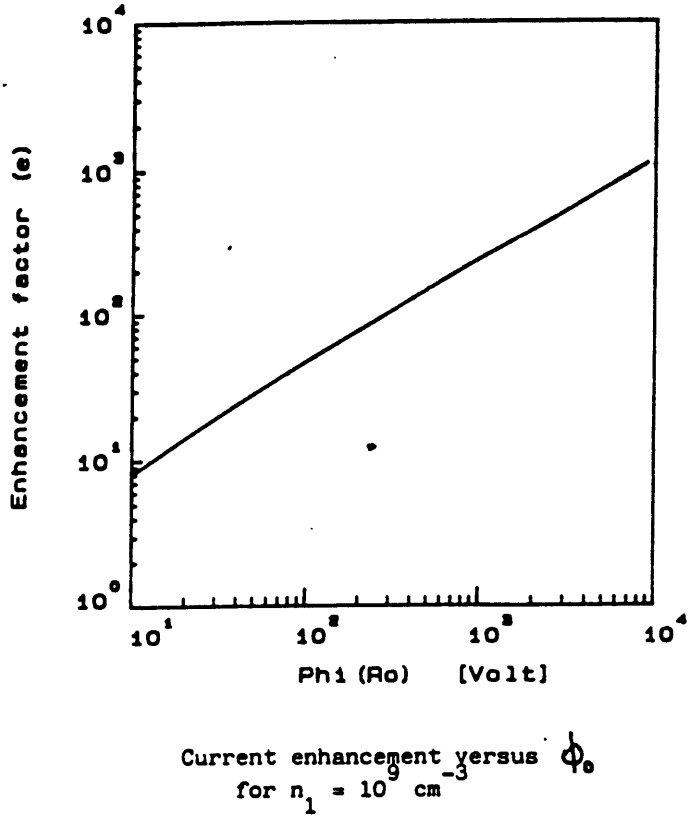

Figure 2.6: Current enhancement vs. Potential; Dobrowolny and Iess quasineutral model [25]

$$\hat{\phi}(\hat{r} \to \infty) = 0 \tag{2.54}$$

The boundary condition in Eq. 2.54 provides a unique solution to the problem while the boundary condition at infinity allows the collected current, I_e, to be solved as an eigenvalue within the equation for mass conservation of electrons.

When analytically solving Eq. 2.51, three regions of plasma interaction are demarcated. Since $\tilde{\phi}_o \gg 1$ in the inner region, the pressure gradient and inertia terms in Eq. 2.51 are considered negligible. In the far field region, $\tilde{\phi} \ll 1$, so that the drift velocity required by the electrons is then too low to trigger instability and the region may be considered collisionless. The difficulty then lies in matching the collisional intermediate region with the other two regimes. Taking $n_1 = 10^9\, cm^{-3}$, the gain is determined as a function of ϕ_o (Figure 2.6) and as a function of the hollow cathode plasma density n_1 (Figure 2.7). The total current obtained is plotted in Figure 2.8.

In their most recent treatment of the plasma contacting process [42], the fluid

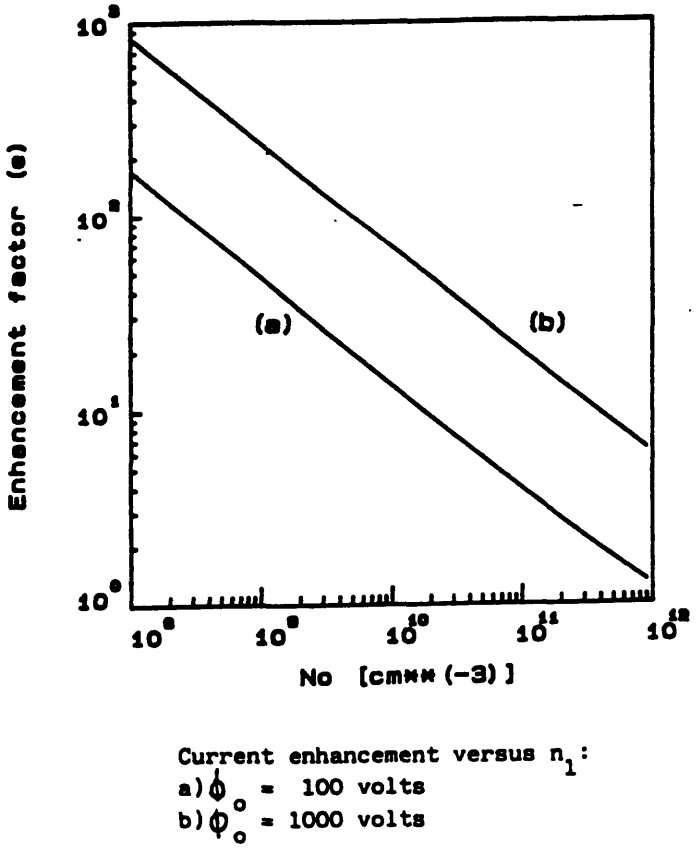

Figure 2.7: Current enhancement vs. Density; Dobrowolny and Iess quasineutral model [25]

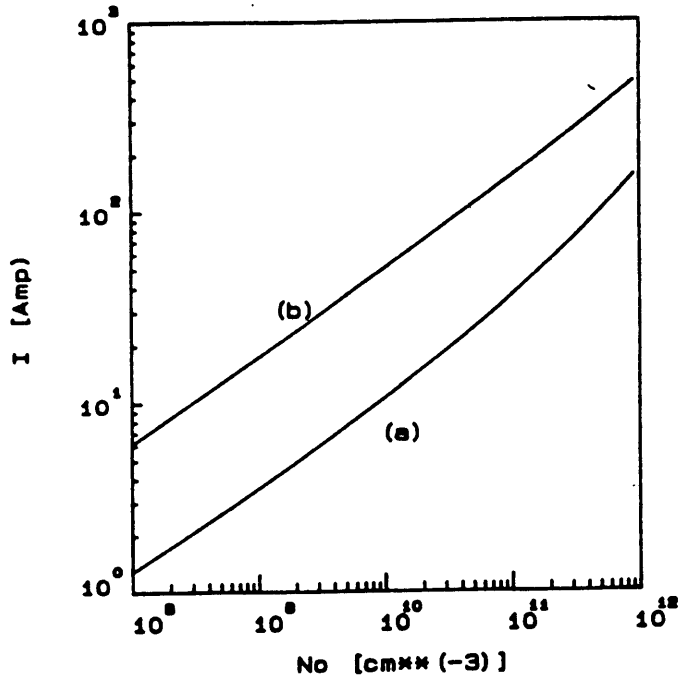

Figure 2.8: Total plasma current vs. Density; Dobrowolny and Iess quasineutral model [25]

equations are fully solved in a continuation of their model as a spherically symmetric, stationary, fluid including collisional transport. As before, a differential equation is established of the form,

$$\frac{d\phi}{dr} = \frac{F(r,\phi,I_e)}{G(r,\phi,I_e)} \tag{2.55}$$

When this solution is singular, *i.e.* when $G(r,\phi,I_e) = 0$, it in fact contains a turning point. Solutions containing such turning points are multivalued and do not represent true physical situations. The quasineutral hypothesis is clearly invalidated for such cases. This is apparent since there exist large potential gradients in the solutions obtained. The solution may be developed around these turning points as,

$$r - r^* = \frac{1}{2}\left(\frac{d^2\phi}{dr^2}\right)^{-2}_{r=r^*}(\phi - \phi^*)^2, \tag{2.56}$$

with r^* and ϕ^* representing the coordinates of the singular point in the r,ϕ

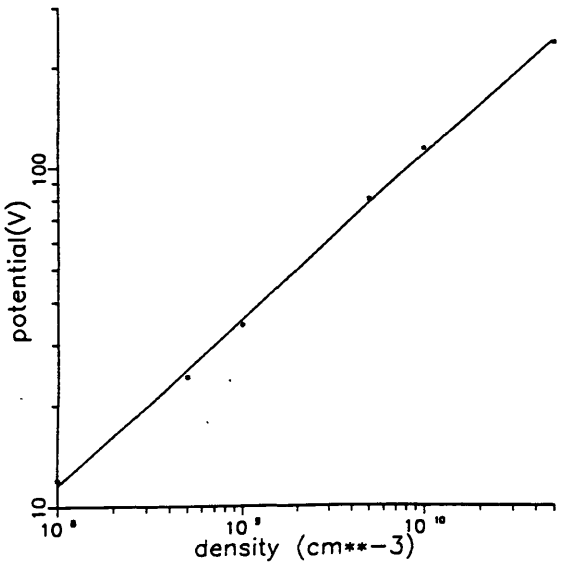

Figure 2.9: Boundary between regular and singular solutions in the Dobrowolny and Iess quasineutral fluid model [42]

system.

The numerical results of Dobrowolny and Iess indicate that these multivalued solutions occur for high values of ϕ_o and low contactor plasma density, n_1. By running numerous cases altering ϕ_o and n_1 parametrically, they obtained the range of ϕ_o and n_1 over which single-valued solutions can be obtained. In Figure 2.9, the boundary between regular and singular solutions is plotted, for parameter values of $T_{e1} = 5\,eV$, $T_{e2} = T_{i2} = 0.1\,eV$, $r_o = 10\,cm$, for an Argon plasma expanding into a LEO type plasma. In these cases, overall system gain is also calculated. It was determined that the gain improves for the lower contactor plasma density cases while higher contactor plasma density corresponds to higher total current.

Dobrowolny and Iess have assumed that the ionospheric ions are stationary and therefore they assume that frictional terms may be eliminated from their expression of the momentum equation. They then must keep the anomalous collision contribution negligible when performing the numerical integration. From their results using the approach described in [42], Dobrowolny and Iess state

that I_e increases with a decrease in the collision frequency since such a decrease results in a less resistive plasma core region.

In addition to the consideration of the parameters discussed above, Dobrowolny and Iess analyze the importance of the magnetic field within the context of their model. Based on a comparison of their calculated electric field strength and calculated Lorentz force values, they reach the conclusion that the ratio of these two values is quite large on the region where anomalous transport is dominant and that the magnetic field effects come into play only when the the potential has reached thermal values, where the contact has effectively already occurred. So the spherical symmetry of the model is destroyed only at great distances from the anode and the inclusion of the magnetic field would not change the final solution very much.

2.3.2 The Hastings, et. al. Model

Several regions are described as existing within the plasma contactor cloud [38]. The plasma in close proximity to the contacting device is assumed to be very dense and highly diamagnetic. The bias voltage on the anodic end of the tether system is taken to be much greater than the ambient ion energy in this model. With these conditions, one can assume that the plasma contactor cloud will expand radially, as can be demonstrated by taking into consideration the two directions of anisotropy inherent to the cloud. One is the direction of motion of the whole system and the other is the direction of the magnetic field.

If the motion of the electrons is primarily radial, the magnetic field anisotropy effects are eliminated. With a highly diamagnetic or highly collisional plasma, this elimination of magnetic field effects would also result [36]. The motional electric field anisotropy is shielded from the plasma whenever the plasma is dense enough to permit easy polarization. When these two directions of anisotropy are felt by the plasma, however, the plasma cloud can be divided into three regions, the core region, the transition region, and the outer shell.

The plasma within the core region is shielded from both anisotropy effects and

expands isotropically, bounded by conditions imposed by the contacting device. The transition region is affected by the magnetic field but remains shielded from the motional electric field due to the fact that the contacting device's imposed electric field is dominant over it. The electrons will be magnetized in the transition region with the ions continuing to expand radially under the imposed potential's influence. At the point where the expansion of the ions is halted by the influence of the magnetic field, the transition region is bounded and the ions turn around. Consequently, the transition region boundary will be at roughly one ion gyroradius, given the gyroradius based on the energy gained by the ions dropping through a self-consistent potential [36].

The outer shell will have manifestations of both anisotropies. Ions will be magnetized and drift across the magnetic field with $\vec{E} \times \vec{B}$ drift that is actually determined by the motional electric field, $\vec{E_m} = \vec{V} \times \vec{B}$. This motion guarantees that the ions will come to rest within the ambient plasma, thereby completing the plasma "contacting" process. The electrons will flow along field lines while experiencing $\vec{E} \times \vec{B}$ drift. The outer shell is the sole region where the sweep of the tethered system across Earth's geomagnetic field is felt; the result is that the inner two regions may be analyzed while ignoring the fact that this sweeping is taking place [36].

Definition of Core Radius

A plasma source capable of producing a large enough contactor cloud to draw a high current in space will have a high density, $\omega_{pe} \gg \omega_{ce}$, for some distance out from the anode. Such a plasma is likely to be subject to instabilities which produce an effective electron collision frequency,

$$\nu_e > \omega_{ce}. \tag{2.57}$$

In the region where Eq. 2.57 is satisfied, the electrons will behave like a fluid, unaffected by the magnetic field. The electron fluid will still feel a $\vec{v} \times \vec{B}$ force, but this force is always small compared to the force due to the electric field. Since if Eq. 2.57 is satisfied, the steady state radial velocity, at which the drag

force $\nu_e m_e v_r$ balances the electric force eE, is $eE/m_e\nu_e$. Then the ratio of the electric force to the magnetic force is

$$\frac{E}{v_r B} = \frac{\nu_e m_e}{eB} = \frac{\nu_e}{\omega_{ce}} \gg 1, \tag{2.58}$$

and the electrons are unaffected by the magnetic field. Since, due to the high collision frequency, there cannot be two different velocity components of electrons at the same place in this region, there can be no double layers and quasineutrality will be satisfied everywhere. Since the effective collision rate due to instabilities tends to scale with ω_{pe}, it decreases with distance from the source. Then at some radial distance, r, from the contactor, Eq. 2.57 is no longer satisfied and the electrons no longer behave like an unmagnetized fluid. Even beyond this radius, electrons can diffuse slowly across the magnetic field, and it is shown in Chapter 3 that it may be possible to collect electron current out to a radius r_1. The electron current collected is

$$I_e = 2\pi r_{core}^2 J_e^\infty, \tag{2.59}$$

where r_{core} is at least as great as the radius r where Eq. 2.57 ceases to be satisfied and is equal to the r_1 defined in Chapter 3, if the model described there is applicable. Both possibilities are evaluated, to set upper and lower bounds on I_e. Note that r_{core} must be smaller than the radius r at which the contactor ion density is equal to the ambient ion density and must be smaller than the ion Larmor radius [29].

Equations for Core Region

The core region will satisfy the following equations as given in Ref. [36]: contactor ion density n_i,

$$\frac{1}{r^2}\frac{\partial}{\partial r}\left(r^2 n_i v_i\right) = n_n n_e \langle\sigma v\rangle_{ionization} - n_i n_e \langle\sigma v\rangle_{recombination} \tag{2.60}$$

ambient ion density $n_{ambient}$,

$$n_{ambient} = n_{ambient}(\infty)\exp(-e\phi/T_i) \tag{2.61}$$

neutral density, n_n,

$$\frac{1}{r^2}\frac{\partial}{\partial r}\left(r^2 n_n v_n\right) = -n_i n_e \langle\sigma v\rangle_{recombination} + n_n n_e \langle\sigma v\rangle_{ionization} - 3\frac{m_e}{m_i} n_e e \nu_e (T_e - T_i) \tag{2.62}$$

potential ϕ,

$$\frac{\partial}{\partial r}\left(e(\phi_0 - \phi)\right) = -m_e \frac{I_e}{4\pi r^2 n_e}\frac{\partial}{\partial r}\left(\frac{I_e}{4\pi r^2 n_e}\right) - \frac{\partial T_e}{\partial r} + \frac{m_e \nu_e}{e n_e}\left(\frac{I}{4\pi r^2}\right) - \frac{T_e}{n_e}\frac{\partial n_e}{\partial r} \tag{2.63}$$

electron temperature T_e,

$$-\frac{1}{r^2}\frac{\partial}{\partial r}\left(r^2 \kappa \frac{\partial T_e}{\partial r}\right) = \frac{I_e}{4\pi r^2} E - E_{ion} n_n n_e \langle\sigma v\rangle_{ionization} \tag{2.64}$$

electron density n_e,

$$n_e = n_i + n_{ambient}. \tag{2.65}$$

where $\langle\sigma v\rangle_{ionization}$ and $\langle\sigma v\rangle_{recombination}$ are given in Ref. [34]. In Eq. 2.64 the electrons are taken to be heated ohmically and to lose their energy mainly as a result of ionization. The sources used to produce the plasma cloud typically emit cold ions and hot electrons. Therefore, the ion and neutral temperatures are chosen to be the same, with the neutral velocity v_n given by $v_n = \sqrt{2kT_i/m_i}$. The value of the equivalent temperatures is chosen to be the ambient ion population's temperature with quasineutrality is imposed in Eq. 2.65.

The ion velocity in the core region will be determined from the ion momentum balance. Devices that are used to produce plasma clouds eject ions with a velocity that is on the order of the ion acoustic velocity. In this case the ion velocity, v_i, with v_{i_0} defined as the initial ion velocity, will be given by

$$\frac{1}{2}m_i v_i^2 + e\phi = \frac{1}{2}m_i v_{i_0}^2 + e\phi_0, \tag{2.66}$$

assuming that the ions are weakly collisional in the core. Consequently, ion energy loss from elastic collisions can be neglected. These equations for the core cloud region must be solved subject to the following constraints:

$$I = constant \tag{2.67}$$

while at at $r = r_{anode}$,

$$n_i(r_{anode}) = \frac{I_i}{4\pi e v_{i_0} r_{anode}^2}. \tag{2.68}$$

I_i is the equivalent ion current contained in the plasma flow leaving the source. The initial neutral density is

$$n_n(r_{anode}) = n_i(r_{anode})(1 - f_i)/f_i \tag{2.69}$$

where f_i is the initial ionization fraction. The neutral mass flow rate per unit area associated with plasma cloud is

$$\dot{m} = \frac{3v_n}{4\pi r_{core}^3} M \left(\frac{m_p}{e}\right) I_i(1 - f_i)/f_i. \tag{2.70}$$

M is the atomic weight of the gas atoms and m_p is the mass of a proton. The boundary conditions on electron temperature are:

$$T_e = T_e(r_{anode}) \tag{2.71}$$

and

$$-\kappa \frac{\partial T_e}{\partial r} = \frac{T_e(r_{anode})}{e} \frac{I_c}{4\pi}. \tag{2.72}$$

The electron thermal conductivity expression used is the classical expression [15]:

$$\kappa = 3.2 n_e T_e/(m_e \nu_e). \tag{2.73}$$

The differential velocity between electron and ions is

$$v_D = \frac{I}{4\pi r^2 e n_e}. \tag{2.74}$$

The electron collision frequency is given as

$$\nu_e = \nu_{ei} + \nu_{en} + \nu^*_{acoustic} + \nu^*_{Buneman} \tag{2.75}$$

where for

$$v_D > \frac{c_s}{\sqrt{2}} \left[1 + \left(\frac{T_e}{T_i}\right)^{3/2} \left(\frac{m_i}{m_e}\right)^{1/2} \exp\left(-\frac{3}{2} - \frac{T_e}{2T_i}\right)\right], \tag{2.76}$$

the ion acoustic instability can be triggered and gives [55]

$$\nu^*_{acoustic} = 10^{-2} \frac{T_e}{T_i} \frac{v_D}{v_{the}} \omega_{pe}. \tag{2.77}$$

For $v_D > v_{the}$, the Buneman instability can be triggered, giving [43],

$$\nu^*_{Buneman} = 0.53 \left(\frac{m_e}{m_i}\right)^{0.61} \omega_{pe}. \tag{2.78}$$

The magnetic field is chosen to be the diamagnetically modified field. The diamagnetically modified field is that in which $B = 0$ for $\beta \geq 1$ and $B = B_{ambient}\sqrt{1 - \beta}$ for $\beta < 1$. The plasma parameter β is defined as:

$$\beta = n_e(T_e + T_i)/(B^2/2\mu_0). \tag{2.79}$$

Discussion of Solutions

In order to evaluate a lower bound on r_{core}, the equations for the core region, given in the preceding section are solved, for the definition of r_{core} given by Eq. 2.57. The equations are solved by making a guess on the incoming electron current and then marching forward in radius from the plasma contactor until the appropriate condition, Eq. 2.57, is satisfied. The electron saturation current across $r = r_{core}$ is then calculated and compared to the initial guess. If the two did not agree, a new guess for the incoming electron current is chosen and the process repeated. This iterative procedure is continued until the electron current entering the central anode is consistent with the electron saturation current crossing the core radius.

This model has been extensively discussed in Ref. [36]. Typical gains were close to 1. This low gain is due to the fact that the core region where Eq. 2.57 is satisfied is too small to collect much electron current. In the collisionless double layer model, much higher gains, over 100, are possible. These high gains occur because electrons are collected across the magnetic field due to the force resulting from the very large potential drop across the double layer. This large potential drop in turn reduces the efficiency of the tether. It may then be more efficient to produce ion current than to collect electron current across such a large potential.

The current collected through a quasineutral cloud is shown against the far field electron saturation current density for a one ampere ion source current in Figures 3.20 and 3.21, using $\frac{d\phi}{dr} > \frac{vB}{c}$ as the boundary condition, alternatively expressed as $E_r > v_{e_r} B$. This condition provides an upper bound on the core radius available with this quasineutral solution [36]. This is the macroscopic fluid approach and implies that the electric field forces dominate the magnetic field forces if the radial electric field component of force exerted on the electron fluid is greater than the swirling magnetic force on the electron fluid. It can be seen that this yields a finite core radius since for $r \rightarrow \infty$, the potential drops as a function of the inverse square of this radius r, and since $v_{e_r} r^2 \rightarrow Constant$, $E_r / v_{e_r} B \sim 1/r \rightarrow 0$ is obtained. Therefore, if $E_r / v_{e_r} B > 1$ is an initial condition,

Table 2.1: Load power and efficiency of quasineutral contactor

$R_{load}\ \Omega$	I(A)	$\phi_0\ (V)$	$P_{load}(W)$	η
10	25	27	6260	4.7%
100	17.5	26.3	30670	33.2%
1000	4.38	24	19180	83%
5000	1.01	21.7	5113	95.7%

r_{core} has a finite value.

The numerical results for this quasineutral model are plotted in Figure 3.20. The gain calculated is at most on the order of 2 and varies by about a factor of 3 for the four order of magnitude variation in the source. In Figure 3.21, the current voltage characteristic is plotted for a quasineutral contactor with a far field electron saturation current density of $2 \times 10^{-3}\, A/m^{-2}$ and with $T_e(r_{anode}) = 2.5\, eV$. The current is mainly composed of outgoing ions with a low voltage drop of $\simeq 20\, Volts$. (These plots are included in Chapter 3 since they also contain results from the modelling presented in that chapter.)

Table 2.1 shows the load power P_{load} and efficiency $\eta = R_{load}I/\phi_{total}$ for different values of R_{load}. These values are calculated using the ambient plasma and tether parameters $B_o = 0.33 \times 10^{-4}\, T$, spacecraft orbital velocity $v_o = 8\, km/s$, tether length $L = 20\, km$, tether impedance $R_t = 200\, \Omega$, average ionospheric electron saturation current density $J_e^{\infty} = 2 \times 10^{-3}\, A/m^2$, and using the potential ϕ_0 obtained for the quasineutral model (with $T_e = 2.5\, eV$ at r_{anode}), $\phi_0 = 21.7I^{0.0676}$ [29].

In this case, the maximum power obtained at $\simeq$ 80% efficiency is $19\, kW$, much higher than in in Table 3.2. In comparision with the collisionless double layer model results, the energetic cost of producing amperes of ion current with the collisional quasineutral model must be weighed against the cost of the high potential associated with the space charge limited double layer.

In Chapter 3, a model is explored that is similar to the collisionless double layer model in the behavior of electrons along the magnetic field, but is colli-

sional and quasineutral across the magnetic field. This anisotropic model has characteristics that fall between those of the collisionless double layer and collisional quasineutral model. The anisotropic contactor model permits modest gains, typically 2 to 10, at moderately low potential drops. Also presented in Chapter 3 are the results of analyzing the figures of merit for a contactor plasma with a one-dimensional radial expansion through a collisional quasineutral core attached to a collisionless double layer that bridges the gap to the ambient plasma.

2.4 The Katz, et. al. Model

In [58], Parks and Katz decribe a model of a hollow cathode plasma contactor for use in conjunction with an electrodynamic tether system. Their theory addresses the potential profile of a plasma in the vicinity of a sphere with a diameter greater than a Debye length. They assume that the spherical body operates at a constant current and attracts electrons across a space-charge-limited sheath. Three different regimes of current collection are characterized:

$$I_i < \sqrt{m_e/m_i} I_e \tag{2.80}$$

$$\sqrt{m_e/m_i} I_e < I_i < I_e \tag{2.81}$$

$$I_p > I_e \tag{2.82}$$

Their work in analyzing these regimes led them to the conclusion that a plasma contactor generated plasma would eliminate the space-charge sheath. This was a desirable result since such sheaths create a high impedance that impacts the efficiency of a system such as a tethered satellite. Eq. 2.81 predicts a high-impedance space-charge-limited sheath collecting surface while Eq. 2.82 provides a resistive quasineutral transport mechanism. The third region in Eq. 2.82 yields low-impedance ion transport. Region 2 appears as the optimal choice for modelling efforts.

However, the availability of chamber data indicating the formation of double layers during plasma contactor experiments has prompted Katz, et. al., to examine this particular phenomenon. In [24], Davis et. al. further develop the model

with the intention of accounting for the two component of electrons observed primarily in the laboratory experiments of Wilbur [85,86,87,91,92] and Patterson [61,62]. This two component flow occurs for current collection greater than 100 mA when the contactor plasma is in ignited mode, undergoing ionization. It is believed that the electrons are accelerated significantly enough through the double layer to ionize contactor emitted neutrals. Subsequently created ions leave the high density core region and the newly created electrons are collected to the contactor anode along with the high energy electrons. The core region for this case is taken to be the ignited plasma region.

Outside of the region of the ignited plasma, the electron population once again consists of two components. A Maxwellian component is measured at an energy of $4-8\,eV$ and a low density monoenergetic component is present with an energy equivalent to the difference between the source electrons and the ambient plasma.

Davis built this version of the model upon the Wei and Wilbur [83] double diode model described in Section 2.2.1. Her addition to the model is the inclusion of finite temperature effects and as well as an accounting of the repelled species. Ionization of contactor neutrals within the plume is considered critical to the model and the primary mechanism for current enhancement. Within this scheme the contactor plasma is comprised of accelerated ions, thermal electrons and neutrals expanding radially. The ambient plasma contains background neutrals in addition to the ambient ions and electrons present. Poisson's equation as given below is solved self-consistently for an all-inclusive charge density,

$$-\nabla^2\phi = \rho = e(n_{ic} + n_{iz} + n_{ec}) + \rho_a \tag{2.83}$$

where ρ_a is charge density of the charged particles of ambient plasma and n_{iz} is the number density of ions created through ionization in the plasma core and all other variables are defined as before. The boundary conditions used are

$$\phi = \phi_k \qquad \textit{at a small sphere of radius} \qquad r_{min} \tag{2.84}$$

$$\phi = 0 \quad \textit{at outer boundary of calculation space} \quad r_{amb}. \tag{2.85}$$

Additional boundary constraints are also applied within the model depending upon the physical nature of the chamber experiment or the spacecraft under

study. Spherical symmetry is assumed in the expansion of the plasma and in the formation of the double layer. Some calculations have been done with a cylindrically symmetric plasma cloud but the results have not yet been presented.

The ionization fraction of the contactor neutrals is considered to be determined by the accelerated electron population that has passed through the double layer. Note, however, that the interaction produced ions do not affect the charge-exchange plasma flow but do alter the local density. Due to the high thermal component of electrons, angular momentum is be taken into account. This angular momentum consideration yields peak electron density estimates that are more in line with the electron density measurements taken in the experiments mentioned at the start of this section.

A plasma with the electron, ion, and neutral components described within the Davis, et. al. model forms a double layer if the value of ϕ_k is significant enough. This presence of a double layer is obtained through the solution of a multiple root problem by Katz and Davis [44]. The charge density equation has a single root at r_{min} and at r_{amb}. However, within the region between these two radii, the charge density equation is found to have three roots. It is assumed that the plasma potential profile is adjusted so that the root with the higher potential value is present at the inner edge of the double layer and the lower potential value root at the outer edge of the double layer. If there is to be a continuous plasma profile, quasineutrality cannot be maintained within the double layer so that charge separation then develops.

Katz and Davis describe the multiple root theory as a "Van der Waals-like" theory. The analogy is made between Van der Waals theory for liquid-gas phase transitions and the theory they present for the formation of double layers between two different plasmas. In this theory they identify the parameter r_{DL} as the radius at which a double layer forms in a case of a spherically expanding plasma in which Poisson's equation is satisfied. The charge density expressions used in their formulation are limited to those double layers where $r_{d.l.} \ll r_i$ and are collisionless.

2.5 Contrast and Comparison of Modelling Efforts

In this section, a comparative study is undertaken of the theoretical plasma contactor models to gauge the plasma contactor's capability to enhance current collection. This section is intended to supplement the examination of the individual theories performed in the preceding sections. This comparison is made among all of the models presented thus far in this work. The model for electron current collection by a plasma contactor presented by Dobrowolny and Iess [25,42] and by Hastings and Blandino is that of quasineutral flow. Solutions have been obtained by Dobrowolny and Iess in which double layers have been included. Numerical simulations have been run to verify this analytic solution. Data have been obtained that yield a current collection enhancement factor differing from the model in order of magnitude as well as from the Hastings and Blandino model. In contrast, the Wilbur, et. al. model is based upon space-charge-limited current flow. A numerical solution to the spherical double sheath problem has been determined. Various hollow cathode operating conditions have been examined in an effort to under the hollow cathode and "ambient" plasma interactions. The modelling of Katz, et. al., has included both quasineutrality and double layers.

The Wei and Wilbur model is not adequate for the purposes of most required modelling when used by itself since it does not offer enough of a description of the plasma process. The thin collisionless double layer does not appear naturally under most operational conditions for a plasma contactor. So it is necessary to place additional constraints upon the model and to use it in conjunction with other modelling tools to reasonably reflect the contacting process. This model also does not apply to LEO conditions as it stands without appropriately set current collection bounds. Analysis and numerical simulations detailed in Chapter 3 build upon this model.

Note that the Wei and Wilbur collisionless unmagnetized space-charge-limited spherical double layer model is essentially identical to the collisional fluid model

of Parks and Katz [59] in the limit that the resistivity η is sufficiently small and $e\eta J \ll \nabla P$, given P as the pressure and J as the current density. In this case, the potential gradient $e\nabla\phi = \nabla P + e\eta J$ is dominated by the potential gradient term ∇P, known in Katz' terminology as the barometric term. The major difference between these two models lies in the treatment of ionization. Wei and Wilbur have a completely collisionless double layer that can model relatively thin sheaths rather well while Katz et. al. have set out to include ionization and extend the theory to thicker layers. This extension is necessary so that the collisonal processes upon which high system gain with low impedance is predicated can be effectively taken into account. However, it is not necessarily beneficial to the contacting system to rely on the ionization of background and source neutrals for this high gain, as is discussed in Chapter 3

The Dobrowolny and Iess approach is self-consistent and offers a solution in one dimension, but at the expense of an oversimplification of the system. Consequently, its results have rather limited applicability to the primary region of interest, space. The greatest deficiency is in the neglect of the magnetic field effects on the contacting plasma. The other models either make some attempt to incorporate those effects, or there exists a natural step that can be taken to include it, as is done with the Wei and Wilbur model in Chapter 3. There is no credible justification for the neglect of the magnetic fields effects on the travel of the electrons to the anode, despite the presence of anomalous resistivity. That is especially true when $\omega_{ce} \geq \omega_{pe}$. Their analysis of the magnetic field effects is limited since it pertains to the one dimensional flow regime and it is clear that the modelling should be at least two-dimensional to consider both the direction along and the direction perpendicular to the magnetic field lines.

However, Dobrowolny and Iess do account for the formation of double layers within their model, in a manner similar to the Katz and Davis multiple root theory. In their full solution of their fluid model using Eq. 2.55, Dobrowolny and Iess can obtain solutions that are singular. Such cases represent the formation of double layers where quasineutrality breaks down and Poisson's equation must be solve to obtain the plasma potential profile. Dobrowolny and Iess primarily solved for regular solutions of Eq. 2.55 with their numerical techniques. Katz

and Davis, on the other hand, formulated a multiple root solution using charge density as function of potential to solve Poisson's equation. This allowed them not only to solve for the potential profile but also to determine at what radius the double layer forms. Despite this inclusion of double layers within their model, the gains calculated by Dobrowolny and Iess are still less than those predicted by the collisionless space-charge-limited theories.

The Hastings and Blandino collisional quasineutral model is handicapped by its contention that there can be no significant electron current collected from those regions where $\nu < \omega_{ce}$. As will be shown in Section 3.2, a contactor cloud can in fact collect current in those regions. It should be noted that the collisionality stopping condition, ν_e/ω_{ce}, provides an essentially nondimensional collision frequency since ω_{ce} remains roughly the same beyond the point where the plasma β parameter is of order unity. The numerical work of Blandino [10] showed that the E/vB stopping condition yields a core radius significantly larger than the ν_e/ω_{ce} stopping condition as the contactor output ion current increases. This is primarily due to the fact that the ν_e/ω_{ce} curve indicates the increasing resistance in the plasma cloud. Another key point brought out by Blandino's numerical results is that the collisions within the core are quite insensitive to the ambient neutral density. This is due to the fact that the dominant collision frequencies are those between the electrons and the contactor ions and between the electrons and the contactor neutrals. His study found that at contactor ion emission currents at or below 1.0A, ionization did nothing to increase the gain of the system. Blandino's conclusion based upon those results was that random thermal current collection was the primary factor determining the gain of the contacting system. Blandino [10] offers further discussion on the collisionality stopping condition versus the E/vB stopping condition.

Both the Dobrowolny and Iess model and the Hastings, et. al. model require a substantial amount of turbulence to attain the required collisionality for the electrons within the core region. The gains calculated with the Dobrowolny and Iess quasineutral model are much higher than those calculated with the Hastings, et. al., quasineutral model. While the Dobrowolny and Iess model neglects entirely the magnetic field effect, Hastings, et. al. accomodates this

effect. In the Hastings and Gatsonis [38] two-dimensional quasineutral theory, this is accomplished by allowing the cloud to expand to r_{core} at which point the electrons become trapped on their gyroorbits. This effect is manifested in a "free expansion" of the cloud along the magnetic field lines, but also makes diffusion across the field lines extremely difficult,

$$\frac{\partial}{\partial l} \ll \frac{\partial}{\partial r_{\perp}}, \tag{2.86}$$

where l is measured along the field lines and $r_{\perp}$ across the field lines. This equation reflects the fact that perpendicular plasma variations are much more rapid than parallel plasma fluctuations. Eq. 2.86 is valid only when the core is significantly diamagnetic. Such a plasma cloud takes on the cigar shape to be explored in Section 3.2. The plasma β parameter may be used as a measure for both of the quasineutral theories assumption that the core region is in fact highly diamagnetic. The magnetic shielding required by the two theories is valid only if $\beta > 1$.

There exists a notable difference in the Dobrowolny and Iess and the Hastings et. al. in expressions for $\nu^{*}_{acoustic}$. The Hastings expression for the anomalous collision frequency is taken from Papadopoulos [55]. This expression is more appropriate for the problem at hand since it is based upon transport equations for a turbulent stationary state, where stationary connotes a time averaged stability and not a temporal independence. Observations in the laboratory and spaceborne data sets indicate the existence of plasma instabilities in tandem with a stable current. This is significant for plasma contacting since it can lead to a more collisional plasma. It is critical to include turbulent scattering in the modelling since it plays a role in maintaining an efficient contacting process. The data presented in the following sections illustrates the points in this discussion on modelling.

The four core criteria presented at the outset of this chapter are actually not as disparate they appear. In fact, they could all be treated within one model. For the collisionless regime, the pressure balance stopping condition is manifested in the formation of a space-charge-limited sheath. Across that sheath, one can maintain a regular, self-consistent potential. The trick is to then preserve the regularity of the solution at the boundaries of that sheath and the

collisional quasineutral regions on either side. Clearly a return to ambient densities occurs just past the outer edge of such a sheath and the density matching condition may be satisfied. A theoretical model is needed that can accomodate the singularities encounterd during transitions from collisionless to collisional regimes while preserving the various considerations of r_{core}. The existing models adequately predict low current unignited plasma flow between a plasma contactor and the surrounding plasma for high pressure and high density conditions. But those conditions are typically found in laboratory situations and not in the LEO environment of interest for the application of electrodynamic tethers.

2.6 Discussion of Laboratory Data

In this section, the plasma contactor experimental setups and their resultant data sets are presented. This information is used to analyze a plasma contactor's capability to enhance current collection. The work presented is by members of Instituto di Fisica dello Spazio Interplanetario (IFSI), Frascati, Italy, by P. Wilbur and colleagues at CSU, by M.J. Patterson of NASA LeRC, and by R. Stenzel and J.-M. Urrutia of UCLA. The experimental parameters for a number of the cases chosen for direct comparison study are shown in Table 2.2, with the exception of Stenzel and Urrutia. Their work was not set up in a manner to specifically test plasma contactors, but to examine current collection processes, and so their experimental setup does not lend itself to the format of Table 2.2. The electron velocity is calculated according to Eq. 2.87. The data for the Frascati chamber is that of the tiny chamber in Table 2.2.

2.6.1 Instituto di Fisica dello Spazio Interplanetario Laboratory Data

Experiments have been carried out by Vannaroni, et al., [79] in both the Freiburg plasma chamber and the $0.5\,m^3$ Frascati vacuum chamber. The experiments pursued in the smaller Frascati chamber can be viewed as a characteriza-

Table 2.2: Experimental Cases

Exp.	Pressure	Gas		H.C.	Anode		$v_{e\|\|}$	$\Delta\Phi$		Ignited
Loc.	(torr)	H.C.	P.S.	Bias(V)	Bias(V)	Dia.(cm)	(m/s)	(V)	α	Flow
Frascati	2.4×10^{-3}	Xe	N/A	+18.5	+12.5	4.2	N/A	N/A	N/A	Yes
Freiburg	3.2×10^{-4}	Xe	Ar	0	+11.0	4.2	1.33×10^{6}	5	2	Yes
CSU	4.3×10^{-6}	Xe	Xe	+12.0-20.0	Bias Pt.	3.0	4.05×10^{6}	40	0.8-$\simeq$1.0	Yes
LeRC	2.3×10^{-6}	Xe	Ar	+50.0-250.0	Bias Pt.	24.0	3.75×10^{6}	42	$\simeq 0.9$	Plume

tion of the hollow cathode device later used in the Freiburg plasma facility. No plasma simulator was used at Frascati in the small chamber. The new, larger plasma chamber at Frascati has just recently come on line and data that has been taken thus far has yet to be released for study.

The dimensions of the Freiburg facility are $2.5\,m$ in diameter and $5.5\,m$ in length, with a Kaufman thruster used to simulate the ionospheric plasma. External Helmholtz coils were used to compensate for Earth's magnetic field as well as to generate field components within the chamber if desired. Only the data set for which the terrestrial magnetic field compensation occurred has been released to date. However, preliminary analysis [41] of the data indicates that the plasma parameters show a 10-20% variation when the plasma is magnetized with the Helmholtz coils. The Kaufman thruster is operated with Argon. The Ar^{+} was expelled from the thruster at an energy of $60\,eV$. The thruster plasma source and the hollow cathode assembly were separated by $370\,cm$.

There were two electrical connections available for the hollow cathode assembly,

1. To the system ammeter for characterization of the hollow cathode I-V curve
2. To a voltage source to polarize it with respect to the chamber wall

For the hollow cathode device, a cathode to anode/keeper discharge current is expected to result in a high density region of weakly ionized, highly collisional plasma freely expanding into the surrounding vacuum. Upon expansion to large

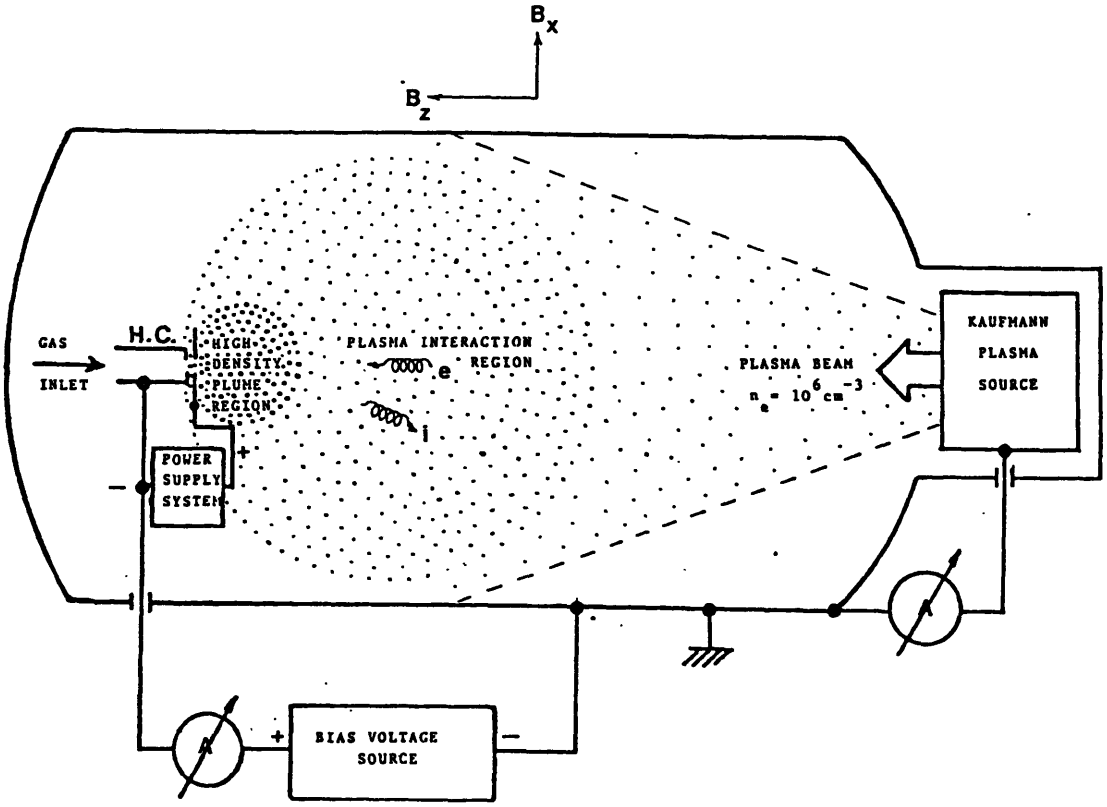

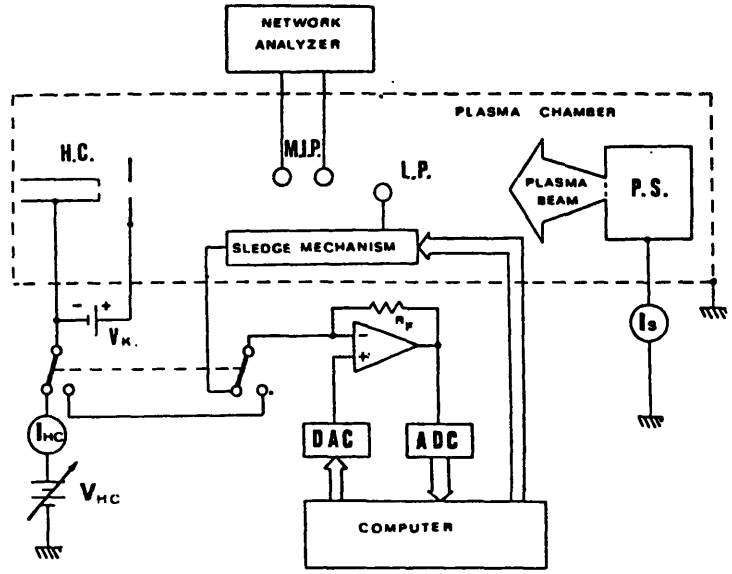

Figure 2.10: Freiburg Test Apparatus [79]

distances away from the contactor, the cloud is taken to be low density and collisionless. Experimentally, the Langmuir probe is used to obtain the plasma profile and it is assumed that the plasma potential in the plasma immediately surrounding the hollow cathode is equal to the keeper voltage, thereby normalizing the values of the plasma potential in order that plasma variation may be studied.

Fig. 2.11 shows the case where only the plasma simulator was operating and characterizes the plasma potential, electron and ion density, and electron temperature. The data are plotted, along with solid lines indicating the theoretical conical expansion mentioned above. It is believed that saturation of the Langmuir probe used for these measurements resulted in the electron deviation from theory in the region of proximity to the plasma source.

Fig. 2.12 shows similar plasma parameter maps for the case of the hollow cathode operating biased with respect to the plasma chamber wall at $V_{HC} = 0\,V$ and with the plasma simulator off. The Langmuir probe obtained the plasma profile and it is assumed that the plasma potential in the plasma immediately surrounding the hollow cathode was equal to the keeper voltage, thereby normalizing the values of the plasma potential in order that plasma variation may be studied.

The third operating condition studied was with the hollow cathode and the plasma simulator functioning simultaneously. With both plasma sources operating, the chamber pressure was $3.2 \times 10^{-4}\,Torr$. For this portion of the experiment, the plasma simulator was electrically connected to the chamber wall and the hollow cathode was then polarized with respect to the plasma simulator. With the hollow cathode assembly at the same potential as the plasma simulator and the anode of the hollow cathode at $+11\,V$, an increase in the temperature of the electron population was detected along with an appreciable $d\phi/dr$ located between $15\,cm$ and $30\,cm$ from the hollow cathode plasma source. This interaction study was hindered by the fact that the resolution of the Langmuir probe was not fine enough to fully examine the potential profile and that the profile did not span the entire distance along the chamber axis between the hollow cathode and the plasma simulator.

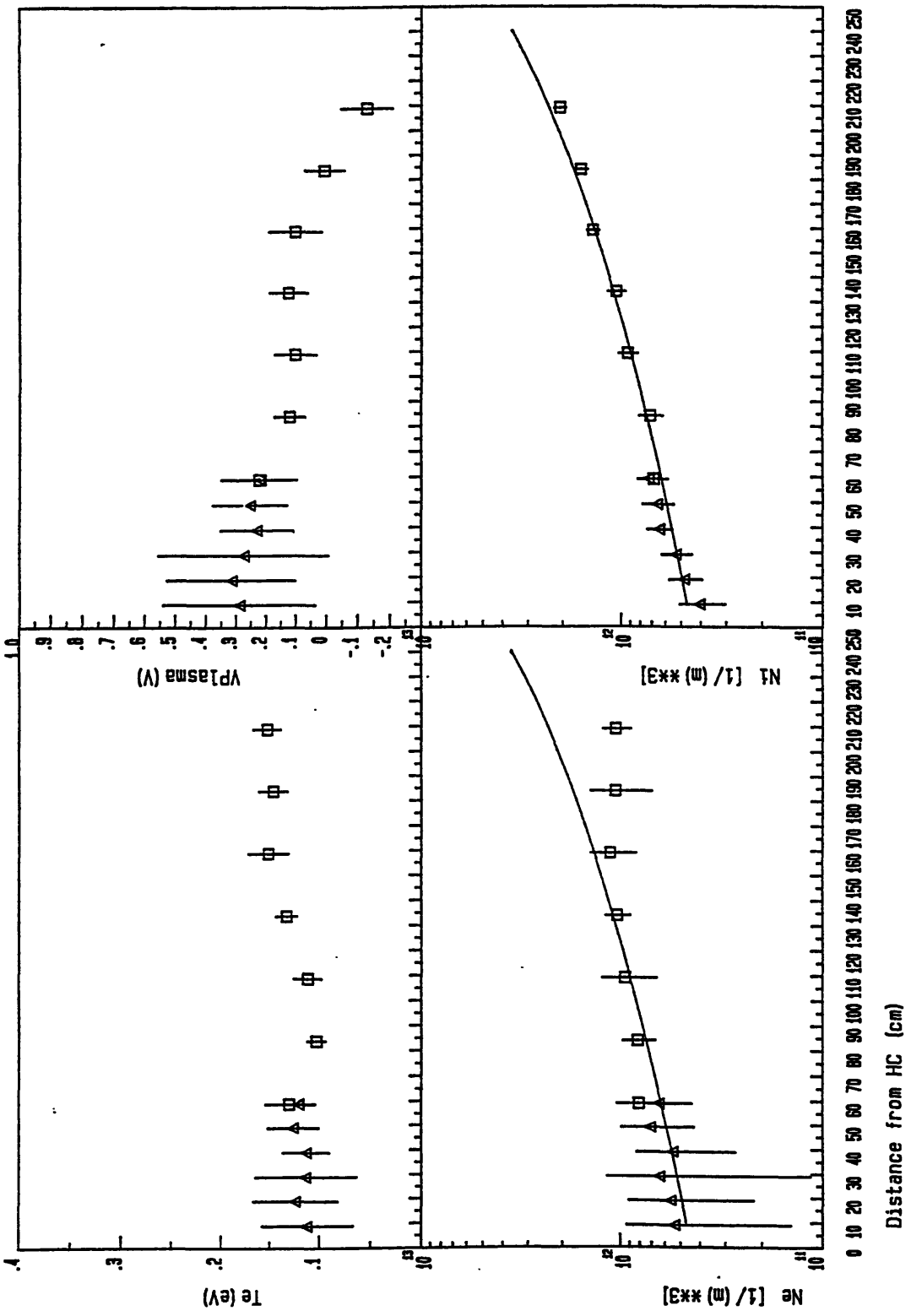

Figure 2.11: Kaufman Thruster Plasma Parameter Maps [79]

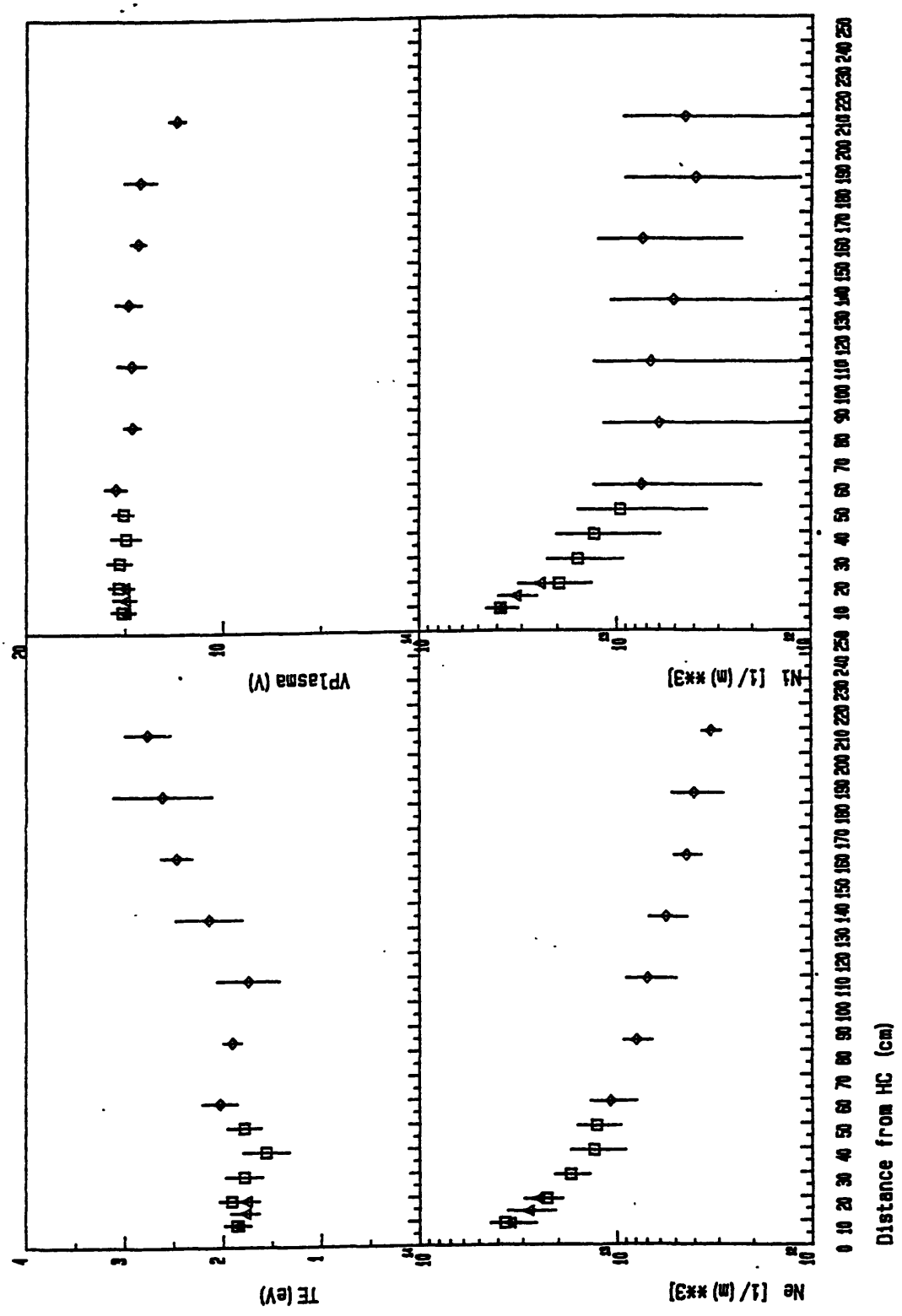

Figure 2.12: Hollow Cathode Plasma Parameter Maps [79]

2.6.2 Colorado State University/NASA Lewis Research Center Laboratory Data

The plasma contactor laboratory testing conducted under Wilbur's direction has been accomplished with the apparatus depicted in Fig. 2.13 . This test setup includes two separate hollow cathode devices, one simulating the ambient space plasma and the other coupling to this "ambient" plasma as a spaceborne hollow cathode would. An anode design was chosen for the contactor hollow cathode such that the size of the contactor anode could be altered. This design was chosen for the contactor so that the effect of altering the contactor anode on the electron collection process could be examined. The capability existed to bias the contactor with respect to the "ambient" plasma, the simulator, and the chamber wall. When the contactor is operating in electron collection mode, the case of interest within the context of this paper, the two switches A and B in Fig. 2.13 are placed in Position 1. In this configuration, the hollow contactor was biased with respect to the simulator, which was electrically connected to the chamber wall.

Wilbur has done extensive work operating the plasma contactor at one set colleciton current, flowrate, and discharge power level so that numerical models could be compared to experimental data. For the $12\,cm$ anode diameter case with a bias voltage of $+18.0\,V$ and effective flow rate of Xenon at $230\,mA-eq$, the electron current collected through the double sheath was $750\,mA$ while the ion emission current was calculated to be approximately $1\,mA$. This case indicated the presence of a high gain, thin double layer was present at the collector. The data collected indicate that a potential profile such as that depicted in Figure 2.14 existed under these plasma conditions. Figure 2.15 gives a magnified graphical view of the sheath structure at the collector.

When the effects of anode size were investigated, a 3 cm anode was chosen to measure the contactor's performance relative to the 12 cm anode. The major differences found between the two cases were the higher voltage drops, lower overall system gain, a spreading of the double layer, and a reduction in the core size of the contactor plasma. Consequently, it appears that the inner radius of

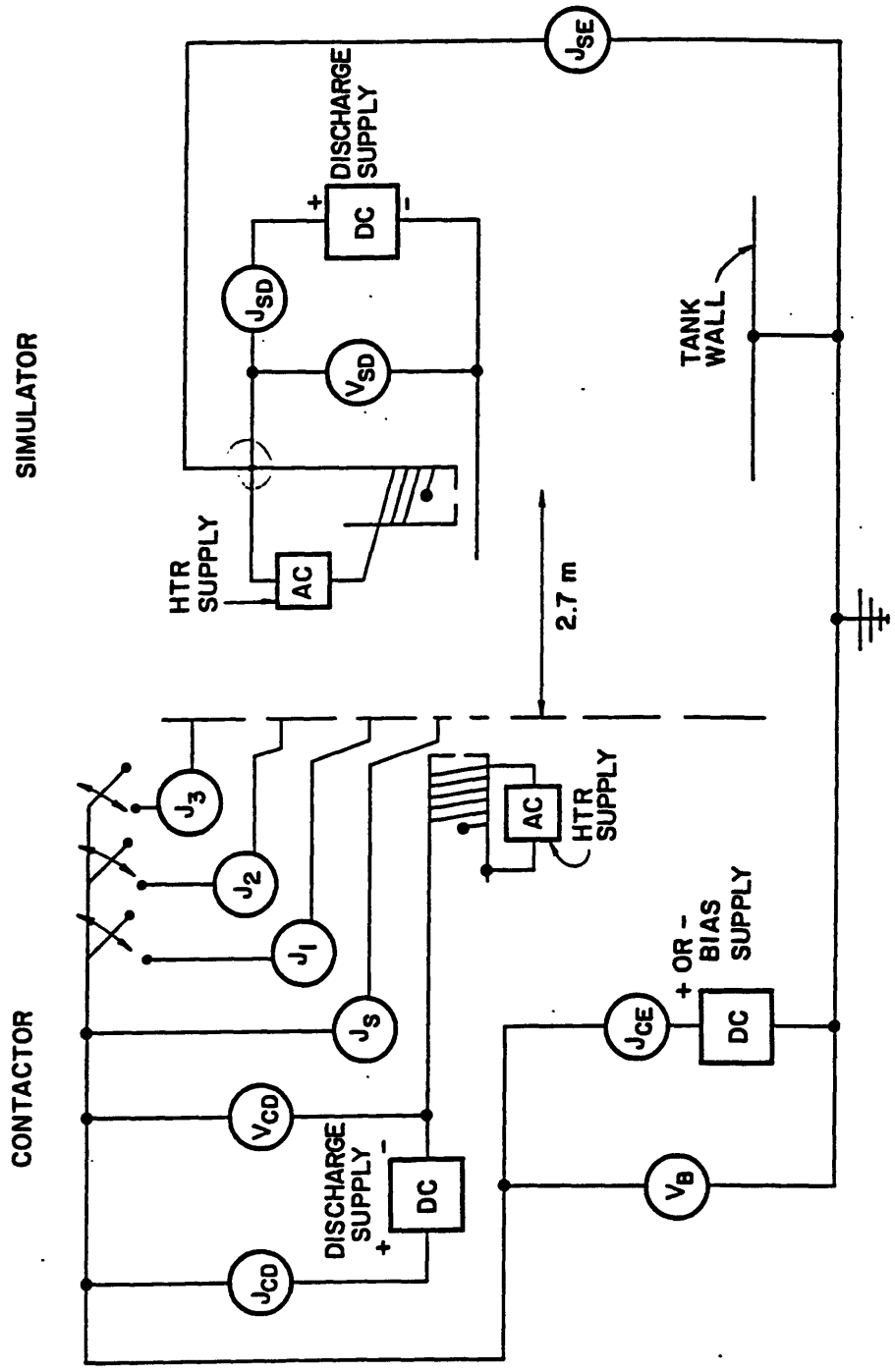

Figure 2.13: CSU Test Apparatus Schematic [85]

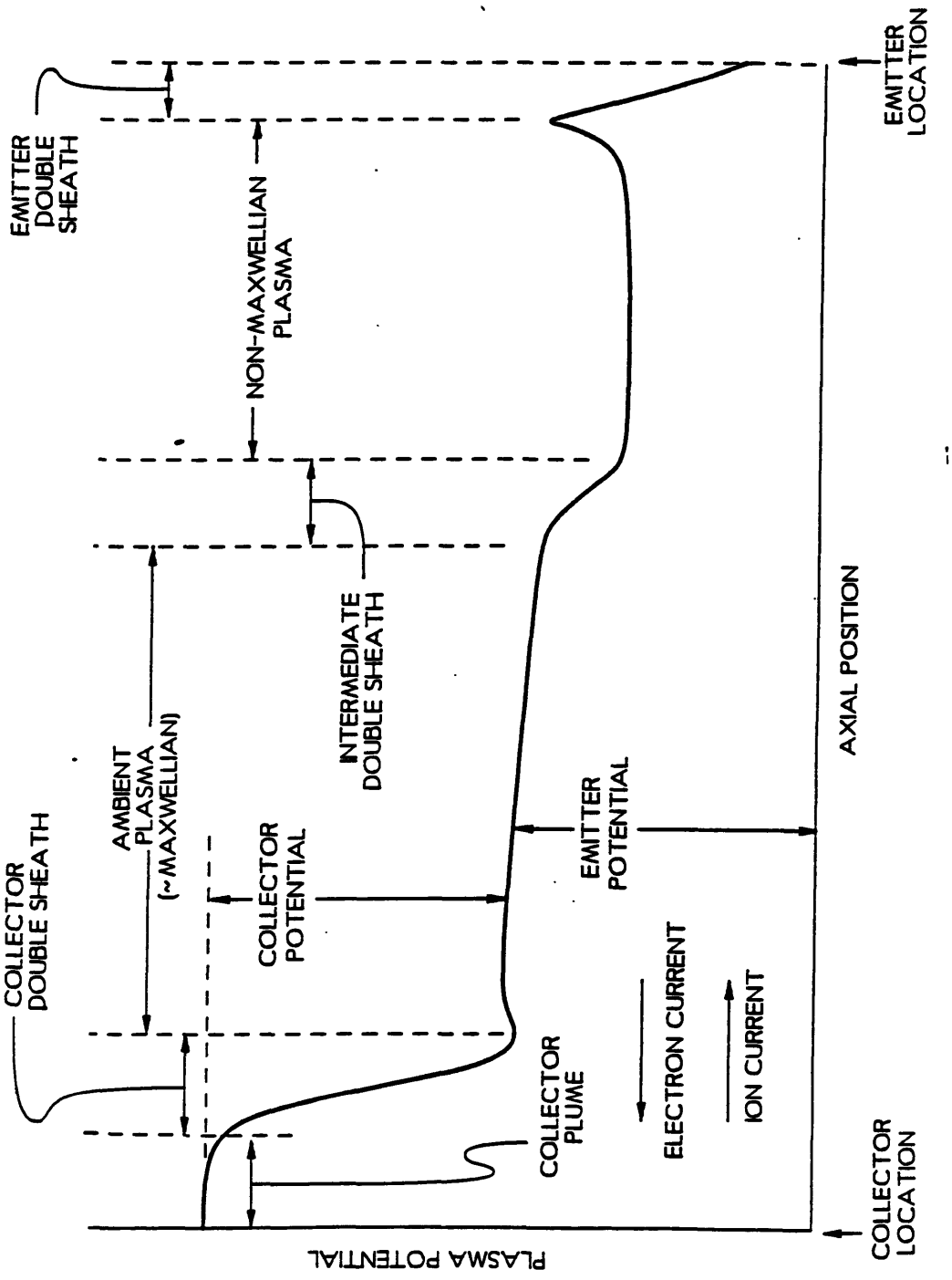

Figure 2.14: Plasma Potential Profile along the length of the Test Chamber [89]

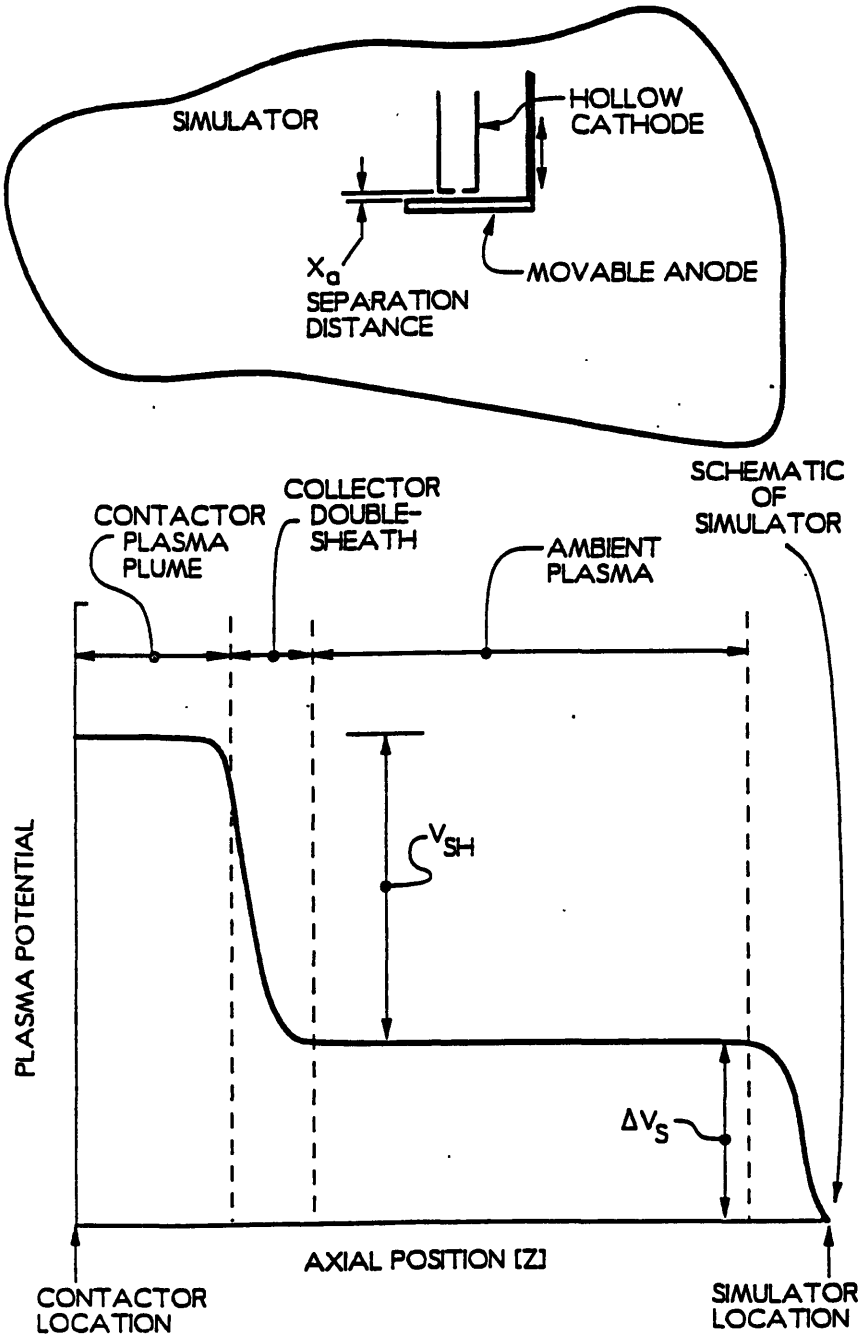

Figure 2.15: Plasma Potential Profile along the length of the Test Chamber at the Collector [89]

the double layer is "anchored" to the anode radius unless there is significant pressure due to ionization to displace it farther from the anode. When such displacement occurs, the double layer spherical symmetry breaks down.

Patterson [62] has conducted a series of plasma contactor studies at NASA LeRC using the apparatus depicted in Figure 2.16. Chamber tests of the CSU contactor and simulator have also been performed in conjunction with Patterson at NASA LeRC [85]. Patterson [61] has tested principally four different contactor geometries, a 30 cm ring cusp contactor with a repressor grid, 30 cm ring cusp contactor with a baffle, a 12/24 cm circular anode and a 12 cm closed drift discharge contactor. While the electrical configurations of the hollow cathode and the plasma simulator in both the CSU and NASA LeRC test facilities remain the same, the pressure conditions of the two facilities do not, as Table 2.2 shows.

Patterson's data set for the 24 cm anode presents a very clear progression from spherical double-sheath formation at low current to ionization at high current and breakdown of the spherical double layer symmetry. The case listed in Table 2.2 is that of double sheath formation at low current. The plasma potential contours for this case are indicated in Figure 2.17. Viewing the potential contours along the axial direction, it appears that a double layer of $r_r \simeq 0.8$ developed at 50 cm. Further experiments performed by Patterson at LeRC demonstrated the double sheath broke down at emitted ion currents greater than 1 A. This indicated that the wider the double sheath became, the greater its asymmetry and likelihood that the plasma flow would ignite, causing volume ionization. This is shown in Figure 2.18 in which the experimentally measured double layer radius ratios are plotted against those predicted by Wei and Wilbur [83]. A number of different space plasma simulators, SPS units numbered 1-4, were used by Patterson in this investigation.

Facility effects on the contactor performance could be evaluated using the combined data sets of Wilbur and Patterson [61,85]. Figure 2.19 compares the current-voltage characteristics obtained using the CSU 12 cm anode contactor in the CSU and NASA LeRC test facilities. In the NASA LeRC chamber, the separation distance between the contactor and the ambient plasma simulator

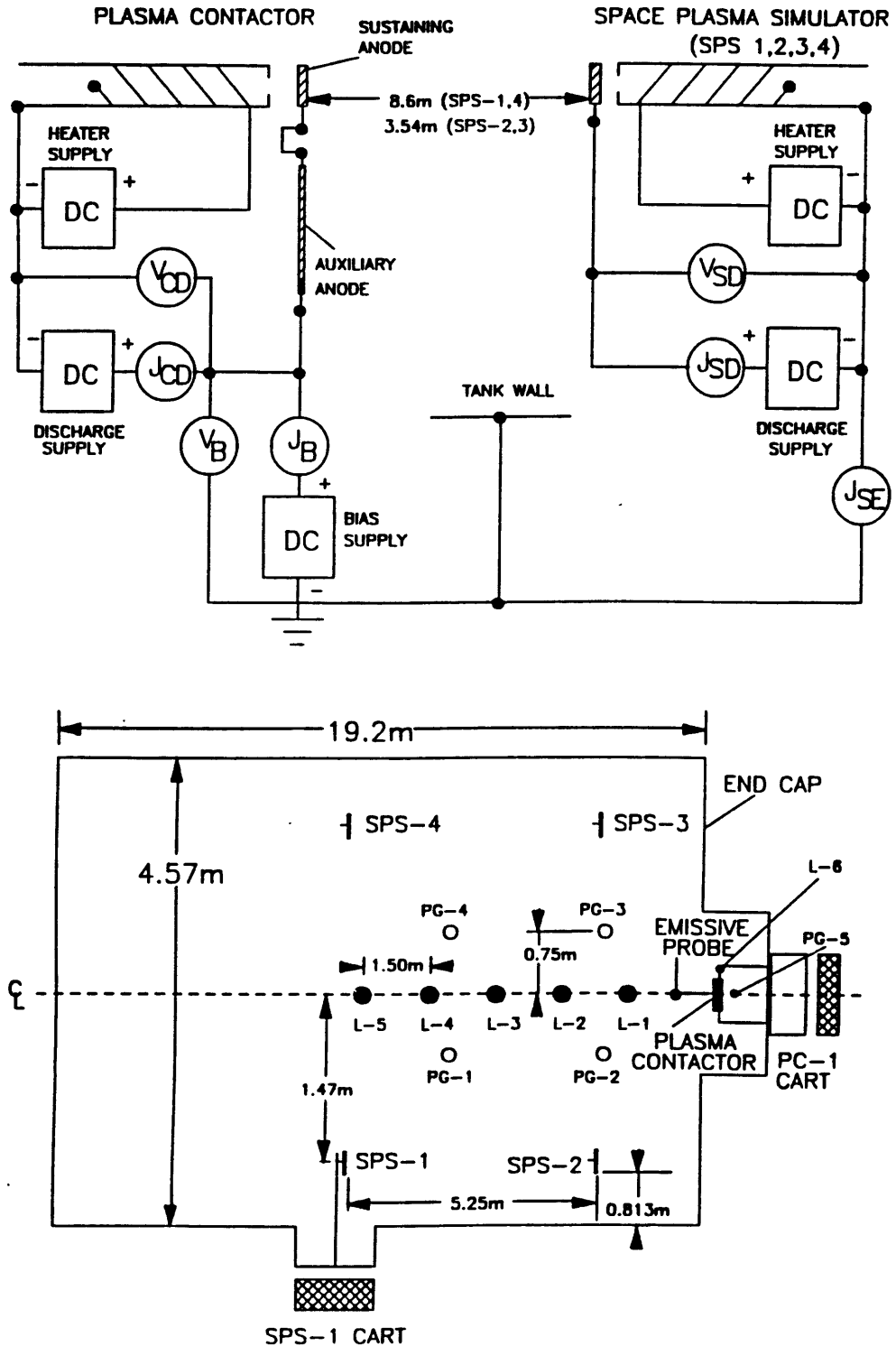

Figure 2.16: NASA LeRC Test Apparatus Schematic [61]

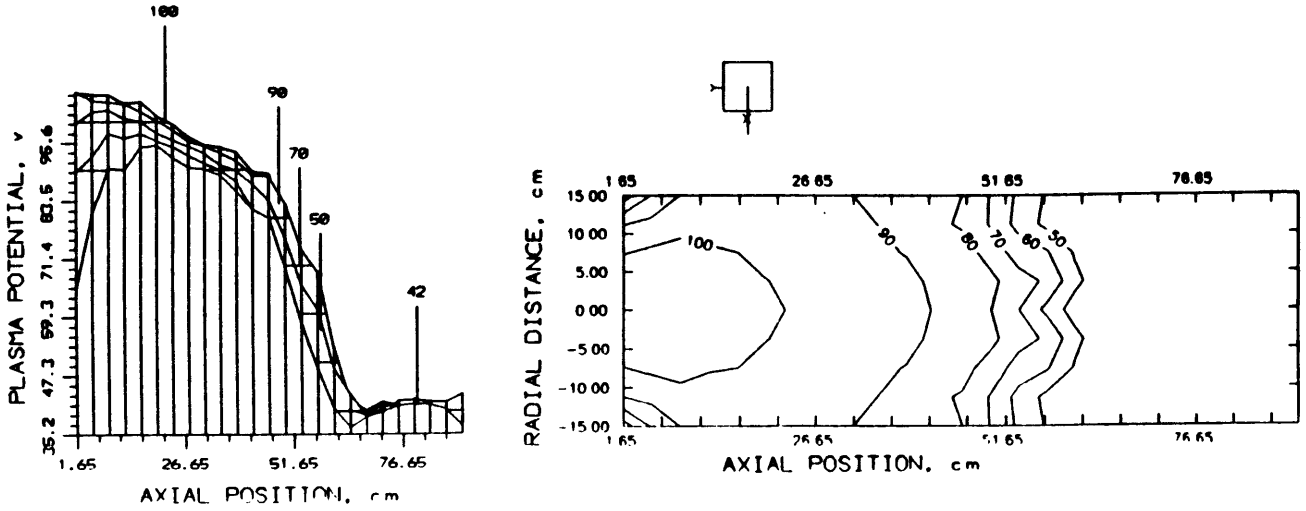

Figure 2.17: NASA LeRC 24 cm anode plasma contactor, with collected electron current = 0.23 A [61]

was $8.6\,m$, three times greater than the separation distance available in the CSU chamber. Given the larger tank size, the background pressure was lower for comparable gas flow rates of both the contactor and the simulator. The performance of the contactor in the CSU facility is very close to desired levels since the contactor potential maintained is nearly constant over the range of currents measured. This performance was inferior in the NASA LeRC facility where higher contactor potentials were required to attain similar collected electron current levels.

2.6.3 The Stenzel and Urrutia (UCLA) Laboratory Data

Stenzel and Urrutia have focussed on the analysis of various current configurations in order to determine the feasibility of the tether circuit envisioned for spaceflight. They studied current propagation and magnetic field effects upon a magnetoplasma in the laboratory in an effort to come to an understanding of the

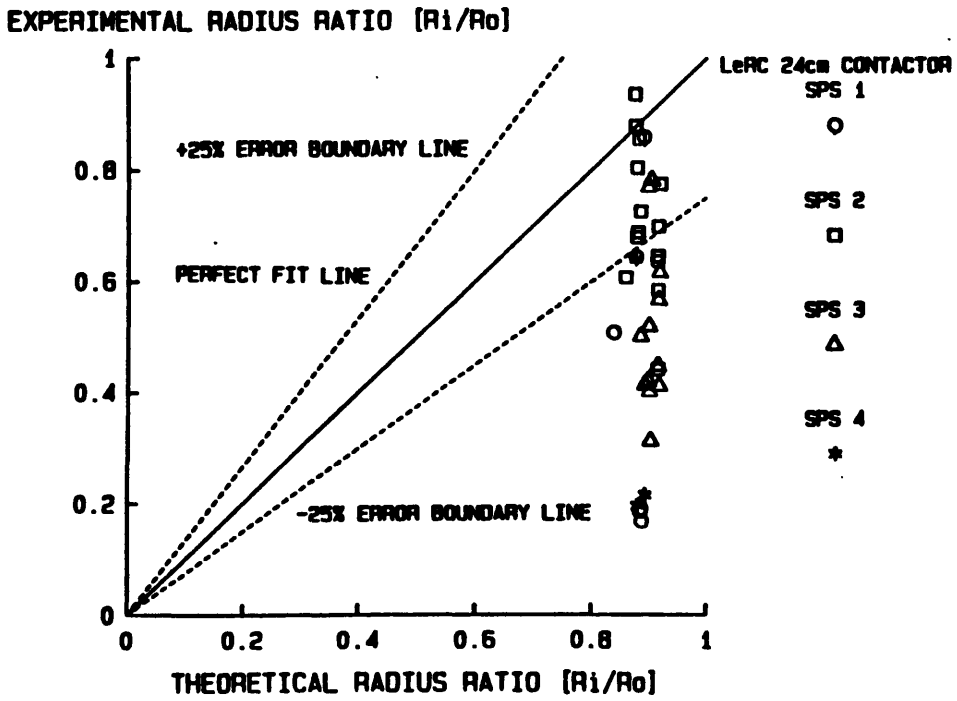

Figure 2.18: NASA LeRC 24 cm anode plasma contactor - Experimental Radius Ratio vs. Theoretical Radius Ratio [61]

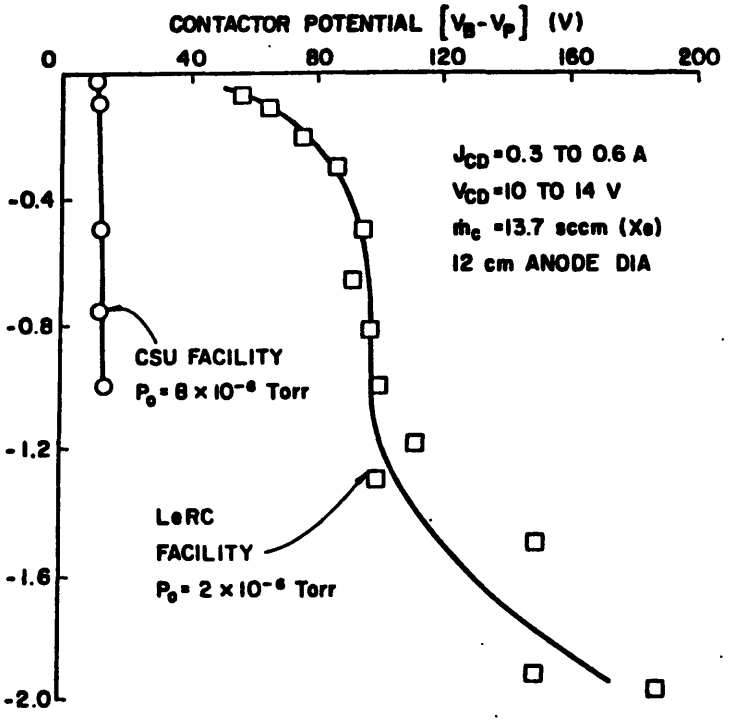

Figure 2.19: CSU 12 cm anode plasma contactor IV curves in both the CSU and NASA LeRC test chambers [61,85]

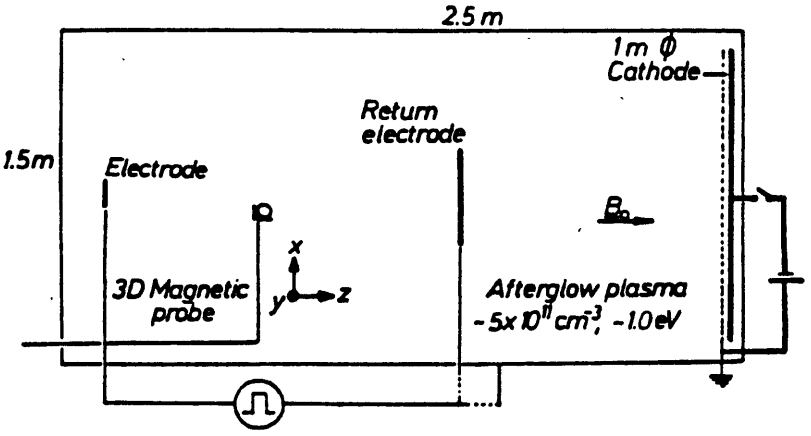

Figure 2.20: Schematic of UCLA Experimental Apparatus [78]

circuit of an electrodynamic tether in LEO. Their experimental setup, depicted in Figure 2.20 [78], had the chamber walls, the anode, and the electrodes themselves acting as reference electrodes. A pulsed Argon plasma was produced so that the experiments could be performed in its afterglow. An external solenoid was used to generate a dc magnetic field. Transmission lines used were insulated thin wires placed either perpendicular or parallel to the chamber's z-axis. The time-varying magnetic field induced by the current switching was measured in three dimensions [78].

Stenzel's and Urrutia's experimental results have led them to the conclusion that the current transport is set not by the current-carrying particles speed but by the electromagnetic waves in the plasma and the time derivative of the currents. The electrons dominate the wave mode selection due to their higher mobility. Given the plasma parameters in the experiment, the whistler mode was selected by the plasma [78]. The domination of the current transport by the electrons ends when the ions achieve inertial steady-state, a condition that does not seem likely to occur in the LEO regime. Conductivity along the magnetic field lines is greater than across it so that field-aligned-currents are not the obvious result. The direction of current flow was found to be dependent upon the electric fields present which were directly affected by the anode geometry. In the event of non-linearity, Urrutia and Stenzel concluded that these self-consistent electric fields could dominate the conductive anisotropy, therefore

opening the way for anomalous cross field transport to occur.

2.6.4 Agreement of Laboratory Data with Theoretical Models

In the UCLA chamber experiments, the electron Larmor radius was small with respect to the plasma potential. Consequently, diffusion of electrons across the magnetic field due to anomalous transport played a significant role in the plasma cloud dynamics. Urrutia and Stenzel measured an electron collection current at their anode a few factors larger than the electron saturation current that passed through the flux tube of magnetic field lines intersecting the anode. This effect remained pronounced even when the effective collision frequency was less than the electron cyclotron frequency. Urrutia and Stenzel attribute this anomalous cross field transport to ion acoustic instabilites arising as a result of $\vec{E} \times \vec{B}$ electron drift relative to the unmagnetized ions. Such a situation would produce azimuthal wave electric fields that in turn excit radial $\vec{E} \times \vec{B}$ drifts.

Another significant phenomenon recorded by Urrutia and Stenzel is that the enhanced electron current was not continuous in time but occurred in periodic bursts. This temporal oscillation in current collection was the result of the periodic nature of the plasma instabilities present during the experiment. It is not clear whether these instabilities are the result of initial conditions relevant to the nature of the experimental setup or are an artifact of this type of anomalous cross field diffusion.

Note that the UCLA data has a high β condition so that the electric field measured is completely out of character for any collisionless model. The current versus time profiles under different operating conditions show the following characteristics at different operating pressures,

At 10^{-3} Torr,

1. Growth of anomalously large currents

2. Large currents present due to ionization
3. Current disruption, due to neutral gas depletion

At 10^{-4} Torr,
1. Current driven instabilities
2. Current disruption due to ion expulsion by the anomalous electric fields
3. Velocity space is slow to replenish with ions through diffusion
4. Repetition in time of current peaks at the roughly the same amplitude

Stenzel and Urrutia measured a time-varying enhancement of the system gain, leading to the conclusion that there will exist modes where the plasma contacting process is an oscillatory one.

The spherically symmetric space-charge-limited collisionless double layer model outlined in Section 2.2.2 agrees well with the vacuum chamber experiments of Wilbur [87] at CSU, in those conditions where that type of double layer was seen. In these experiments, one of the plasma contactor anodes used had a radius $r_{anode} = 6\,cm$. The radius of the virtual anode, however, where most of the ionization occurred, was $r_{source} \approx 2\,cm$. ϕ_0 varied from 0 to $70\,V$ and the collected electron current varied from 0 to $1\,A$. At higher operating currents, the effective collision frequency, due to streaming instabilities, was too high for collisionless double layer theory to be valid.

Neutral gas, Xenon, was introduced at the center of the anode at a rate varying from 1.8 to $13.7\,sccm$. This corresponded to a neutral density ranging from 3×10^{11} to $10^{12}\,cm^{-3}$, concentrated within r_{source} of the origin. For ϕ_0 above some critical value, dependent upon the neutral density, ambient electrons accelerated in the double layer had enough energy to ionize the gas. With the occurence of such ionization, the contactor cloud underwent a transition to an "ignited mode". This ionization was then the major source of emitted ion current. The electron temperature and density and the plasma potential were measured as functions of position. The ambient ion temperature was much lower than the electron temperatures.

In a typical case, with $\phi_0 = 37\,V$, the bulk of the potential drop, $25\,V$, occurred in a double layer that was roughly spherical and was located between $r_i = 8\,cm$ and $r_o = 11\,cm$ as measured by Wilbur's chamber apparatus. The rest of the potential drop occurred between the anode and r_i. The potential profile was virtually flat outside r_o. The ambient electron temperature was $5.5\,eV$, and the ambient electron density was $3 \times 10^7\,cm^{-3}$. These electrons had a Larmor radius of about $15\,cm$ in the earth's magnetic field, which is greater than $r_o - r_i$. Once they crossed the double layer, they had a Larmor radius of about $50\,cm$, which is greater than $r_o^2/2r_{anode}$. Consequently, the electrons can reach the anode according to the criterion established by Parker and Murphy [57] (see Section 3.1.3). The assumption in the two component model of unmagnetized electrons appears then to be valid.

The assumption of collisionless electrons can also be satisfied if the Parks and Katz estimate [59] of an effective collision frequency $\nu_e \approx 0.1\omega_{pe}$ is used. At r_o one finds $\nu_e = 3 \times 10^7\,s^{-1}$, and the electron mean free path is about $3\,cm$, comparable to the width of the double layer. While at r_i one finds $\nu_e = 2 \times 10^7\,s^{-1}$ and the mean free path of the accelerated ambient electrons is about $10\,cm$, comparable to r_i. Note that at densities a few times higher, the electron mean free path would be less than the double layer width, and a double layer could not exist since it is required that $r_{d.l} \gg \lambda_D$, as stated at the outset of Section 2.2.2. This is in agreement with observations at currents above $1\,A$, as discussed at the end of Section 2.6.2. There was also a $40\,eV$ ambient electron component the "primary" electrons, of density $3 \times 10^6\,cm^{-3}$. Such a component of electrons was not included in the two component model presented in Section 2.2.2, but their effect can be included by using an effective $T_{ea} \approx 9\,eV$, which would give the same electron saturation current as that obtained from the $5.5\,eV$ and $40\,eV$ components.

The collected electron current, $370\,mA$, was in good agreement with the electron saturation current integrated over the area of the double layer $2\pi r_o^2$. The integration is not taken over $4\pi r_o^2$ since the collection area was actually a half sphere. The electrons in the contactor cloud had a temperature $T_{ec} = 2\,eV$ and a density ranging from $8 \times 10^8\,cm^{-3}$ at r_{source} to $2 \times 10^7\,cm^{-3}$ at r_i. The

ratio of $n_e(r_{source})/n_e(r_i)$ is close to the value given by Eq. 2.25. The emitted ion current I_i would then be $2\pi r_{source}^2 e n_e(r_{source})(T_{ec}/m_i)^{1/2} = 0.4\,mA$, fairly close to the ion current required by Eq. 2.39, $0.7\,mA$. The observed width of the double layer, $r_{d.l.} \approx 3\,cm$, is a few times greater than the width of $0.6\,cm$ predicted by Eq.(18), but it is likely that the measured width is smeared out by fluctuations in the instrumentation used to record the measurements as well as the time-varying changes in the double layer structure.

2.7 Limitations in Ground-Based Experiments

As mentioned in Section 2.6.4, there are conditions that result in chamber interference with measuring a plasma experiment's critical parameters. This section discusses those limitations and difficulties encountered in the laboratory.

Double layer formation is seen in the Wilbur and Patterson data sets at low levels of electron current collection. According to Patterson, at high current levels, *i.e.* $> 1.0\,A$, deviations from the spherical double-sheath theory [83] are seen in the data due to the development of sheath asymmetry and bulk ionization. Wilbur [85], however, found a clearly demarcated double layer region at $1.2\,A$ at a standoff distance from the hollow cathode between approximately 25 to $40\,cm$. This data was taken for the $12\,cm$ anode contactor, with the test conducted at NASA LeRC. Due to lack of resolution in the Frascati data set, the question remains as to whether hollow cathode/plasma simulator configurations besides that of CSU/LeRC yield the double layer result at low, or even high, electron current collection levels. Upcoming experiments in the new Frascati plasma facility will address such questions. It is interesting to note, however, that the $3\,cm$ anode used by Wilbur yields results indicating that the double sheath spreads may well correspond to a similar phenomenon in the Freiburg $3\,cm$ anode case.

The $24\,cm$ anode LeRC contactor and the $12\,cm$ CSU contactor tested separately in the LeRC facility demonstrate an order of magnitude difference in current collected, favoring the larger anode size. This type of observation has also

been noted at the CSU facility when the hollow cathode anode size was varied under the same plasma simulator operating conditions. Chamber wall effects and Langmuir probe saturation hindered the measurement of hollow cathode current collection in the Freiburg experiments; analysis of isolated cases of the hollow cathode biased with respect to the plasma source indicated that the current collected was an order of magnitude less than predicted by the Dobrowolny and Iess model [25,42]. The smaller anode size used with the Frascati contactor can be compared with the smaller size anode used by Wilbur and Williams [86].

The data indicates that there are five regions of plasma contactor operation occuring within the laboratory setting. The first region, with currents less than $100\,mA$ being collected, does not offer any particular structure in the plasma profile. In this case, apparently, the emitted ion density is less than the ambient density even at the anode, so any potential drop will occur in a sheath at the anode, rather than in a double layer, and the collected current will just be the ambient saturation current over the area of the anode. A transition region then exists for current levels just above $100\,mA$ in which a spherical double layer [83] appears to be present but the contactor plume is unignited, *i.e.* there is no diffuse glow. The third region, traversing the current range up to $1\,A$, has breakdown of the spherical double layer and multiple as well as cylindrical double layers appear; this region also is ignited flow, *i.e.* there is a diffuse glow. Just above $1\,A$, the ignited flow causes increased ionization. Presumably, streaming instabilities occur in this fourth region. The spherical double layer model is completely invalid in this region. Plume domination then occurs in the fifth region, where currents are well in excess of 10A. The term plume domination refers to the neutral gas plume emanating from the plasma contactor. The ionization of this neutral gas creates ions which then dominate the contactor plasma plume ions in the electron collection process.

A sizable measured radial electric field component does not offer enough information to justify the existence of a double layer. The density measurements between the plasma contactor and the ambient plasma simulator must be made more accurately to assist in the determination of the boundaries between plasma regions. There is a clear need for better spatial resolution in the probe measure-

ments made in the chamber experiments. It is hoped that such information will be forthcoming from future experiments.

With regard to the difficulties encountered when Langmuir probe saturation occurs, it is useful to review the work of Parrot, et. al. [60]. They developed a theory of cylindrical and spherical Langmuir probes for collisionless plasmas in which the ratio of the Debye length to probe radius, the Debye number, vanishes. Their modelling results indicated that, for cases where the electron and ion temperatures were equal in the presheath surrounding the probe and where quasineutrality was maintained, the potential and density distributions seemed to have infinite slope at the surface of the probe. As the probe potential was increased relative to the potential of the surrounding plasma, the current saturated asymptotically, at a value $\simeq 45\%$ greater than the ambient plasma value. Such an occurrence would have a rather dramatic effect on data collection. Results within the contactor core cloud would be affected when $T_{ea} \simeq T_{ic}$ and the probe potential was greater than the potential of the plasma within the core cloud. This situation was seen by Williams and Wilbur [86] in results obtained as they moved their Langmuir probe closer to the anode surface and observed that it saturated in the high density core region. Measurements in close proximity to the anode are therefore likely to be compromised due to probe saturation. The probe potential must be then set carefully to avoid this saturation problem.

There have been interactions of the magnetic field with the plasma that induce significanct effects on the outcome of experiments, notably Urrutia and Stenzel and the Frascati group. These studies are critical in assessing which results model the space environment and which results are purely a function of chamber effects. One such chamber effect is the possibility of preferential diffusion of the electron population in the chamber, indicating magnetic field effects. Better dynamic range of the plasma probes in all three dimensions in the chamber would answer this and other such questions.

In assessing the relevance of the UCLA data set to LEO conditions, it is not clear whether behavior similar to that described in Section 2.6.4 would occur in the regime of free electron flow along the magnetic field and collisional flow across the magnetic field. Certain conditions, such as those in the UCLA experiments,

could produce ion acoustic instabilities but it is not known at this time whether the periodic nature of the instabilities inherent to the contacting system in space would be akin to those seen in the chamber experiments. It would be useful to quantify the self-consistent electric fields' effects on anomalous cross-field-transport. Such data could then be used to verify the need for anomalous resistivity as required by both Dobrowolony and Iess and Hastings.

2.7.1 The Double Layer Correlation Question

Since the chamber experiments are intended to achieve a simulation of the ionospheric plasma conditions, it is fair to compare the plasma generated to the ambient ionospheric plasma to determine if the same plasma mechanisms are at work. Assuming that the plasma simulators are producing "ionospheric" electrons and that the plasma contactors attract electrons while not expelling any into the interaction region, the electron velocity may be taken as:

$$v_{e\|} = -\sqrt{2}\left[\frac{e\Phi}{m_e} - \frac{T_e}{m_e}\ln\left(\frac{n_e}{n_{ambient}(\infty)}\right)\right]^{1/2} \tag{2.87}$$

Double layers may very often produce noise, *i.e.* rapid and irregular variations within a broad band of frequencies [1]. Noise may well cause greater scattering of the electrons in the double layer than do collisions. Due to the double layer, there is a broadening of the electron energy spectrum and plasma expansion occurs perpendicular to the magnetic field. One of the drawbacks of the prevailing models is their inability to account for such noise. Additionally, the experiments performed to date have not been equipped to detect such noise and use the measurement as a means of identifying a double layer.

When two very different plasmas meet at a juncture in space, some process must set up in which the potential and density differences are handled. In the case of plasma contactor emission into the ambient space environment, such a process is required. This type of process must also be considered when assessing the formation of naturally occuring double layers in the auroral regions of the ionosphere. It would therefore be useful in the course of this work to examine

such naturally occurring double layers for insight into the possible formation of double layers with plasma contactors in space.

The literature concerning the natural formation of double layers in space indicates that the magnetosphere will provide the significant parallel electron velocity, $v_{e\|}$, required for one of the double layer triggering mechanisms along the earth's auroral field lines [51]. These double layers form as a current is driven through a plasma that is greater than the current carrying ability of the charge carriers in the plasma. If an experimental situation in space is such that the divergence of the electric field is not equal to zero, $\vec{\nabla} \cdot \vec{E} \neq 0$, ionospheric conductivity is high enough, and the parallel electron current, $j_{e\|}$, exceeds that which can be carried along the field lines, significant parallel electron velocity will result and conditions for a double layer are set. The expulsion of plasma from a spaceborne hollow cathode could set up a double layer, then, if it met the condition that a region of divergent electric field was generated within the expelled plasma or along the field lines attached to this conducting plasma.

The Role of Supersonic Ambient Electrons in Sheath Formation

The double layer theory developed in Section 2.2.2 assumed that $T_{ea} \gg T_{ia}$, an approximation allowing the definition of a sharp boundary r_o for the double layer and the neglect of the ambient ion density within the double layer. These assumptions are satisfied in ground-based vacuum chamber experiments, but not in the equatorial LEO regime, where $T_{ea} \approx T_{ia}$. The question arises as to whether a double layer equilibrium potential $\phi(r)$, can join smoothly onto a quasineutral potential at $r > r_o$ in this case. For that matter, it has not been properly demonstrated that such an equilibrium is possible even when $T_{ea} \gg T_{ia}$, since there is no consideration of the very outer edge of the double layer.

That outer edge consideration is important where the ambient ion density is comparable to the ambient electron density, at the transition from the interior of the double layer, where the ambient ion density is negligible, to the quasineutral region. It turns out that a double layer equilibrium exists for any T_{ea}/T_{ia}. This can be shown explicitly for $T_{ea} \gg T_{ia}$ and for $T_{ea} \ll T_{ia}$; it has already

been shown by Alpert, Gurevich and Pitaevskii [2] for the more difficult case of $T_{ea} = T_{ia}$ [29].

In order to have a potential $\phi(r)$ asymtotically approaching the quasineutral solution at large r, it is necessary to have

$$\frac{d}{d\phi}(n_e - n_i) > 0. \tag{2.88}$$

In other words, the electrons must be supersonic as they approach the double layer from the outer, *i.e.* low potential, side. A similar condition exists with an opposite sign convention for the existence at a wall of a Debye sheath that joins smoothly onto a quasineutral plasma with a potential that is positive with respect to the wall. In that case, the requirement is that the ions be supersonic as they approach the sheath. This case applies to the double layer on the inner, *i.e.* high potential, side.

The question of why the ions are always supersonic as they enter the sheath was considered by Tonks and Langmuir [75], and later by Bohm [14]. Bohm showed that an electric field, the "Bohm presheath", must exist wherever there is a plasma source in a quasineutral region. He also showed that this presheath always accelerates ions to supersonic velocities before they reach the sheath. On the outer side of the double layer there is no plasma source, but there is a quasineutral presheath, *viz.* the potential rise of order T_{ia} associated with the empty region of electron velocity space due to the fact that electrons are not emitted from the double layer. This presheath plays the same role in accelerating electrons that the Bohm presheath plays in accelerating ions. When $T_{ea} \gg T_{ia}$, this potential is given by Eqs. 2.28 and 2.29. At r_o, the potential is $T_{ia} \ln 2$. In the vicinity of r_o, *i.e.* for $\phi(r) \ll T_{ea}$, the ambient electron density, from Eq. 2.32, is,

$$n_e(r) \approx \frac{n_\infty}{2}\left(1 - \frac{2}{\sqrt{\pi}}\sqrt{\frac{\phi}{T_{ea}}}\right) \tag{2.89}$$

and $dn_e/d\phi$, evaluated at $\phi = T_{ia} \ln 2$, is $-(4\pi \ln 2)^{-1/2} n_\infty (T_{ia} T_{ea})^{-1/2}$. The ambient ion density is simply

$$n_i(r) = n_\infty e^{(-\phi/T_{ia})}, \tag{2.90}$$

so that $dn_i/d\phi$, evaluated at $\phi = T_{ia}\ln 2$, is $-(n_\infty/2)T_{ia}^{-1}$. Then Eq. 2.88 is always satisfied if $T_{ea} \gg T_{ia}$. Note that this would not be true if there were no presheath outside the double layer, since that case results in a singularity where $dn_e/d\phi$ blows up for $\phi = 0$.

When $T_{ia} \gg T_{ea}$, the ambient electron density is greatly affected by the presheath. Therefore, to find $\phi(r_o)$ one must set $n_e(r)$ from Eq. 2.32 equal to $n_i(r)$ from Eq. 2.90, in the limit that $\phi \gg T_{ea}$. In this limit, Eq. 2.32 becomes

$$n_e(r) \approx \frac{n_\infty}{2\sqrt{\pi}}\left(\frac{T_{ea}}{\phi}\right)^{1/2}. \tag{2.91}$$

One then finds $\phi(r_o) \approx \frac{1}{2}T_{ia}\ln(T_{ia}/T_{ea})$, yielding a potential greater than T_{ia} by a logarithmic factor. It is obvious in this case that the electrons are supersonic and Eq. 2.88 is satisfied. Since Eq. 2.88 is satisfied for either $T_{ia} \gg T_{ea}$ or $T_{ia} \ll T_{ea}$, and since it is known from Alpert, Gurevich and Pitaevskii [2] that it is also satisfied for $T_{ia} = T_{ea}$, it appears very likely that it is satisfied for all T_{ea}/T_{ia}, although a simple proof of this has not been found. It is worth noting that Eq. 2.88, and the analogous condition for the inner side of the double layer, are only satisfied because of processes going on some distance away from the double layer. Consequently, misleading results could be obtained from computer simulations of double layers that consider only near-field effects, and do not properly treat the plasma coming into the double layer [29]. It should be noted, when treating this problem with a computer simulation, that the use of a relatively small number of particles per Debye length within the simulation can cause artificially high levels of thermal fluctuations to be manifested [18].

2.7.2 Correlation of Laboratory Results to Limited Space-borne Experimental Data Sets

The Space Electric Rocket Test II, SERT II, was a sounding rocket experiment carried out at 1000 km. It was demonstrated on that flight that an ion could be charge and current neutralized through the use of a plasma contactor. The Applied Technology Satellite 6, ATS-6, carried plasma contactors to study

active control of spacecraft potential, but its ion engine tests also provided a great deal of information on potential control through plasma emission. ATS-6 flew in a geosynchronous orbit but the results obtained have applicability within the scope of this present work. Both of these shots provided valuable information on charge control techniques [54,84].

With ATS-6, it was found that both the ion engines and ion neutralizers could effectively discharge large negative potentials over the full range of ambient plasma parameters. It was demonstrated that plasma emission could control spacecraft potential and did not generate the differential charging that results when an electron beam is used for charge control. It was also shown that the ion sources on both SERT II and ATS-6 were adequate for potential control even though not optimally designed for that role. The ATS-6 data set indicated that $1\,A$ of emitted ion current was sufficient to control the spacecraft [54]. Also notable in the ATS-6 data set was a lack of return ion flux, indicating that ion contamination of the spacecraft with a plasma contactor may be unlikely.

The Spacecraft Charging at High Altitude, SCATHA, satellite was also a geosynchronous satellite. When discussing the charging of SCATHA during active plasma emissions, it is useful to be aware of the composition of the exterior of the spacecraft. SCATHA was a cylinder $1.75\,m$ long and $1.75\,m$ in diameter. One end of this cylinder was a conductor tied to ground while the other end housed the rocket motor. The remainder of SCATHA's cylindrical surface area was covered with varying dielectric materials.

SCATHA carried the SC-4 charge ejection payload into orbit to make quantitative measurements related to charge ejection on satellites [22]. The plasma source it contained was used to discharge spacecraft ground potential. Ions could be ejected with both high, keV, and low, eV, energies. In discharging spacecraft ground with the plasma source, a number of characteristics were studied, minimum and optimum electron and ion currents required, the electron and ion current relation, and the physical processes that appeared to make this discharge mechanism effective. It was determined that spacecraft ground was most efficiently discharge using high energy ions. It also appeared that a fraction of the electrons ejected from the heated filament of the neutralizer (not the

hollow cathode also onboard) left the spacecraft, creating a sort of plasma-wire. This plasma-wire [22] apparently sustained low-impedance current flow from the spacecraft skin to the ambient plasma and helped keep SCATHA discharged.

Space Experiments with Particle Acceleration (SEPAC) was a mission carried out onboard the Spacelab 1 (STS-9) flight in 1983. Included in its experiments was the injection of a high density plasma plume with a high power electron beam. In an attempt to neutralize the Orbiter's potential, an MPD plasma plume was injected 0.5 seconds after the electron beam emission commenced in the execution of SEPAC Functional Objectives FO-7-1 and FO-7-2. (In STS parlance, FO's indicate a particular experiment performed within the entire mission sequence.) During these particular FO's, an electron beam of $5\,kV$ at $0.3\,A$ was pulsed with a 5 second pulsewidth. The MPD arcjet firing was held for $1\,msec$ starting 0.5 seconds after the commencement of each electron gun pulse. It was determined that the Orbiter's neutralization time ranged from $6-20\,msec$ with a recovery time to the original potential value sometimes lasting up to $100\,msec$. The return current electrons during these interactive experiments with the electron beam and the MPD arcject had spectra confined to energies below that of the beam energy, $5\,kV$. The spacecraft potential was shown to be clamped $\simeq 1\,V$. When this same electron beam was fired without the MPD arcjet injecting plasma into its vicinity, the electron energy spectrum peaked at 1.1 keV and significant fluxes of electrons above the beam energy were measured. The conclusion was therefore drawn that the plasma injection served to control the charging of the spacecraft [69]. However, no data appears available with which one could study the MPD plasma plume dynamics during these interactive operations. Such data are a particularly critical need for assessing the capacity of the plasma contactor to act as a vehicle neutralization device.

The CHARGE 2 rocket was launched in December of 1985 and recent analysis of the data gathered from its flight has pointed to electron collection enhancement as a direct result of the firing of neutral gas jets [30]. CHARGE 2 was a mother-daughter rocket experiment in which the mother and daughter payloads were connected by an electrically conductive tether. An electron beam was mounted on the mother payload. The mother and daughter payloads used

cold nitrogen gas in the thrusters of their attitude control systems. The vehicle potential was seen to be controlled by the injection of the nitrogen gas into the ambient plasma and subsequent ionization of this neutral gas.

Prior to the flight of the ECHO 7 [93] sounding rocket early in 1988, the University of Minnesota had launched six sounding rockets that carried high energy electron beam experiments to study the reflection of these electrons off of the conjugate hemisphere and to study the interaction of these electrons with the various plasma regions encountered [3,94,95]. All six of those flights yielded similar data in terms of spacecraft charging and neutralization, but the bulk of the published results center around the ECHO 3 and 6 flights. ECHO 7 was a collaborative venture between Winckler's University of Minnesota group, Arnoldy's University of New Hampshire group, the Space Physics Division of the Air Force Geophysics Laboratory, AFGL (now GL), and Hallinan's group at University of Alaska.

In both the ECHO 3 and 6 flights, the equilibrium spacecraft potential occurred at $-1.2\,V$. During the modulated electron beam emissions at $2\,msec$ pulse intervals, the spacecraft achieved highly positive potentials. The analysis of these potential levels and the surrounding plasma densities has been impeded due to the presence of scattering, thermalization, and secondary emissions. The best estimates indicate that the spacecraft charged to $+10\,V$ for approximately one ion gyroperiod right after the firing of the electron guns began. After that initial ion gyroperiod passed, it is unknown to what positive potential the vehicle returned.

Directly following the shutdown of the electron beam, the vehicle potential dropped to a potential of $\simeq -4\,V$ within $4\,msec$. If the beam had been fired up along the magnetic field lines, the vehicle potential returned to $-1.2\,V$ within $4\,msec$. If this direction was reversed and the beam fired down the field lines, the electron beam mirrored at the conjugate point and returned to vehicle, resulting in a potential held at $\simeq 3\,V$ until $16\,msec$ post beam shutdown.

The studies undertaken with the photometers and current detectors flown on board these rockets indicate that the return current to the vehicle is not

sustained by the ambient plasma alone. Wave-plasma interactions result from the beam operations and cause heating and ionization of neutrals around the vehicle. Hotter than ambient electron and ion spectra were measured both during and immediately following electron beam operations. Probe data measured this hot interaction region to be roughly $100\,m$ in diameter. From these studies, it was concluded that the bulk of the return current was carried by low energy electron, $< 10\,eV$, and that the return current did not exhibit a strong pitch angle dependence. In addition, the photometers and current detectors observed a periodicity in the return current that peaked near $20\,Hz$. This periodicity was most probably the result of the existence of a cylindrical sheath, in place along the rocket's semimajor axis, that oscillated radially as the ions executed gyromotion in and out of plane.

ECHO 7 was launched in order to study the electric and magnetic field configurations associated with the diffusion and energization of electrons moving along magnetic field lines that cross the equatorial plane between 6 and 10 R_E and to study the dynamics of beam-plasma interactions [93]. The analysis of payload sheath structures and payload potentials during the active experimentation is of paramount interest in this present work. ECHO 7 carried a tethered probe, known as TETHER AFGL, that moved away from the vehicle to measure the plasma potential profile between the main payload housing and the external plasma sheath region. The TETHER collecting area was $0.1\,m^2$ and the potential difference between the TETHER payload and the MAIN payload was measured with a $10^9\,\Omega$ voltmeter. The potential difference measured with only the electron generator firing went as high as $3\,kV$. When that electron beam injection was immediately preceded by a gas thruster firing, the payload potential difference reached only $600\,V$. This indicated the neutralizing effect of a plasma release, results quite similar to those seen on CHARGE 2.

The data sets for spaceborne plasma contactor experiments are not extremely extensive and tend to be mostly for contactors intended to control spacecraft potential. This is due in part to the fact that a number of "contactor" experiments were recorded purely by chance, *e.g.* CHARGE 2. Such experiments were often not fully instrumented to make the necessary measurements of plasma param-

eters to assess the performance of the contacting process. The other problem is that not a great deal of the work has been published on these spaceborne contactor experiments, allowing for only basic qualitative assessments of the contactor's performance in space.

2.8 Experiments Recommended for Furthering Knowledge of the Plasma Contacting Process in Space Conditions

As can be seen from the preceding sections, the process of extrapolating knowledge gained from laboratory experiments to the environment of space is not straightforward. Making this correlation even more difficult is the nature of the differences between the two approaches to a scientific query. Laboratory experiments offer a proliferation of data, run a relatively low risk at reasonably low cost and provide rapid data turnaround. The disadvantage of a laboratory regime relative to the plasma contactor electron current collection process is the lack of nonlinear theories to extract clear conclusions from the data sets. Spaceborne experiments have an extremely long lead time, are very expensive and run high risks. Consequently, there is a paucity of data from spaceborne experiments in this field. If an increase in understanding of the plasma contacting process occurring in space is to be achieved, it is critical that a laboratory-based understanding of the contacting process be obtained and its application to the regime of space be well understood. The necessary follow-on to such laboratory work is the execution of carefully planned spaceborne contactor experiments.

Such carefully controlled experiments require a higher degree of spatial resolution of densities, plasma potential profile, core radius, transition region dimensions, contacting boundary, and temperatures in order that the evolutionary process at work in plasma contacting be quantified. In Section 2.7.2, triggering mechanisms for double layers within plasmas were discussed. For effective scaling of laboratory investigations to spaceborne experiments, it is crucial that the triggering mechanisms of double layers in laboratory plasma contacting experi-

ments be examined closely. This may be accomplished by stepping through the various contactor operating modes matrixed against a range of plasma simulator injection electron velocities. A search for preferential Maxwellian diffusion as indicative of magnetic field effects should be undertaken in an effort to distinguish chamber phenomena from the plasma phenomena that will naturally occur in the lower density and lower pressure LEO regime. From the data presented, it has been clearly demonstrated that there is a need for effective probe placement in all three dimensions within the chamber experiments to completely analyze the contacting region. Mikhailovskii [53] pointed out that an electron streaming instability results from a finite separation between an anode and a cathode. This phenomenon should be addressed by performing further interaction studies centered on the distance between the contactor and the ambient plasma simulator, building upon the chamber tests previously performed by Wilbur and Patterson.

2.8.1 Spaceflight Recommendations

The data presented in Section 2.7.2 clearly indicates the need for further spaceborne experiments in order to determine the nature of the plasma contacting process. If plasma contactors are to be used on spacecraft flying in the auroral regions of the ionosphere or in geosynchronous orbits, then additional considerations should be made, especially in light of the information gained from the auroral and geosychronous missions presented in Section 2.7.2. In the event that magnetospheric substorm or storm activity were to occur during such flights, conditions would most probably result in electric fields that would cause the formation of natural double layers. An interesting question to address would be whether the interaction of this type of magnetospheric activity with an on-orbit artificially generated plasma would result in a predisposition towards double layer formation and if so how this would affect the efficiency of the device in its role either as an amplifier of system power or as an active charge control device. It is imperative that spaceborne plasma contacting systems be instrumented with boom packages that can deploy sensor packages from the contactor anode at varying distances, all the way out to the ambient plasma. Alternatively, a small free-flying satellite should flown in the vicinity of the contactor

experiment to obtain the necessary plasma profiles. Currently the major electrodynamic tether mission planned utilizing a plasma contacting system is the Tethered Satellite System 1, TSS-1. There are boom sensor packages mounted on the TSS-1 subsatellite, but none on the Orbiter and there will be no free flyer in the vicinity of the Orbiter. The measurements of any sheaths that form around the Orbiter will be restricted to those made by experiments fixed in the payload bay.

Opportunities Available on TSS-1

TSS-1 is manifested for flight in May 1991 and presents a number of opportunities for performing the type of experiments necessary to validate theoretical modelling of the plasma contacting process. Included among the experiments to be flown as part of the TSS-1 complement is the Hollow Cathode Plasma Bridge (HCPB) to be provided by J. McCoy of Johnson Space Center.

The primary objectives of the HCPB are to:

1. Stabilize the potential of the Orbiter ground with respect to to the ambient ionosphere during deployment of the TSS-1 Satellite,
2. Allow flow of tether currents exceeding 1 Amp into the ionosphere, without a need for large potential drops at the Orbiter end of the tethered system,
3. Measure Orbiter ground current flow during operation of the onboard electron guns and tether deployment,
4. Provide a calibrated, controlled plasma and neutral gas cloud on the Orbiter.

The HCPB will be operated in a variety of modes to provide data to enhance knowledge in such critical areas as the ionization processes associated with plasma contactor operation, interactions between plasma clouds and the ambient plasma, interactions between neutral clouds and the ambient plasma, and processes analogous to the formation, dynamics and decay of comets [6] .

The HCPB will provide the opportunity to study the interaction of a continuous plasma emission from a moving vehicle with the ambient ionospheric plasma at Shuttle altitude. The experiment will provide a configuration of a steady-state nature in that a balance will be achieved between gas and plasma efflux and cloud growth tied to ion loss processes. This balance will be determined by the relationship between the conducting plasma cloud, the ambient plasma and the earth's magnetic field.

The HCPB will provide a neutral flow of either Xenon or Argon at a rate of $10^{19} - 10^{22}$ neutrals/sec. The matter expelled will be one of the following, depending on the HCPB mode of operation,

1. Cold gas jet,
2. With internal heater on, hot gas ($\sim T = 1000 \circ K$),
3. Hot gas plume plus plasma generated with application of $8 - 15\,V$ HCPB external anode.

Prior to tether deployment, the HCPB can be used as an electron collector in experiments where the Orbiter potential with respect to the ambient plasma is driven positive. During deployed operations, the HCPB will act as an electron emitter and is expected to prove that a plasma contactor emits electrons in a much less energetically expensive manner than an electron beam system does.

The TSS-1 instrument complement will measure a number of plasma parameters of interest in the study of the contacting process. On the Orbiter, measurements of n_i, n_e, T_i, T_e, $\Phi_{Orbiter}$ (with respect to the ambient plasma), return currents to the Orbiter, and the magnetic field as experienced in the payload bay. Such measurements will provide details on the spatial and temporal development of the plasma cloud and its interaction with the ambient plasma as well as critical data regarding the contactor's ability to control the discharge of the Orbiter's potential. The TSS-1 satellite may be thought of as a Langmuir probe as it provides measurements on the cloud interactions in addition to those listed above as it deploys out to its $20\,km$ stop on station, and during its retrieval. As an example of this concept, a sudden $\Delta\Phi_{Satellite}$ with respect to

the Orbiter measured along with changes in species density and energy as the satellite is deploying through the plasma interaction region would be indicative of an encounter with the boundary of a double layer.

Making the tie to the need for planned laboratory and space correlations, there are chamber tests planned for the HCPB which involve instrumentation for measuring its interaction with a simulated plasma and with the TSS-1 electron guns. These tests will allow the development of a much needed data base in terms of planning the experiment operations for TSS-1. Without interactive chamber testing of all of the active experiments and the measurement packages prior to flight of TSS-1, it will be nearly impossible to understand in real-time what interactions are taking place on and in close proximity to the Orbiter, making reliable execution of the mission debatable. Without the inclusion of the HCPB in the TSS-1 mission, the establishment of large amplitude currents in the tether at maximum deployed length would be compromised.

Chapter 3
Extension of Plasma Contactor Modelling to Space

3.1 Application of Space-Charge-Limited Double Layer Theory

3.1.1 Introduction

A variety of theories and data sets have been already presented in Chapter 2. In the following chapter, extensions of existing theories will be presented and the numerical results of these extensions evaluated. In addition, a new theory will be presented that makes use of the extension of the space-charge-limited double layer to space conditions.

3.1.2 Determining Critical Potential for Transition of the Plasma to Ignited Mode

In this section, the crossover point from contactor plume mode to contactor spot mode will be addressed. Plume mode is the contactor mode in which there is high-voltage, low-current plasma discharge while spot, alternatively termed ignited, mode is that in which there is high-current, low-voltage plasma discharge. Such ignited flow was described in Chapter 2 with regards to a variety of experiments. The spot, or ignited, mode refers to the discharge in which the neutral gas outside of the contacting device has become ionized.

The emitted ion current in the chamber experiments described in Section 2.6 is comprised of a rather small ion current I_o produced by the hollow cathode source that is independent of the incoming electron current plus a current of ions produced by ionization of neutral gas caused by the incoming ambient electrons. These ambient electrons have been accelerated by a double layer separating the high density core cloud and the ambient plasma. The expression of this total ion current is given by

$$I_i = I_o + I_e \int dr n_o(r)\sigma, \tag{3.1}$$

where $n_o(r)$ is the neutral density, and σ is the electron ionization cross-section at the energy of the incoming ambient electrons, $\phi_o + T_{ea}$. For a thin double layer, $I_i = (m_e/m_i)^{1/2} I_e$, so it then follows from Eq. 3.1 that

$$I_e = I_o \left[(m_e/m_i)^{1/2} - \int dr n_o(r)\sigma \right]^{-1}. \tag{3.2}$$

Eq. 3.2 sets the radius of the double layer since I_e must be equal to the saturation current integrated over the surface of the double layer, $I_e = 2\pi r_o^2 J_e^{\infty}$. The expression for I_e is self-consistent if it gives $r_o \gg \lambda_{De}(\phi_o/T_{ea})^{3/4}$. Otherwise, the double layer will not be thin, and $(m_e/m_i)^{1/2}$ must be increased by the enhancement factor presented in Section 2.2.1, further reducing r_o and I_e. A consequence of Eq. 3.2 is that, as ϕ_o and, hence, σ are increased from zero, I_e will gradually increase until ϕ_o reaches a critical value, where

$$\int dr\ n_o(r)\sigma = (m_e/m_i)^{1/2} \tag{3.3}$$

At this ϕ_o, according to Eq. 3.2, I_e will blow up. In practice, I_e will not become infinite, but will be limited by several factors:

1) If r_o is too much greater than r_{anode}, the incoming electrons will not be able to converge completely on the source, and consequently, they will not all be available for ionization;

2) r_o cannot be greater than the size of the tank.

However, one can expect qualitatively that at this critical ϕ_o, there will be a sudden increase in I_e and in r_o, and that the critical ϕ_o will be a decreasing function of neutral line density $\int dr\ n_o$. At this critical value the plasma will undergo a transition from plume mode to spot mode. Such a transition to

Table 3.1: Transition to ignited mode

ϕ_o (Volts)	σ (cm^2)	$\int dr\, n_o$ (cm^{-2})	Gas flow (sccm)
11	2.3×10^{-16}	9×10^{12}	13.7
16	3.3×10^{-16}	6×10^{12}	9.6
19	3.6×10^{-16}	5.4×10^{12}	6.8
27	4.8×10^{-16}	4×10^{12}	4.1
36	5.5×10^{-16}	3.4×10^{12}	2.7

that ignited mode at a critical ϕ_o was seen in the Frascati data [26,79,80,81] and in Wilbur's [87] and Patterson's [61,62] experiments, as was pointed out in Section 2.6. Table 3.1 [29] gives σ, for Xenon, at electron energy $\phi_o + T_{ea}$, with $T_{ea} = 9\,eV$, the required neutral line density for this transition to occur at each of several values of ϕ_o, and the gas flow rate at which the transition was observed, for each value of ϕ_o.

Measurements of the spatial distribution of neutral gas were made by the CSU and NASA LeRC experimenters, within $r_{anode} \approx 2\,cm$ of the center of the anode, yielding neutral line densities in good agreement with the theoretical values shown in Table 3.1. However, the neutral line density near the center of the anode may not be the critical neutral line density. Measurements were made of the density and energy of the incoming hot electrons as a function of radius inside the contactor cloud. While the energies were within the expected range of values of $\phi(r) + T_{ea}$, and the density at r_i was close to the ambient density multiplied by $[T_{ea}/\phi(r_i)]^{1/2}$, the density increased more slowly than r^{-2} at smaller r and was only a factor of 3 greater at r_{anode} than at r_i. This indicates that the incoming electrons were not converging to within r_{anode} of the center of the anode, but instead spread out over much of the full anode radius of this $6\,cm$ anode case chosen for examination. Alternatively, this could indicate that the neutral gas expansion did not adhere to spherical symmetry and that the expected number of electron-neutral collisions did not occur, thereby yielding a measured electron density lower than that expected from using the overly simplified spherically symmetric geometry. The proper treatment of the problem

needs to account for both the more complex geometry of the interaction and the effect of angular momentum on the geometry.

The failure of the electrons to fully converge may be due in part to their angular momentum and perhaps in part to the effect of the ambient magnetic field, effects which were not included in the model examined in Section 2.2.2. The neutral line density over most of this area was considerably lower than it was within r_{anode} of the center of the anode. This gives a neutral line density that, according to Eq. 3.3, is lower than that required for the transition to the ignited mode. A possible explanation for this discrepancy is that there may have been a substantial flux of secondary emission electrons in the vicinity of the anode, contributing to the ionization rate. Note, however, that this secondary population should be attracted to the positively biased anode while the newly liberated secondary ions will move out from the anode. One should also note that probe saturation due to the high density and temperature of the electrons could have affected the measurements and the true state of the plasma may in fact not have been measured.

3.1.3 Extension of Wei and Wilbur Model to Magnetized Electrons and Finite Anode Size

In order to extend the Wei and Wilbur spherically symmetric space-charge-limited double layer model to the conditions present in the LEO environment, one must account for the fact that the path taken by the electrons on their way to the anode is affected by their angular momentum and by the fact that the plasma contactor has a finite anode. This is done by using the Parker-Murphy condition (see Section 3.1.3) to set the value of the outer edge of the double layer, r_o. For comparison, r_o is also set to equal the electron gyroradius. The equations describing this model are discussed in this section.

In Wilbur's ground based experiments [85,86,87,91] in which the $6\,cm$ anode was used, the Larmor radius of the ambient electrons in the earth's magnetic field was about $20\,cm$, much greater than the $3\,cm$ thickness of the double layer

observed for those experimental conditions. Under those conditions, the magnetic field did not significantly deflect the electrons as they crossed the double layer. After the electrons covered the distance across the double layer, they had a Larmor radius of about $50\,cm$. In the $8\,cm$ the electrons then had to traverse to reach the plasma contactor's collection surface, the anode, they were deflected deflected by about $\frac{1}{2}(8)^2/50 = 0.7\,cm$, less than the $6\,cm$ radius of the anode. Consequently, the magnetic field did not inhibit the electrons from reaching the anode [57]. Hence the model which assumed unmagnetized electrons ought to be valid under plasma conditions similar to those for the case given above. An additional critical requirement of the model, $r_i > r_{anode}$, is obviously also satisfied in those chamber experiments. Given the restrictions on the mechanical range of the probes, it is not possible to fully determine the chamber wall effects on the double layer structure and the chamber wall sheath characteristics.

In space, on the other hand, the ambient electron temperature in the equatorial region is much less than that of the simulated ambient plasma in the chamber experiments, only about $0.1\,eV$. The Larmor radius, then, is about $2.5\,cm$ and the ambient density is much less than that produced in the ground based experiments, roughly $10^5\,cm^{-3}$ as opposed to $3 \times 10^7\,cm^{-3}$. Therefore, to collect an electron current of several amps from the ambient plasma requires an outer radius r_o of tens of meters, much greater than the electron Larmor radius. The electrons can traverse such a distance only if they undergo collisions or effective collisions due to some kind of instability. If the electrons can gain enough energy as they cross the double layer to remain effectively unmagnetized until they reach the anode, they will also be able to traverse the very wide double layer. The latter possibility has been considered and it has been found that, even with rather optimistic assumptions, an undesirably large sheath potential drop is required, since the result is that most of the tether potential drop occurrs in the sheath. It is apparent that effective collisions of some kind are needed in a plasma contactor in space, in order to collect a large electron current from the ambient plasma with an acceptable potential drop. However, in lieu of a collisional space-charge-limited double layer model, the Parker-Murphy condition and the gyroradius limit are employed to extend the space-charge-limited collisionless spherical double sheath to LEO conditions, underscoring the fact

that this model results in a rather inefficient contacting system.

Validity of Parker-Murphy Limit

One of the primary motivations, as has been mentioned, in flying plasma contactors in space is to actively control spacecraft potential. In the LEO plasma regime, the magnetic field is strong enough to prevent cross field electron transport, effectively handicapping efforts to keep a spacecraft's potential close to that of the ambient plasma through which it is flying. This problem was addressed by Parker and Murphy [57]. Dissipation of potential buildup through the use of electron beams was treated by them. The theory they applied to that problem can also be applied to the plasma contacting process under consideration in this thesis.

Parker and Murphy developed a theory of drift approximation that led to the numerical solution of a differential equation. In solving that equation,they assumed that the potential surrounding the spacecraft is an axially symmetric function. In the case of very large potentials, when the drift approximation is invalidated, they used the nonrelativistic constants of motion of an electron to determine a rigorous analytic bound on the current collected to the satellite. In pursuit of their theory, Parker and Murphy made a number of assumptions that will be examined below for their validity under space conditions.

Within their theory, Parker and Murphy assumed that the electron gyroradii are orders of magnitude less than the radius of the satellite and that the collisional mean free paths are of the order of kilometers [57]. They then state that the electrons travel freely along the magnetic field lines, while remaining fixed to those field lines and executing tight spirals around them. With this assumption, diffusion across field lines was neglected and the concern was exclusively with $\vec{E} \times \vec{B}$ electron drift. Neglecting the motional electric field effects, the electrons are then collected solely from the area of the magnetic flux tube that intersects the area of the satellite and are taken to be collected from infinity at the ends of such a flux tube. The cross-sectional area of the flux tube is only slightly larger than the cross-sectional area of the satellite which is perpendicular to the

magnetic field lines as a result of finite electron cyclotron radius. Parker and Murphy assumed that this difference in cross-sectional area is negligible since the electron cyclotron radius is negligible compared with the satellite radius. Therefore, the maximum current collected would be the thermal current passing into the area $2\pi a^2$, with a equal to the radius of the satellite. Parker and Murphy also assumed that the magnetic flux tube supplying the electrons from infinity is not depleted, allowing them to proceed with their derivation of an upper limit on current collected to the satellite. Also, they neglected the distortion of the local magnetic field due to induced currents circulating through the satellite and the surrounding ionospheric plasma.

For current collection according to drift theory, Parker and Murphy chose the cylindrical coordinates, r, θ, and z, to represent the radial, azimuthal, and axial coordinates of the electron motion. The origin of the coordinate system was taken to be the center of the spherical satellite, with the magnetic field uniform and parallel to the z axis. An electron then experiences a radial drift normal to the axis of the system given by

$$v_r = -(v_z/m_e\omega_{ce}^2)\frac{\partial^2\Phi}{\partial r \partial z}, \tag{3.4}$$

where v_r and v_z are the radial and axial components of the drift velocity of the electron's guiding center. The electron's electrostatic potential energy is given by $\Phi(r, z)$. The electron gyrofrequency is given by ω_{ce}, and m_e denotes the mass of an electron. Approximating the electric field with an attractive Coulomb field, the electron's guiding center motion along the magnetic field line then also experiences drift so that, in Eq. 3.4, the axial component of the electron's guiding center drift velocity would be negative as would the $\partial^2\Phi/\partial r\partial z$ term, causing the radial component of the electron's guiding center drift velocity to be negative. Consequently, the electron's guiding center maps a helical path around the axis of the coordinate system, meeting the surface of the magnetic flux tube as it executes this spiralling motion. Such radial drift is a result of the $\vec{E} \times \vec{B}$ drift as the electron travels toward the satellite. Eq. 3.4 holds for $|v_r/v_z| < 1$, the condition of validity for this drift approximation, because v_r is a drift term of higher order than v_z [57].

Parker and Murphy obtained, in a collisionless model and for $e\phi_o \gg T_{ea}$, a necessary condition which must be satisfied for electrons that have reached r_o to then reach the plasma contactor anode is

$$r_{PM}^2/r_{anode}^2 < 1 + (8e\phi_o/m_e\omega_{ce}^2 r_{anode}^2)^{1/2}. \tag{3.5}$$

Eq. 3.5 provides the rigorous upper bound on current collection for a satellite at known potential.

In the majority of the previous analyses of the collisionless space-charge-limited double layer problem, there was no consideration of angular momentum. An angular momentum consideration was invoked in [24] and taken up in Section 3.1.3. Introduction of Eq. 3.5 allows the angular momentum consideration desired in Section 3.1.3. Eq. 3.5 can also be taken as a sufficient condition for collection of electrons to the anode if all of the potential drop occurs in a thin double layer. However, if the double layer is thick, or if a significant part of the potential drop occurs in the quasineutral regions on either side of the double layer, then a further condition must be satisfied if the electrons are to be collected by the plasma contactor anode. Another condition that must be satisfied is $r_i \geq r_{anode}$. The work in this thesis shows that for LEO plasma parameters of interest, the $r_i \geq r_{anode}$ condition is more physically realistic than Eq. 3.5 as an upper limit when considering thick, collisionless, space-charge-limited double layers.

The Parker-Murphy bound on current collection, while offering a means of including magnetic field effects in the collisionless space-charge-limited double layer model, has deficiencies that should be addressed, so that the reader is aware that the complete solution that provides the necessary condition for electron collection to the anode remains undetermined. Consider the following application of the Parker-Murphy drift approximation theory. Let $j_o^{\parallel}$ equal the component of the ambient mean thermal current density parallel to the magnetic field direction, and then,

$$j_o^{\parallel} = n_e q \langle v_e \rangle = n_e q \sqrt{\frac{8kT}{\pi m_e}}. \tag{3.6}$$

For this example, assume that a $1\,A$ electron beam is injected into the ionosphere at an approximate altitude of $300\,km$ and the following values used for the

variables in Eq. 3.6,

$$\begin{aligned} n_e &\simeq 2 \times 10^{11}/m^3 \\ q &= 1.6022 \times 10^{-19}\, C \\ k &= 1.38 \times 10^{-23} J/^\circ K \\ T &\simeq 1000^\circ K \simeq 0.09\, eV \\ m_e &= 9.109 \times 10^{-31}\, kg \\ a &= 1.5\, m \\ B &= 0.5\, Gauss \end{aligned}$$

As a result, $j_o^{\parallel}$ equals $6.29\, mA/m^2$ and the thermal current collected would equal $88.97\, mA$. Substituting these values into Eq. 3.5, the potential required on the satellite is $12934\, V$. Therefore, according to the Parker-Murphy upper bound on current collection, a satellite potential on the order of $10^4\, V$ is necessary to achieve current balance when emitting a $1\, A$ electron beam.

This prediction flies in the face of experimental data. Winckler, et. al., in [94], describes the flight of the Echo I beam experiment and the data collected. This experiment proved that for an $80\, mA$ electron beam current, both the unbiased metallic rocket body and the rocket body biased to $30\, V$ acted as effective collection devices and adequately restored current balance to the vehicle. Winckler [94] cites 25 rocket-launched electron beam experiments in which emitted electron beam currents up to $0.8\, A$ were balanced with spacecraft potentials much less than those predicted by the Parker-Murphy bound. These results demonstrate that there is a critical element lacking in the Parker-Murphy theory. Clearly, Parker and Murphy did not account for other mechanisms that must be acting to supplement the return current. One such omission is that of the role played by collisions.

Basically, Parker and Murphy neglect three primary mechanisms for the achievement of current balance:

1) Spacecraft material charging characteristics and secondary and backscattering characteristics

2) Return of secondary currents from the ejected plasma itself

3) Possibility of positively charged vehicle itself accelerating return electron cur-

rent, thereby producing secondaries, in a manner similar to an arc discharge.

Collection of the backscattered electrons, secondaries, and photoelectrons must play a role in the return current process. Note that these three currents are material dependent. Therefore, any calculation of the spacecraft potential necessary to maintain an electron beam discharge while preserving current balance must include these currents. The ejected beam will interact with the plasma and create secondaries, adding another element to the balance. The same effects hold true for ion beam discharges, which create electrons due to ionization in the ambient plasma. Finally, if the satellite surface potential is positive, the electron return current is accelerated towards the spacecraft and additional secondaries are produced, forming an electron avalanche through electron-neutral collisions.

The assumption that the magnetic flux tube that extends to infinity and supplies the collected electrons, cannot be depleted is another point of contention in the Parker-Murphy theory. Consider the example case at $300\,km$. If the $1\,A$ beam is ejected and the plasma parameters are as before, then $1\,Coulomb/sec$ must be returned to the spacecraft to preserve charge balance, charge on one electron equalling the value of q given above. An unperturbed volume of ionospheric plasma at this altitude then contains $1.602 \times 10^{-8}\ C/m^3$. Therefore, $6.24\ m^3/sec$ of space is depleted to provide return current to the spacecraft. This is a substantial drain on the surrounding plasma if one considers such a crude first order approximation valid. Assuming this depleted volume of $6.24\,m^3$ to be spherical, its radius r then equals $3.97\,m$. Then,

$$r \gg \lambda_D, \tag{3.7}$$

with λ_D in the ionosphere at $300\,km$ equal to approximately $6.9 \times 10^{-3}\,m$. The assumption that the flux tube is not depleted appears invalidated by the above example.

This discussion of the validity of the Parker-Murphy theory demonstrates that the system that achieves current balance cannot be simply comprised of a spacecraft's collection area and the ambient mean thermal current density, regardless of whether one is using electron beams or a plasma contactor to discharge a vehicle. Additionally, the arguments against the Parker-Murphy

condition that are presented here apply for the case of collecting electron current. This points out why it is very difficult to apply solely the collisionless theory to the plasma contacting process. It also illustrates why the anisotropic contactor model to be elaborated upon in Section 3.2 is so vital to the success of modelling plasma contactor plasma flow in space. However, the Parker-Murphy limit does have utility under certain restricted conditions and can be used to provide a bound on collected current as is done in the following numerical solutions.

Equations used in the Extension to Space Conditions and the Numerical Method Applied

The solution of the Poisson equation given in Wei and Wilbur [83] was not a straightforward problem. The code developed by this author determined the correct potential profile and associated gradients relatively autonomously, representing a significant improvement over the numerical methods used to date [88,90]. What follows is the explanation of how those solutions are achieved.

Eq 2.17 is written in finite difference form to facilitate its numerical solution,

$$\frac{\phi_{i-1} - 2\phi_i + \phi_{i+1}}{h^2} + \frac{\phi_{i+1} - \phi_{i-1}}{2h} = j_o \left[\sqrt{\frac{1}{\phi_i}} - \frac{1}{\alpha} \sqrt{\frac{1}{1-\phi_i}} \right], \tag{3.8}$$

where is h is the step size in the calculation of the potential versus ρ in an evenly spaced grid,

$$h = \frac{\rho_o - \rho_i}{n+1}, \tag{3.9}$$

and where n equals the number of steps across the grid. The boundary conditions given in Eqs. 2.18- 2.21 are written as,

$$\phi(\rho_i) = 1 \tag{3.10}$$

$$\phi(\rho_o) = 0 \tag{3.11}$$

$$\frac{d\phi}{d\rho}(\rho_i) = 0 \tag{3.12}$$

$$\frac{d\phi}{d\rho}(\rho_o) = 0, \tag{3.13}$$

where,

$$\rho_i = \ln\left(\frac{r_i}{r_o}\right) \tag{3.14}$$

$$\rho_o = \ln\left(\frac{r_o}{r_o}\right). \tag{3.15}$$

The initial guess for the potential profile is obtained by calculating the Laplacian solution to Eq. 3.8. Once a potential profile satisfying Eqs. 3.10 and 3.11 is obtained using Poisson's equation within an inner iterative loop, one then checks if that profile is the unique space-charge-limited solution for the given boundary conditions in an outer iterative loop. The unique solution is obtained if Eqs. 3.12 and 3.13 are satisfied. If Eqs. 3.12 and 3.13 are not satified with the calculated profile, then the outer iterative loop is executed, varying j_o and α until all four boundary conditions are met. Through such a process the space-charge-limited solution unique to a particular set of r_r, j_o, and α can be obtained.

Upon initial inspection of the equation, and considering that it is of the form $\phi'' = f(\rho, \phi, \phi')$, one would be tempted to solve for ϕ_i using Newton's iterative method for nonlinear ordinary differential equations, as described by Burden and Faires [16]. As Eq. 3.8 is written, however, it violates the requirement of Newton's method that the matrix of coefficients used to solve the problem must be diagonally dominant. This and similar iterative schemes all require that

$$f_\phi(\rho, \phi, \phi') > 0, \ for\ all\ (\rho, \phi, \phi'). \tag{3.16}$$

Consequently, the equation and method of solution were modified to permit an iterative solution to be successfully accomplished.

Eq. 3.8 is then rewritten,

$$\left(\frac{1}{h} + \frac{1}{h^2}\right)\phi_{i+1} - \left(\frac{2}{h^2} + \frac{1}{h}\right)\phi_i + \frac{1}{h^2}\phi_{i-1} = f(\phi_i^{old}). \tag{3.17}$$

The function $f(\phi_i^{old})$ is Eq. 3.17 is calculated using the previous loop's potential values and inserting them into the right hand side of Eq. 3.8. Eq. 3.17 can then be solved using the computationally efficient Newton's method since this approach permits the formation of a diagonally dominant coefficient matrix.

The convergence of the solution is very sensitive to the initial guesses of j_o and α when attempting to solve for the potential profile. At the ρ_i boundary, significant overshooting was encountered and, at the ρ_o boundary, significant undershooting developed. To combat this problem and decrease the number of iterations required to achieve convergence, the Picard mixing technique is incorporated into the algorithm.

In order to obtain the space-charge-limited potential profile as accurately as possible, the boundary conditions given in Eqs. 2.20 and 2.21 need to be approached as closely as possible. This matching process is run as an outer loop once the potential profile has been solved according to Eq. 2.17 within acceptable accuracy limits, as mentioned above. As the width of the double layer, $r_{D.L.}$, decreases, those boundary conditions become increasingly difficult to match. This is because the potential gradients are much larger within thinner double layers than within thick layers. Note that the thinner the double layer, the larger its radius ratio. In order to obtain an accurate space-charge-limited potential solution, the ratio of the potential gradient endpoints to the maximum potential gradient value has to be set to a tolerance level that increased with increasing radius ratio,

$$\frac{\frac{d\phi}{d\rho}(\rho_i)}{(\frac{d\phi}{d\rho})_{max}} = Tolerance\ value \tag{3.18}$$

$$\frac{\frac{d\phi}{d\rho}(\rho_o)}{(\frac{d\phi}{d\rho})_{max}} = Tolerance\ value. \tag{3.19}$$

Figures 3.1- 3.6 show examples of three double layer thicknesses and their numerically obtained nondimensionalized potential and potential gradient profiles. These obtained profiles agree reasonably well with those obtained by Wei and Wilbur [83].

The values of j_o and α are then obtained as functions of the radius ratio of the double layer, r_r. A complete set of these three values then fully describes a given double layer and can be used to determine the potential drop across the layer for a given hollow cathode emitted ion current and given ambient electron saturation current density. These functions are plotted in Figures 3.7 and 3.8 and represent an extension of the values found by Wei and Wilbur [83] at the

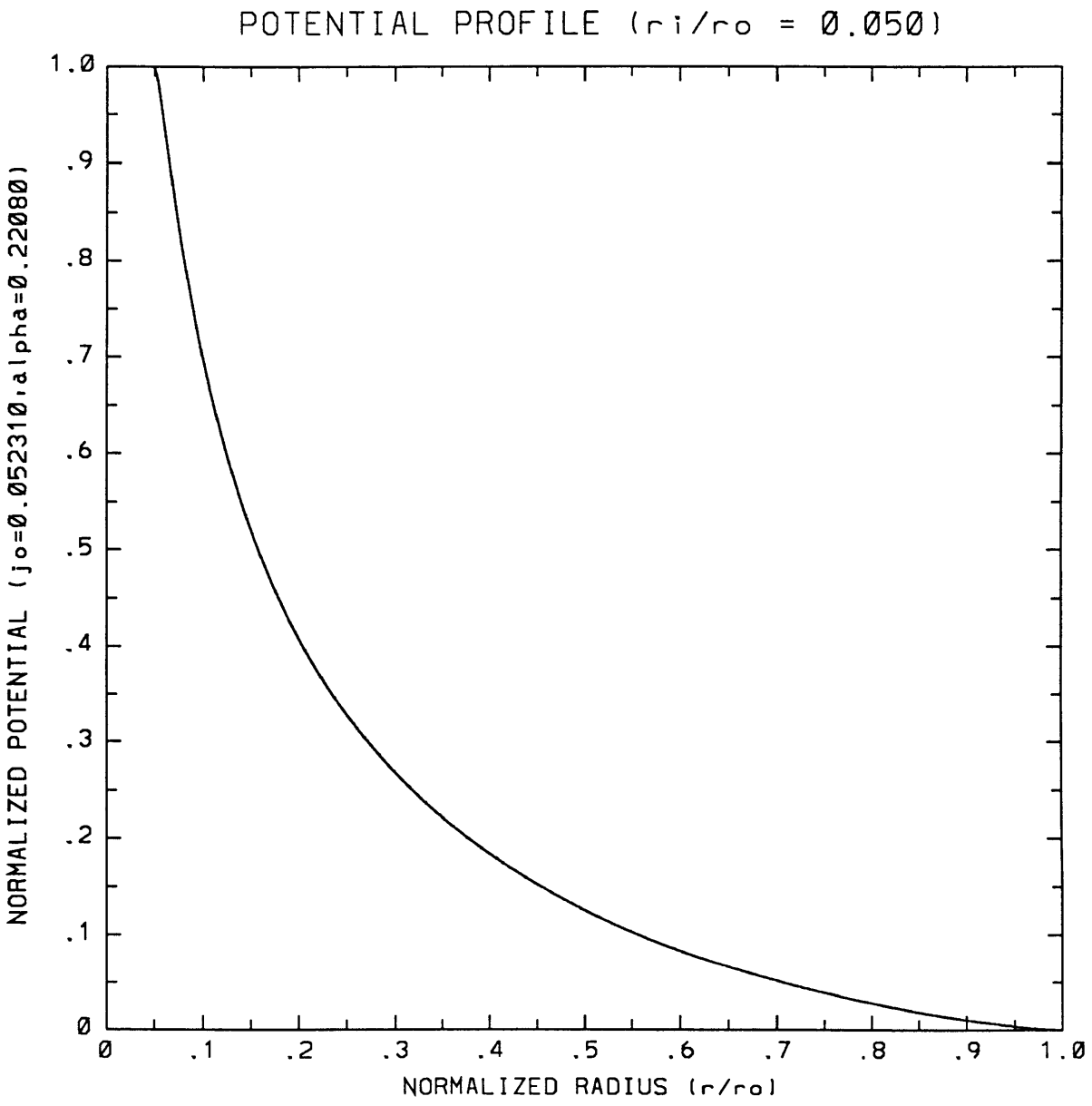

Figure 3.1: Nondimensionalized Potential Profile for $r_r = 0.05$

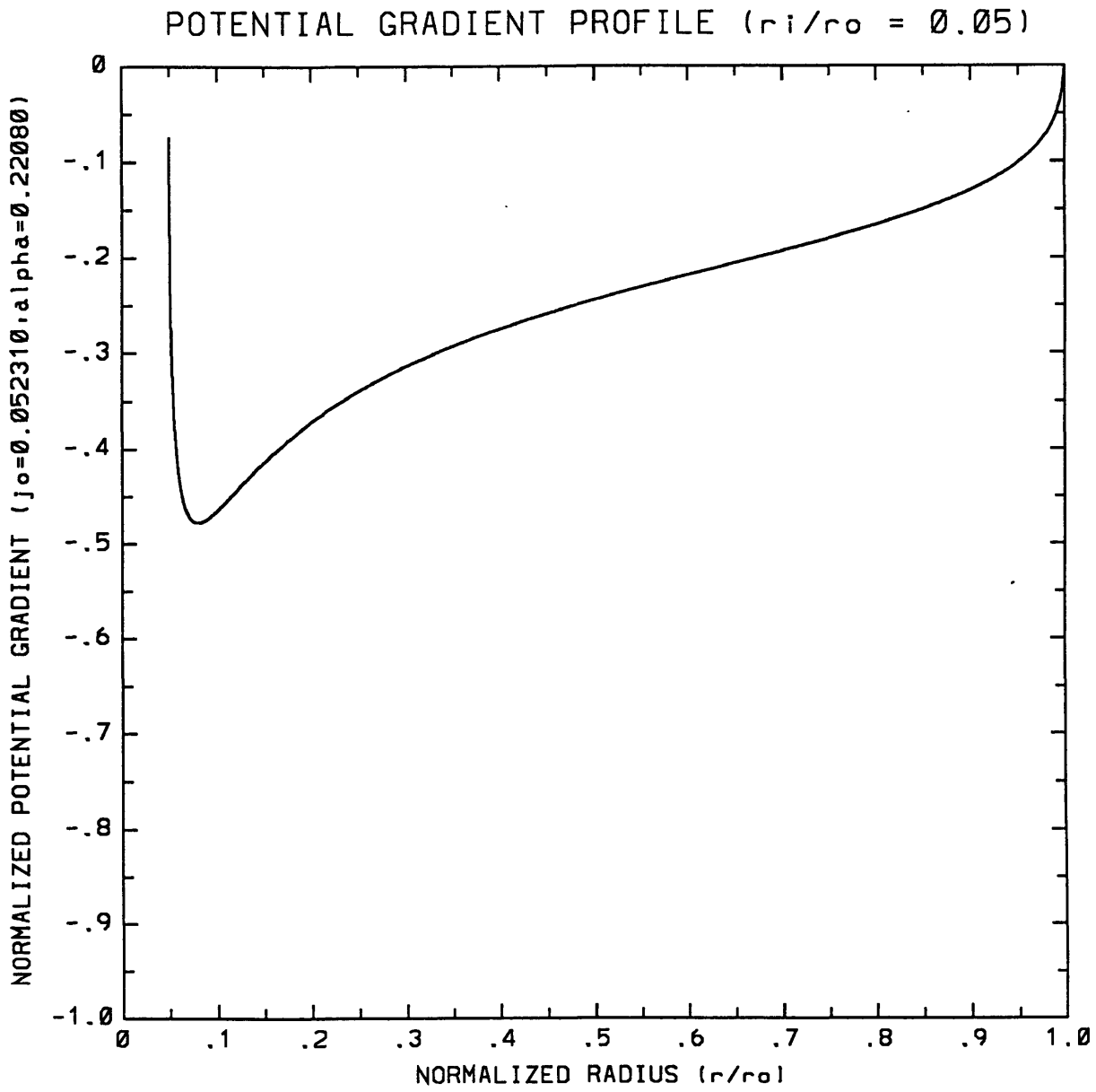

Figure 3.2: Nondimensionalized Potential Gradient Profile for $r_r = 0.05$

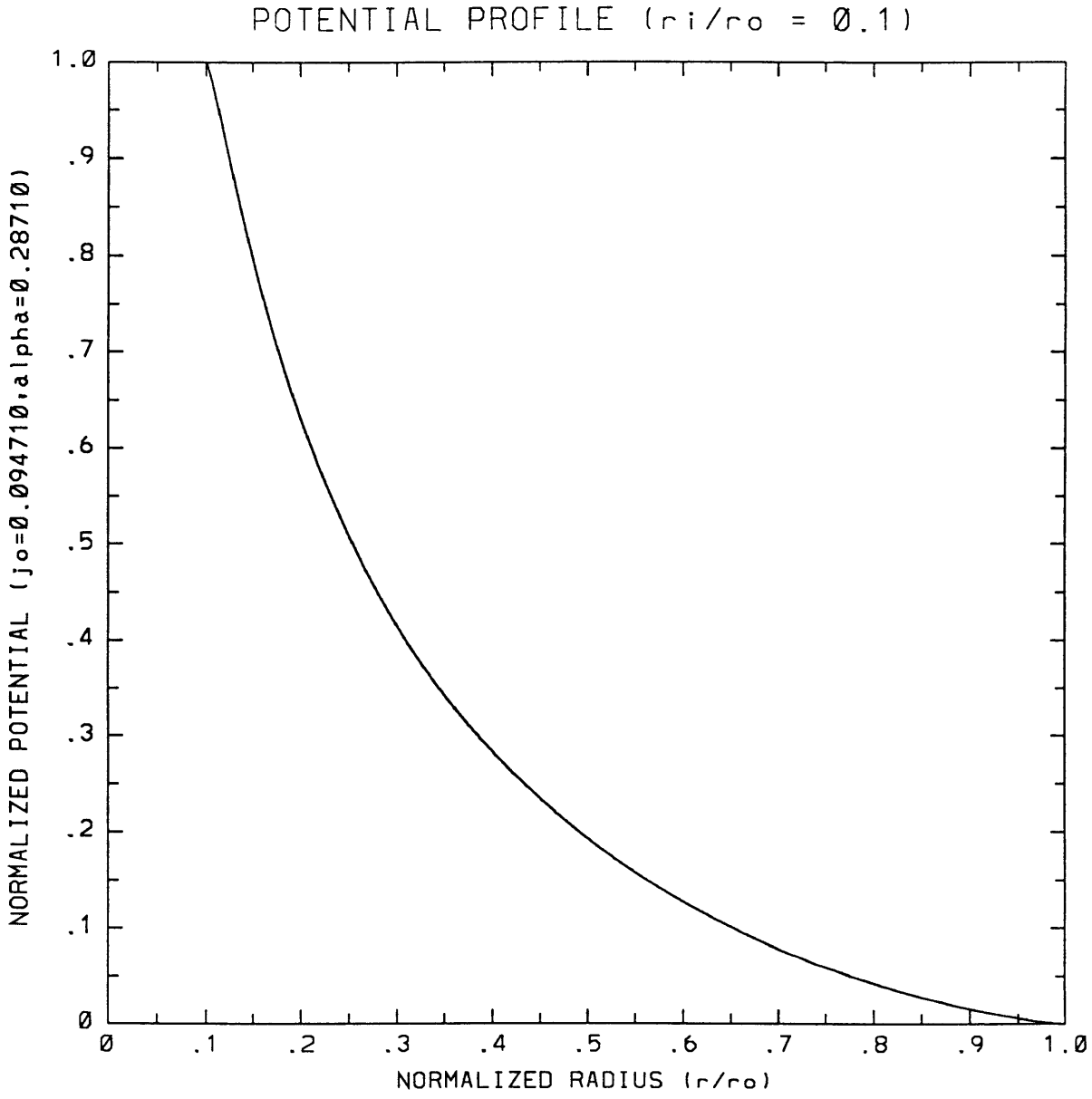

Figure 3.3: Nondimensionalized Potential Profile for $r_r = 0.10$

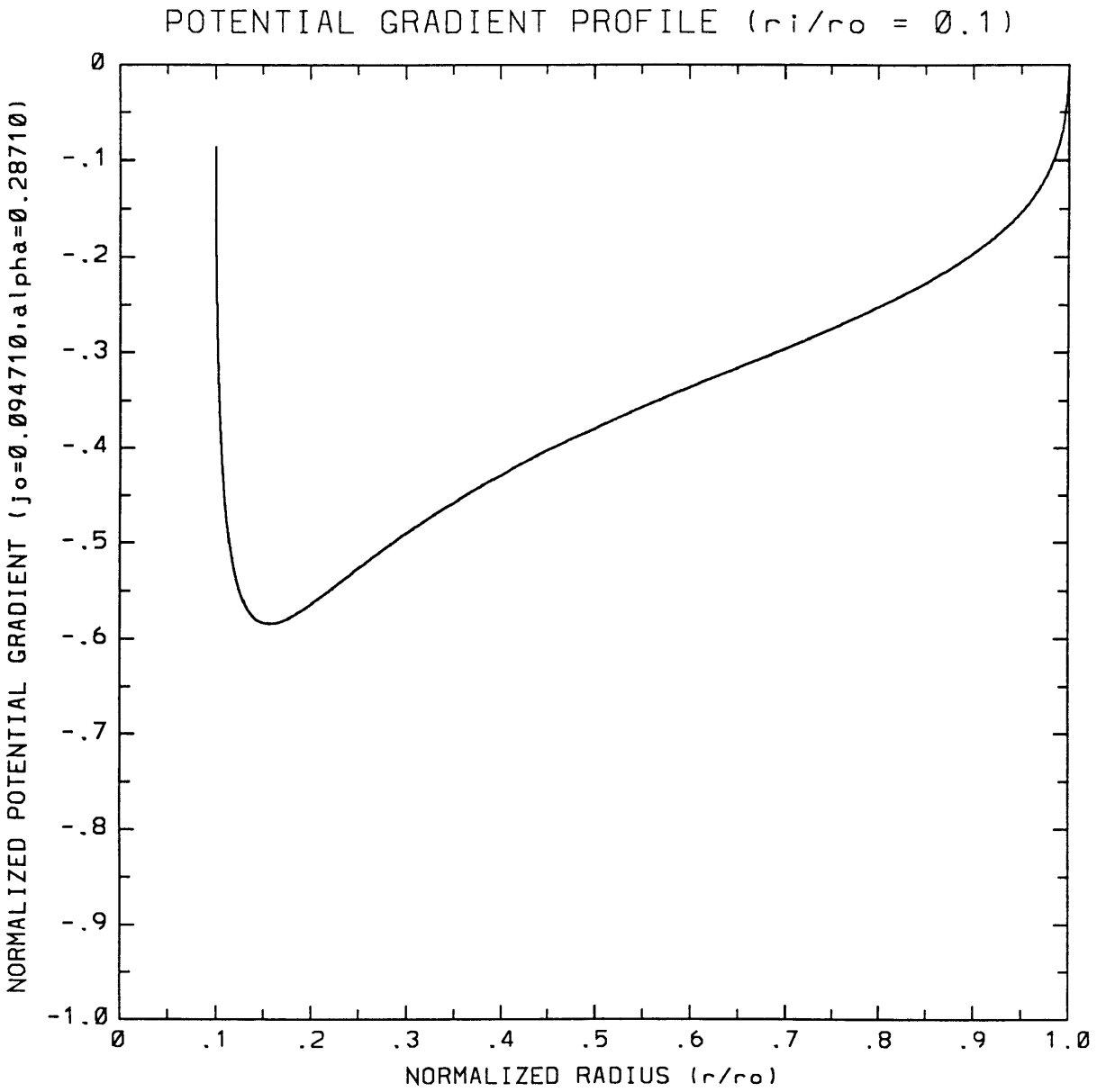

Figure 3.4: Nondimensionalized Potential Gradient Profile for $r_r = 0.10$

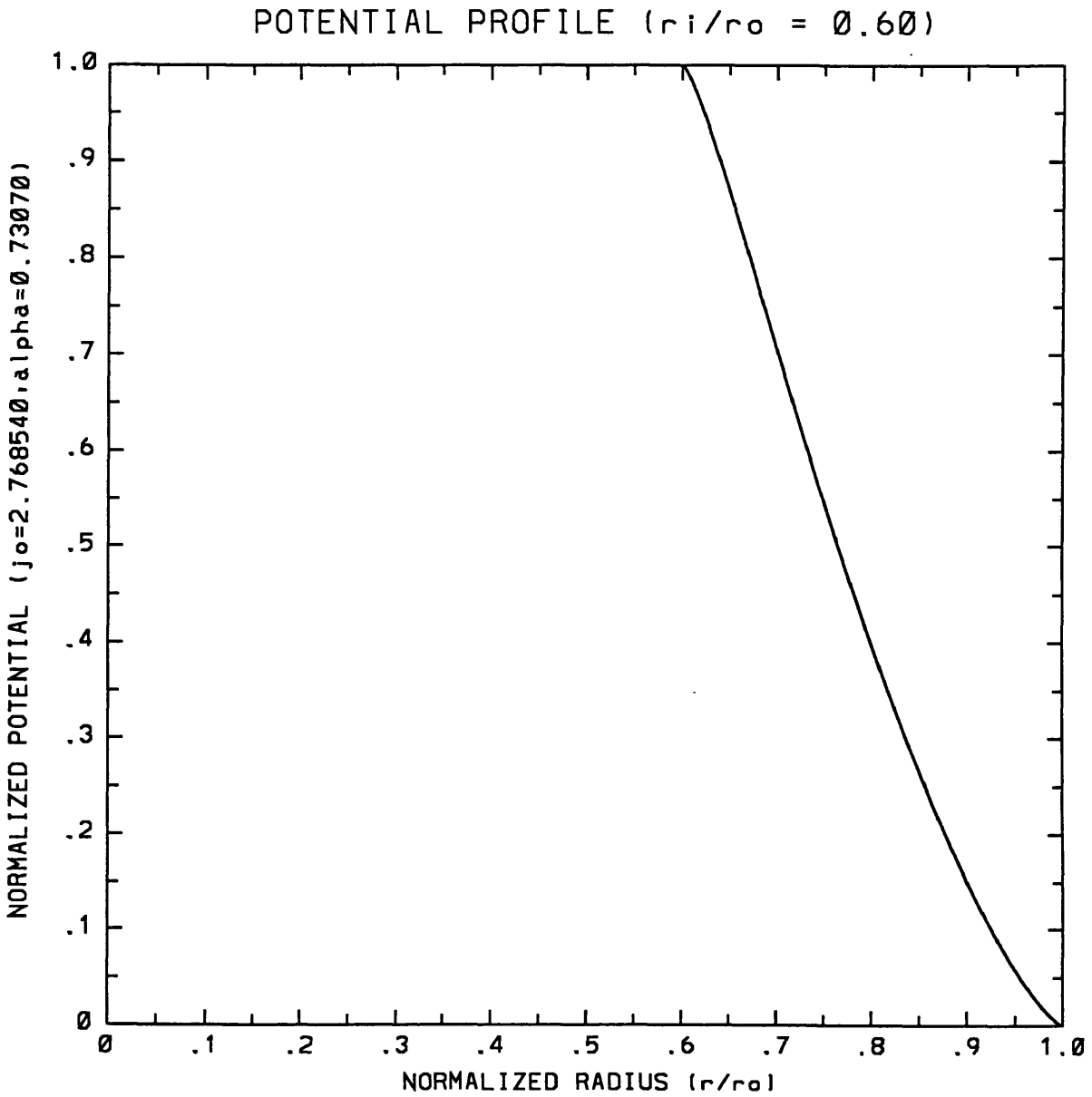

Figure 3.5: Nondimensionalized Potential Profile for $r_r = 0.60$

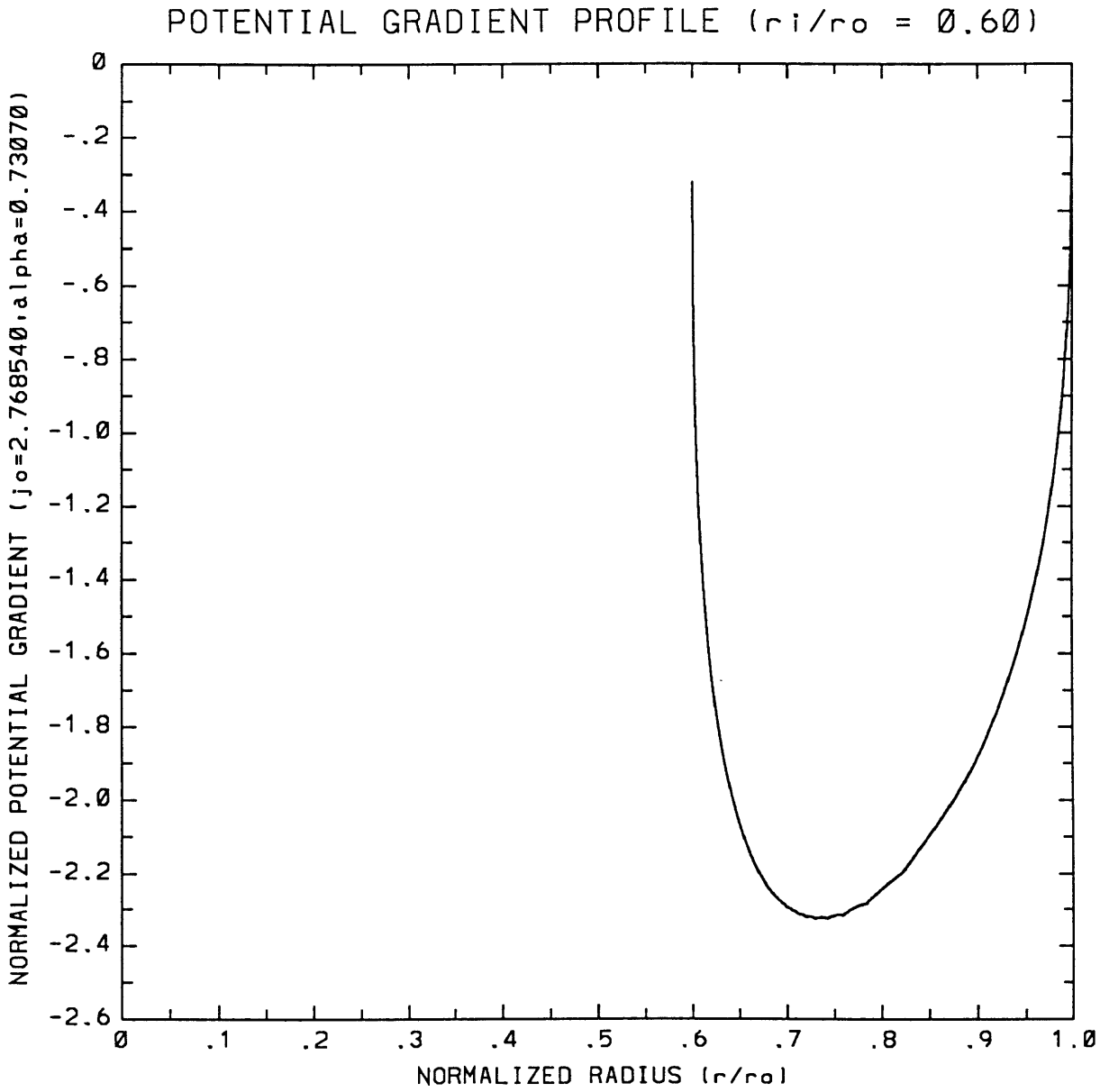

Figure 3.6: Nondimensionalized Potential Gradient Profile for $r_r = 0.60$

boundaries. The tabulated values of the functions are provided for reference in Appendix A.

The extension of the Wei and Wilbur space-charge-limited collisionless double layer model to space conditions requires the use of the radius ratio functions. Since this study is mainly interested in the analysis of contactor use in the LEO regime, the electron saturation density is set as a fixed parameter for each run through the full range of radius ratios from 0.0 to 1.0 and the emitted hollow cathode ion current is obtained numerically from the equations in the extension model. The desired solutions are obtained from the radius ratio functions in the manner described below.

The nondimensionalized gain, given in Eq. 2.16, is used to obtain the total system gain,

$$\xi = \frac{I}{I_i} = 1 + \frac{I_e}{I_i} \simeq \alpha \frac{m_i}{m_e})^{1/2} \approx \frac{I_e}{I_i}, \; for \; \frac{I_e}{I_i} \gg 1. \tag{3.20}$$

Each of those nondimensionalized gain values is a function of a particular radius ratio which allows one to also obtain the nondimensionalized current collected that is a function of that particular radius ratio. The parameters of r_r, ξ, and j_o are used to uniquely determine a solution obtained when either the gyroradius or the Parker-Murphy condition is imposed on the outer radius of the double layer. The solution of the problem can be made purely a function of system gain.

The potential drop across the double layer is expressed for both outer radius limits by manipulating Eq. 2.16 and incorporating Eq. 3.20,

$$\Delta\phi = \left(\frac{I_i \xi}{4\pi\epsilon_o j_o}\right)^{\frac{2}{3}} \left(\frac{m_e}{2e}\right)^{\frac{1}{3}}. \tag{3.21}$$

If the MKS system is used for the standard values in Eq. 3.21,

$$\Delta\phi = 612.364 \left(\frac{I_i \xi}{j_o}\right)^{\frac{2}{3}} \tag{3.22}$$

Setting the outer radius of the double layer equal to the electron gyroradius, $r_o = r_{ce}$, yields the gyroradius limit,

$$r_o = r_{ce} = \sqrt{\frac{2e\Delta\phi}{m_e}} \left(\frac{m_e}{eB}\right) \tag{3.23}$$

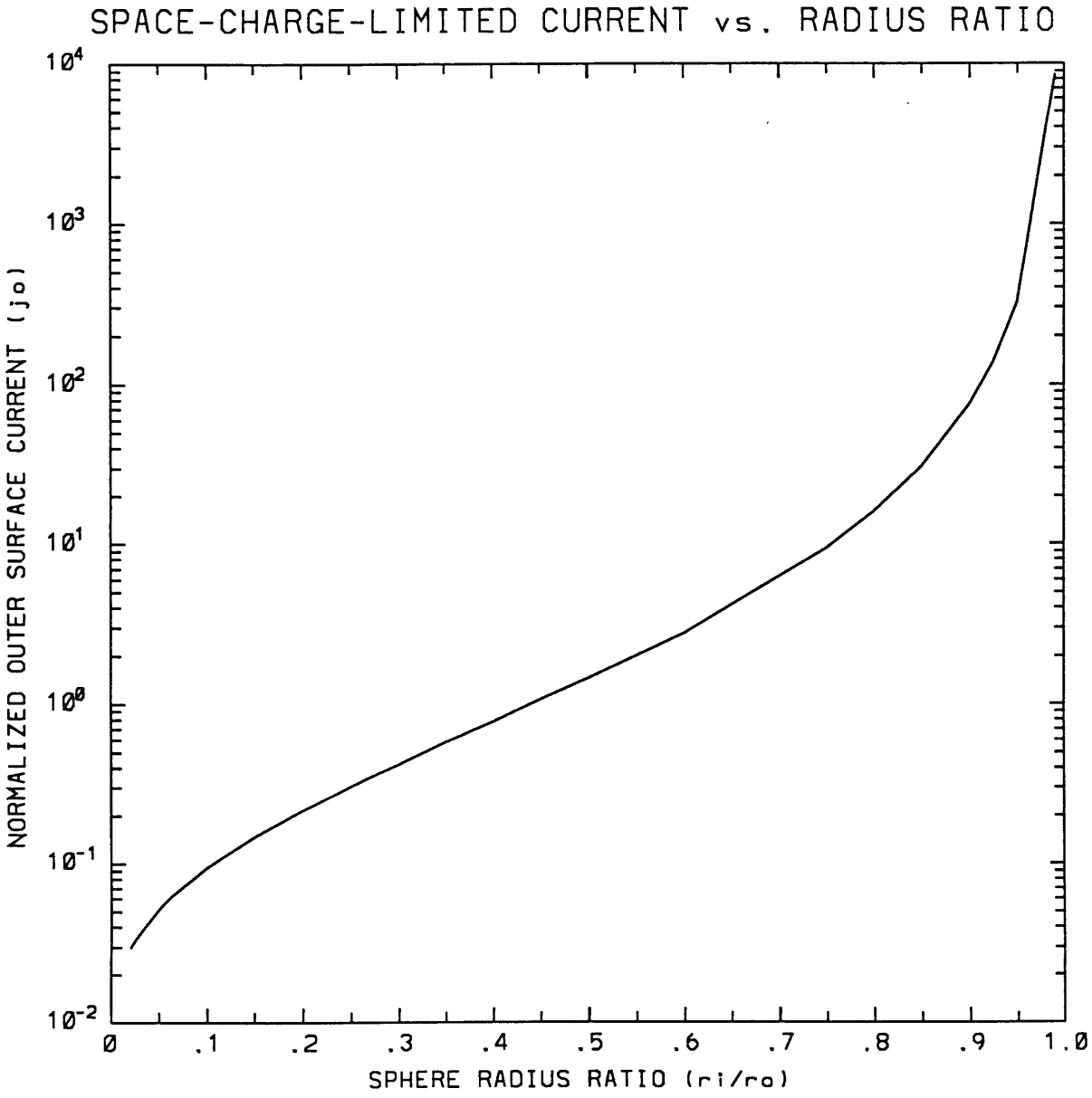

Figure 3.7: Nondimensionalized Space-Charge-Limited Collected Current vs. Radius Ratio

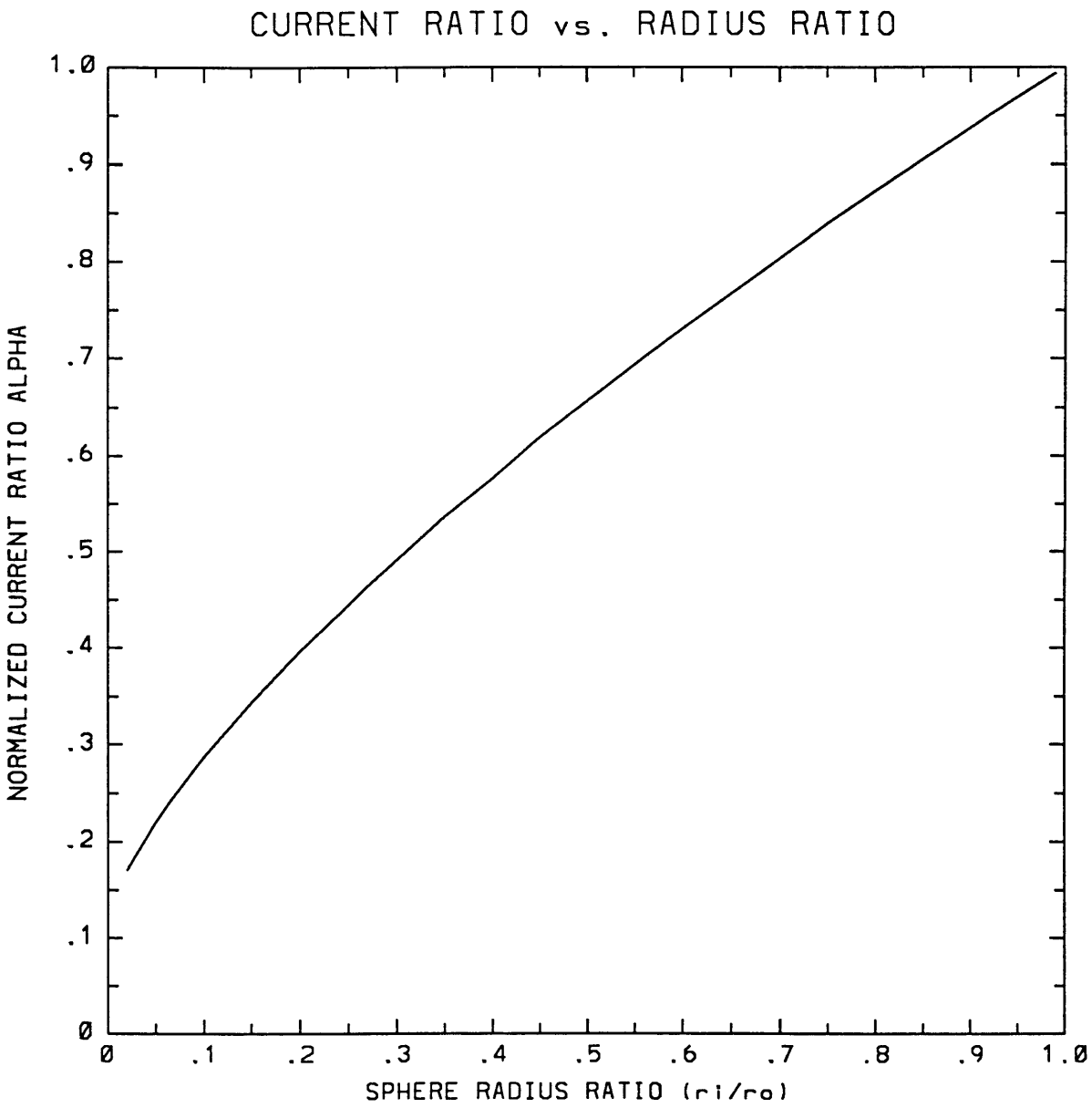

Figure 3.8: Nondimensionalized Gain vs. Radius Ratio

where B is the magnetic field strength. If $B = 0.33 \times 10^{-4}T$, then

$$r_o = 0.102\sqrt{\Delta\phi} \tag{3.24}$$

Eq. 3.25 is obtained by combining Eqs. 3.22 and 3.24,

$$f(\xi) = \xi^{\frac{1}{6}} r_r(\xi) j_o(\xi) = 6.325 \frac{\sqrt{j_e^{\infty}}}{I_i^{\frac{1}{6}}} \tag{3.25}$$

The values of r_r, ξ, and j_o completely specify the left hand side of Eq. 3.25 so that the necessary ion current, I_i, to operate the collisionless space-charge-limited contactor plasma flow under the given ambient conditions for the gyroradius case can be calculated for a given ambient electron saturation current density using Eq. 3.25. After solving Eq. 3.25 directly for I_i, the values of $\Delta\phi$, r_o, r_i, collected electron current I_e, and total current I can be calculated.

For the Parker-Murphy condition case, set $r_o = r_{PM}$, where r_{PM} is determined from Eq. 3.5. The values of r_r, ξ, and j_o plus the electron gyroradius, r_{ce}, anode radius, a, and magnitude of the earth's magnetic field, B, are then specified along with the ambient saturation current density to determine the requisite hollow cathode ion current from

$$\xi = \frac{a^2 j_e^{\infty} 2\pi}{I_i} + \left(\frac{2\pi j_e^{\infty} a}{I_i r_{ce}}\right)\left(\frac{4 I_i \xi e}{j_o m_e \pi \epsilon_o}\right)^{\frac{1}{3}}, \tag{3.26}$$

which can be simplified if the MKS system is used for the standard plasma values to

$$\xi = \frac{a^2 j_e^{\infty} 2\pi}{I_i} + \left(\frac{\xi}{j_o}\right)^{\frac{1}{3}} \frac{j_e^{\infty}}{I_i^{\frac{2}{3}}} \frac{(1.84431 \times 10^8) a}{r_{ce}}. \tag{3.27}$$

A root solver is used to determine I_i to meet the constraints imposed in Eq. 3.27. The potential drop is then calculated along with r_i, r_o, I_e, and I. If, after solving the Parker-Murphy limit, the check loop determines that $r_i < r_{anode} = a$, the calculation is repeated with $r_i = r_{anode}$.

3.1.4 Results of Extending the Wei and Wilbur Model

In Figure 3.17 the gain, ξ, of a contactor using Argon as its neutral gas is plotted versus the ion current for a range of electron saturation current densities

spanning the range experienced in the equatorial LEO environment. The gain for Argon is $\xi = 272\ \alpha$ and appears somewhat weakly dependent on the ion current. Also shown on Figure 3.17 is the line where the contactor plasma passes from the plume mode to the spot mode and was calculated following the method described in Section 3.1.2. Values of gain to the right of this ignition line indicate the range of radius ratios, r_r, where the collisionless model is invalid for the given operating conditions in space since if the flow is ignited there are collisions occurring. This range of r_r values should be matched against the plotted parameters in Figures 3.18-3.21 so that one notes where the collisionless model in invalid when examining all of the figures of merit. In Figure 3.18 the associated potential drop through the double layer is plotted. Typical potential drops are in the range of hundreds to thousands of volts for ion currents in the milliampere range.

In Figure 3.19 the inner and outer radii of the double layer are shown for space conditions. These radii are determined by imposing the Parker-Murphy condition and $r_i \geq r_{anode}$. The double layer extends to many meters for ion currents in the milliampere range. For comparision, the diameter of the CSU tank is shown on the figure. This indicates that finite tank effects would be very important in experiments at realistic LEO plasma densities, except for the very smallest ion currents. One should note that chamber experiments need to have much lower plasma densities than they have had in the past if a reasonable simulation of the LEO environment is to be achieved. In Figure 3.20, the total current is shown as a function of the electron saturation current density. The curve obtained for the collisionless double layer is shown for a fixed ion current of $10\,mA$ while the quasineutral model and the anisotropic contactor model are shown for a fixed ion current of $1\,A$. This figure compares the realistic range of operation for the three models in typical ambient electron saturation current densities. A significant feature of this figure is that as the source varies by two orders of magnitude, the total current collected varies by only a factor of 1.6 for the collisionless double layer model. This would seem to invalidate one of the conclusions made by Martinez-Sanchez and Hastings [52] that plasma contactors would not be useful on the nightside of an equatorial low earth orbit because the collected current would drop to almost nothing. Here the double layer moves

out as the electron pressure drops so that the collected electron current is almost the same.

On the other hand, as seen in Section 3.2 when the anisotropic contactor model is reviewed, the electron current has a stronger dependence on the electron saturation current density when the electron Larmor radius is small compared to the radius of the contactor cloud. The electrons then reach the anode by diffusing across the magnetic field collisionally. In that regime, which is more relevant for high current plasma contactors in low earth orbit, the collected electron current is substantially higher on the dayside than on the nightside. Figure 3.20 shows that the total current is about 4 times higher, and the collected electron current is about 10 times higher, on the dayside ($J_e^\infty \approx 2 \times 10^{-2}\, A/m^2$) than on the nightside ($J_e^\infty \approx 2 \times 10^{-4}\, A/m^2$).

In Figure 3.21, the current voltage characteristic is shown for the range of electron saturation current densities. At constant current in the milliampere range, the voltage is seen to vary by about a factor of 3 for the two order of magnitude variation in source for the collisionless double layer. At constant voltage in the $100\,V$ range, the current varies by about a factor of 3 for the two orders of magnitude source variation. Ampere range currents, mainly collected electron current, require a potential drop of thousands or tens of thousands of volts, no matter what the level of electron saturation current.

With these results, one can calculate the current that could flow through a tether using a plasma contactor. The total potential drop ϕ_{total} across the contactor, tether, load, and electron gun is fixed by the length l of the tether, the earth's magnetic field $B_o = 0.33 \times 10^{-4}\, T$, and the orbital velocity of the spacecraft $v_o = 8\, km/s$. For $L = 20\, km$, one finds $\phi_{total} = v_o B_o L = 5333\, V$. The potential across the load is $\phi_{load} = R_{load}(I_i + I_e)$, where R_{load} is the load impedance. The potential across the tether is $R_t(I_i + I_e)$, where one can take the tether impedance $R_t = 200\,\Omega$. The radiation impedance [40] could be included, but this is typically only about 10Ω, so may be neglected compared to the tether impedance. If one assumes an average ionosphere with $J_e^\infty = 2 \times 10^{-3}\, A/m^2$, a good fit to the numerical results in Figure 3.21 is $\phi_o = b(I_i + I_e)^{0.88}$ where $b = 6.1 \times 10^3$. E_{ion} is the ionization energy of the dominant neutral gas present in

Table 3.2: Load power against efficiency of double layer contactor, modelled with Parker-Murphy condition imposed on outer radius of double layer

η	$I_i(A)$	ξ	$I(A)$	$P_{load}(kW)$
0.1	0.015	49	0.73	0.4
0.3	0.011	51	0.54	0.91
0.5	0.0069	54	0.9	1.06
0.7	0.0035	59	0.21	0.86
0.9	0.0008	70	0.06	0.31

the plasma cloud and $E_{ion} = 45\,V$. For a given load R_{load}, the current $I = I_i + I_e$ may be found by solving

$$\phi_{total} = R_{load}I + R_tI + bI^{0.88} + E_{ion} \tag{28}$$

and one may then find the power across the load $P_{load} = R_{load}I^2$, and the efficiency $\eta = R_{load}I/\phi_{total}$, as functions of R_{load}. Table 3.2 shows P_{load}, and ξ as functions of the efficiency $\eta = R_{load}I/\phi_{total}$.

Note if one were not to employ the Parker-Murphy condition in the absence of collisions, the electrons will be effectively unmagnetized all the way to the anode only if at every radius r either

$$v/\omega_{ce} > r \tag{3.28}$$

i.e. the electron Larmor radius is greater than r, or

$$d\phi/dr > (v/c)B \tag{3.29}$$

In Eq. 3.28 and Eq. 3.29, the electron velocity v is $(e\phi(r)/m_e)^{1/2}$, the velocity the electron gained falling through the potential, assumed to be much greater than its initial thermal velocity $(T_{ea}/m_e)^{1/2}$. The effective outer radius of the double layer, r_o, which determines the electron current collection

$$I_e = 2\pi r_o^2 e n_{ea}(T_{ea}/(2\pi m_e))^{1/2}, \tag{3.30}$$

is the largest radius r at which Eq. 3.28 and Eq. 3.29 are satisfied.

Inside the double layer, $r_o > r > r_i$, where v is small and $d\phi/dr$ is large, Eq. 3.29 is more easily satisfied than Eq. 3.28, while inside the contactor cloud ($r < r_i$), where v reaches its maximum possible value and $d\phi/dr$ is small, Eq. 3.28 is more easily satisfied. Therefore there are two necessary conditions that must be satisfied if the electrons are to be unmagnetized all the way to the anode. The first condition is that Eq. 3.28 must be satisfied at r_i,

$$(e\phi_o/m_e)^{1/2}/\omega_{ce} > r_i \tag{3.31}$$

The second condition is obtained by integrating Eq. 3.29 across the double layer, from r_i to r_o, since Eq. 3.29 must be true integrated across the double layer if it is true for every r within the double layer. Taking $\phi(r_i) \approx \phi_o$,this yields,

$$(e\phi_o/m_e)^{1/2}/\omega_{ce} > (r_o - r_i) \tag{3.32}$$

Note that Eq. 3.31 is the more stringent requirement for a thin double layer, while Eq. 3.32 is the more stringent requirement for a thick double layer. With $r_o \gg r_i$, this just reduces to:

$$(e\phi_o/m_e)^{1/2}/\omega_{ce} > r_o \tag{3.33}$$

Even Eq. 3.33 may not be a sufficient condition for the electrons to reach the anode without collisions, since the deflection of the electron by the magnetic field may make it miss the anode, even if the magnetic field does not bend its orbit around 180°. Similarly, Eq. 3.31 may not be a sufficient condition for the electrons to reach the anode, for a thin double layer.

However, as noted above, this is an optimistic estimate, based on the assumption that only Eq. 3.33 has be satisfied in order for the electrons to get to the anode without collisional transport. The maximum load power may be even lower than this. A lower limit on the maximum load power may be obtained by invoking the Parker-Murphy condition instead of Eq. 3.33 as the condition for the electrons to get to the anode. The resulting current voltage characteristics are shown in Fig. 3.21, and, at $J_e^\infty = 2 \times 10^{-3}\, A/m^2$, a good fit to the numerical results is $\phi_o = b(I_i + I_e)^{0.88}$. Table 3.2 shows the corresponding P_{load} and ξ a functions of η. The maximum load power at 90% efficiency is only $0.31\, kW$ in this case.

On the other hand, if the electrons lose even a small fraction of their energy due to collisions when they are in the double layer or contactor cloud, then they will not be able to escape again, and must eventually end up at the anode. The only question is whether they spend so much time bouncing around the double layer before reaching the anode that their space charge builds up sufficiently to shrink r_o, reducing the current. In short, finding a *sufficient* condition for the electrons to reach the anode is quite difficult, if there is a small degree of collisionality, and may require particle simulations that incorporate particle trapping. However, the Parker-Murphy condition is a robust and simple *necessary* condition; if it is not satisfied, then the electrons have small Larmor orbits within the contactor cloud, and a transport process is certainly required to get them to the anode. Accordingly, the theory must be expanded to include particle trapping at the juncture of the double layer and the core cloud. Such an addition requires time-varying computer simulations to track the particles and is not treated within the scope of this present work.

The maximum power to the load is 1.06kW, but this occurs when the efficiency is only 50%. As noted by Martinez-Sanchez and Hastings [52], in order for tethers to be competitive with other power systems in space, it is necessary for them to operate at high efficiency, at least 80% or 90%. This is because all of the power has to be made up by periodically boosting the tether, but only the load power can be effectively used. If desired system efficiency is 80%, then the maximum load power one can obtain is only 0.5kW. This maximum power may in fact be much less, since Eq. 3.5 is not a sufficient condition for electrons to get across the magnetic field to the anode [57], and is known to be far from sufficient in the regime where $r_o \gg r_i$ which is true at the maximum power.

Figures 3.12- 3.16 plot data sets comparable to Figures 3.17-3.21, where the electron gyroradius is set equal to the outer radius of the double layer. These results are presented to make the point that to achieve effective power generation with a plasma contactor, the virtual anode radius of the contactor must exceed the ambient electron gyroradius as well as to indicate the difference between including and not including the angular momentum consideration with the collisionless double layer model in space. The condition for the electrons to

reach the anode taking into account their deflection by the magnetic field is that found by Parker and Murphy [57] and must be considered, making the results presented in Figures 3.17-3.21 far more applicable to the LEO regime than those presented for the gyroradius limit case.

One may conclude that it is not possible to design a high power contactor which draws electrons straight across a double layer without collisions. Instead, designs should be considered where collisions or, more realistically, effective collisions due to instabilities of some kind transport electrons across the magnetic field to the anode. The following section considers the possibility of joining a collisional quasineutral ignited plasma to a collisionless double layer as a step towards completing the contacting process model.

Necesary Conditions for Development of Ignited Flow

For a partially ionized plasma, it is possible to include the effect of ionization and to show when the plasma will ignite. If one assumes that the neutral density varies with radius as $n_n(r) = n_n(r_{anode})(r_{anode}/r)^2$ and applies conservation of mass from r_{anode} to r_i then one can obtain

$$I_e(r) = I_e(r_i)\exp(\gamma(\Delta\phi)[\frac{r_{anode}}{r} - \frac{r_{anode}}{r_i}]) \tag{3.34}$$

where $\gamma(\Delta\phi) = n_n(r_{anode})r_{anode}\sigma(\Delta\phi + T_{ea})$. From conservation of current, the gain is

$$\xi = 1 + \frac{(\xi(r_i) - 1)\exp(\gamma(1 - \frac{r_{anode}}{r_i}))}{1 + (\xi(r_i) - 1)(1 - \exp(\gamma(1 - \frac{r_{anode}}{r_i})))} \tag{3.35}$$

where $\xi(r_i) = I/I_i(r_i)$. The ion current at the anode of the source in terms of the ion current just inside the double layer is [29]

$$\frac{I_i(r_{anode})}{I_i(r_i)} = 1 + (\xi(r_i) - 1)(1 - \exp(\gamma(1 - \frac{r_{anode}}{r_i})) \tag{3.36}$$

In order to interpret the calculations in Figure 3.17 with ionization present, one must interpret the ion current in the ordinate as $I_i(r_i)$. The relationship in terms of the ion current emitted at the source is given above. From Figure 3.17, it

is obvious that there may be no solution for an ion current for a given ion current at the double layer. Physically this will occur when there is so much neutral gas that the flow mixture of neutrals and plasma particles ignites, precipitating an avalanche of ion current. At this point the collisionless space-charge-limit double layer theory will break down. By setting the source ion current to zero, one can obtain this critical neutral density for ignition as

$$n_{critical} = \frac{\ln(1+1/\xi)}{1 - r_{anode}/r_i} \frac{1}{r_{anode}\sigma} \tag{3.37}$$

If one relates the source neutral density to the ion flow rate and initial fractional ionization, f_i, ignition is obtained for

$$I_i(r_i) > \frac{4\pi r_{anode}^2 c_s e f_i}{1 - f_i} n_{critical} \tag{3.38}$$

In Figure 3.17, this critical ion current is plotted against gain for $r_{anode} = 0.1\,m$, $c_s = 4.89 \times 10^3\,m/s$, $\sigma = \sigma_{max} = 3.21 \times 10^{-20}\,m^{-2}$ (for ionization of Argon) and $f_i = 10^{-4}$, a typical ionization fraction for hollow cathode devices. For ion current and gain pairs which fall to the right of the curve on the figure, the neutral flow will spontaneously ignite. A double layer structure of some asymmetric shape will then establish itself given only a very small seed ionization. This spot mode behavior had been described previously in Section 2.6. In the next section, a model is outlined that will examine the efficacy of ionizing expelled neutrals within the core cloud to enhance gain.

3.1.5 Results of Combining Collisional Quasineutral Core Region with Collisionless Spherical Double Sheath Transition Region

In this section, a model is used to demonstrate that no benefits are derived when a contactor system relies on ionization of expelled neutrals to provide high overall system gain. To prove this point, the quasineutral collisional contactor model is matched in a new model with the collisionless space-charge-limited spherically symmetric double layer model. This combination model is rather limited since it lacks the capacity to invoke collisionality in the double layer and

it is known that there is a clear need to turn on a collisional double layer when the ignition limit is reached. An additional deficiency in this approximation is that the ambient electrons are accelerated directly by the double layer and no presheath is considered.

So, to demonstrate where this combination model loses its validity, *i.e.* where the double layer becomes collisional, the values of $n_{critical}$ and the critical ion current from Eqs. 3.37 and 3.38 are calculated along with ξ, $r_{core} = r_i$, the mass flow rate $\dot{m}$, the potential drop $\Delta\phi$, and the outer edge of the double layer r_o for a given set of parameters. This selected set of parameters fixed the contactor ion current, the initial fractional ionization rate, the ambient electron temperature, initial contactor electron temperature, the ambient ion density, initial density of electrons at the contactor orifice, and the initial potential.

The numerical solution of this problem was achieved by tailoring an existing computer program [10] that iterates to solve for a self-consistent potential profile in a turbulent and collisional quasineutral core and to then match the electron current at the core radius of the quasineutral region to the electron current current collected across the collisionless double layer. This equivalence implies that the core radius of the quasineutral cloud then equals the inner radius of the double layer. The contactor emitted ion current, I_{ic}, is fixed and then the collected electron current at r_o is input as an initial condition to the iterative scheme employing the collisionality stopping condition [10]. When that boundary is reached, the total gain of the system is determined and input to the collisionless double layer model. This gain then uniquely determines a matching double layer solution if there one exists for the given set of parameters. If the double layer solution exists, the total solution is calculated and output.

In solving for the ionospheric parameters of interest using an Argon plasma contactor, it was determined that there was a very limited range of ion currents for which a solution could be obtained. One reason for this is that it is difficult for the quasineutral core cloud to achieve a gain high enough to even match the lowest gains of the collisionless double layer. Without a gain match, the model cannot proceed. For the case studied, the following initial plasma parameters were held fixed for each case studied,

$$
\begin{aligned}
T_{ea} &= 0.1\,eV \\
T_{ec_o} &= 0.5\,eV \\
T_{ic} &= 0.1\,eV \\
n_{ia} &= 2.0 \times 10^{11}/m^3 \\
n_{ec} &= 0.0 \times 10^{11}/m^3
\end{aligned}
$$

Then the initial ionization fraction and contactor ion current were set for each case in which the collected electron current was varied to determine the effects of ionization on the neutral mass flow rate, the size of the double layer, the position of the core radius/inner radius of the double layer, and the potential drop. Cases in which solutions were achievable were rerun with initial guesses of collected electron current varied over a range of four orders of magnitude to determine the stability of the model in its search for the proper solution. In all solved cases for a given set of initial conditions, the solutions varied at most from one another by $\simeq 2\%$. The cases that were insoluble were those in which I_{ic} fell outside of the range of $7.5 \times 10^{-7} < I_{ic} \leq 5. \times 10^{-5}\,A$.

Figure 3.9 shows the relationship between overall system gain and the emitted contactor ion current. This one curve is roughly the same for all four of the initial ionization fractions, f_i, used in the numerical solution. Those ionization fractions used were $1.0 \times 10^{-4}, 1.0 \times 10^{-2}, 1.0 \times 10^{-1}$, and$2.5 \times 10^{-1}$. This result clearly indicates that the current collected is produced by ionization within the inner plasma core region and the initial ionization fraction therefore has little effect. It is evident that ionizing the neutral gas external to the contactor provides no tangible benefits to the system since the gain is not enhanced for varying degrees of ionization within the cloud. The potential drop from the anode to contact with the ambient plasma is plotted in Figure 3.10. This plot illustrates the point once more that there is truly no benefit to be gained through ionization of expelled neutrals; the potential drop is approximately as it was for the earlier collisionless model which was proven to be inefficient and ill-suited to adaptation for a significant fraction of the LEO regime. The degree of ionization could be determined from the densities and currents calculated in the core region.

This model's solutions were also examined to determine if the critical neutral density had been reached and if the critical ion ignition current had been

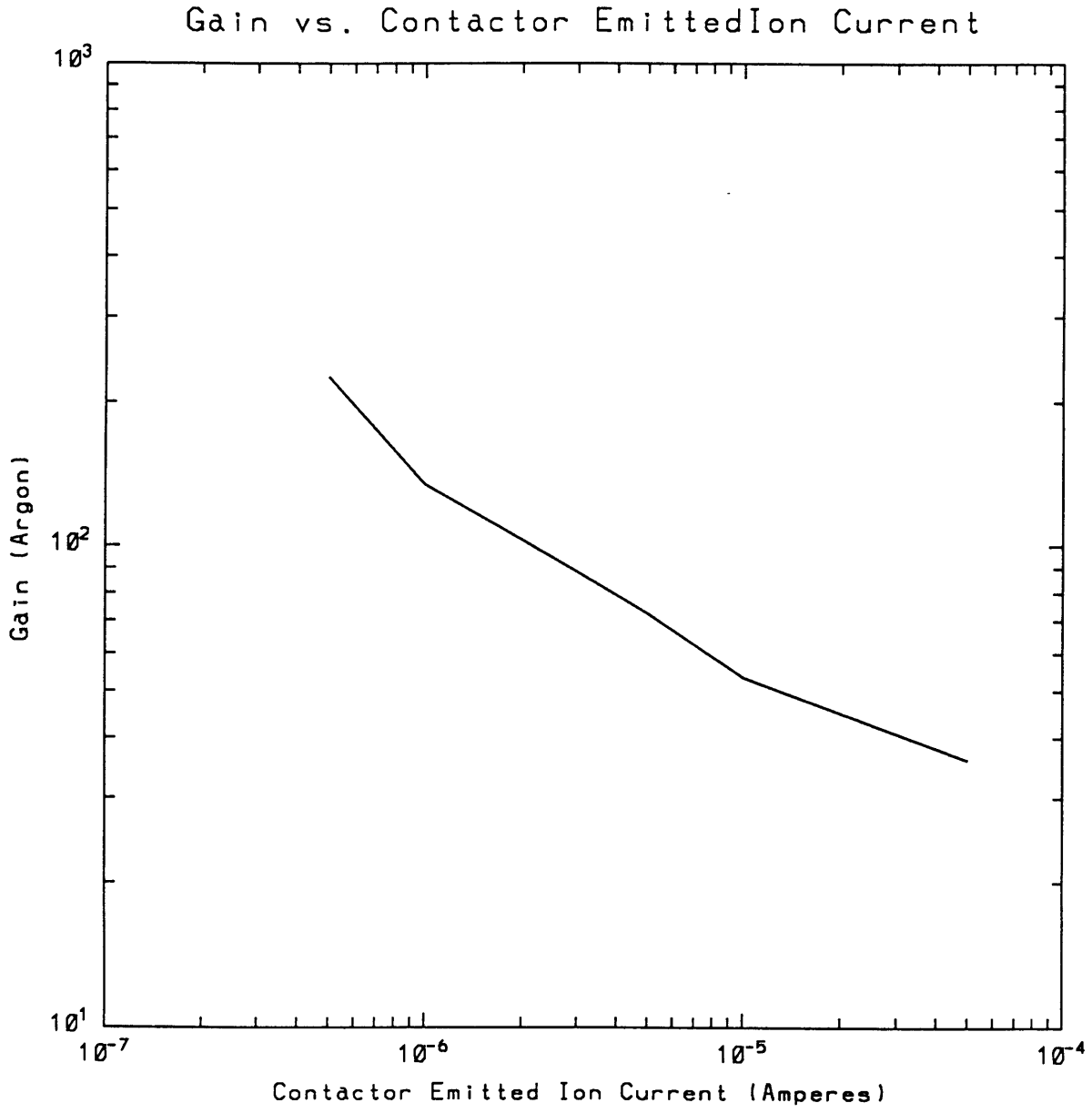

Figure 3.9: Combined Collisional Quasineutral Core with Collisionless Double Layer Transition Region - Gain vs. Contactor Ion Current

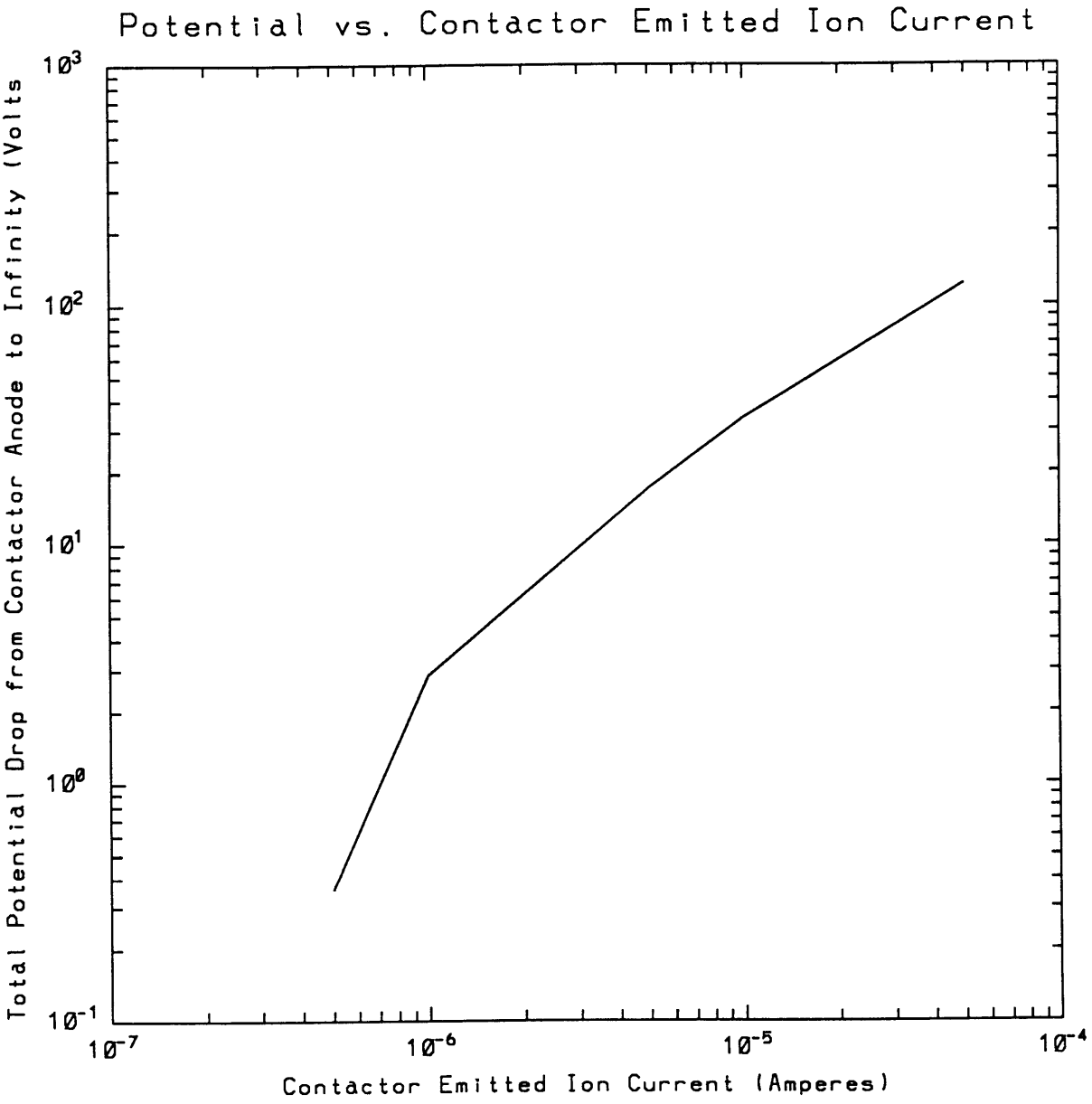

Figure 3.10: Combined Collisional Quasineutral Core with Collisionless Double Layer Transition Region - Potential vs. Contactor Ion Current

Table 3.3: Combination Model Ignited Plasma Parameters

$I_i(A)$	f_i	$r_{core}(m)$	$r_o(m)$	$\dot{m}(kg/s-m^2)$	$n_{critical}(m^{-3})$	$I_{i_{crit}}$
$5.\times10^{-7}$	0.1	0.1025	0.1401	2.04×10^{-7}	5.687×10^{19}	196.8600
$1.\times10^{-6}$	0.1	0.1125	0.3750	3.09×10^{-7}	2.092×10^{19}	72.4280
$5.\times10^{-6}$	0.1	0.1825	2.2813	3.61×10^{-7}	9.566×10^{18}	33.2110
$1.\times10^{-5}$	0.1	0.2225	6.3571	3.99×10^{-7}	1.068×10^{19}	36.9750
$5.\times10^{-5}$	0.1	0.3475	69.5000	5.23×10^{-7}	1.653×10^{19}	57.2200
$5.\times10^{-7}$	0.0001	0.1025	0.1414	2.27×10^{-4}	5.687×10^{19}	0.1772
$1.\times10^{-6}$	0.0001	0.1125	0.3629	3.43×10^{-4}	2.092×10^{19}	0.0652
$5.\times10^{-6}$	0.0001	0.1825	2.2813	4.01×10^{-4}	9.566×10^{18}	0.0298
$1.\times10^{-5}$	0.0001	0.2225	6.3571	4.43×10^{-4}	1.068×10^{19}	0.0333
$5.\times10^{-5}$	0.0001	0.3475	69.5000	5.81×10^{-4}	1.653×10^{19}	0.0520

exceeded. The velocity of the neutrals, v_n, was taken to be that expressed in Section 2.3.2. Given the initial conditions above, $v_n = 489.5m/sec$ for the test cases. With this value and the known mass of the Argon ion, Eq. 2.70 is solved for the neutral mass flow rate. Table 3.3 shows the calculated neutral mass flow rate for selected initial conditions I_i and f_i and calculated r_{core} along with the critical neutral density and critical ion ignition current for the listed case. From the data presented in Table 3.3, it can be seen that the impact of varying the initial ionization fraction is seen only in the mass flow rate which then impacts the critical ignition parameters. It is readily apparent where the deficiencies in this model exist if one examines the thicker double layers that develop for the higher emitted ion currents, which clearly violate the requirement that the mean free path of the electrons for the ionization of neutrals be greater than the width of the double layer, if the double layer is to remain collisionless. One should also note the difference between this model's calculated critical neutral density and that determined by Cooke and Katz [23]; their values for an ionized plasma are on the order of 10^{16} particles per volume element.

Note that this model was driven by the need to maintain the plasma pressure balance and match boundary currents. Ideally, this transition should be achieved much more smoothly at the r_{core} singularity. Considerable difficulty exists in

matching the quasineutral core with its typically low gain and the double layer with its typically high gain, indicating that it is not particularly useful to attach a collisionless double layer as a transition region to a collisional quasineutral cloud when attempting to model core cloud ionization and the connection process of this core cloud to the ambient plasma surrounding it. This underscores the need for a model of a collisional double layer, possibly a critical need for the successful application of the anisotropic contactor model under certain operating conditions.

3.2 Anisotropic Contactor Model

3.2.1 Derivation

Recent work [29] has produced a new model that enables one to combine the virtues of the collisional quasineutral theory with those of the spherically symmetric space-charge-limited double layer theory in order to more closely model the plasma contacting process. In the region where the effective electron collision frequency ν_e is less than the electron cyclotron frequency ω_{ce}, the contactor cloud will be anisotropic. The cloud will extend further in a direction along the magnetic field than across the magnetic field. Therefore, the cylindrical coordinates z and r are used, where r now refers only to the distance across the magnetic field, not to the total distance from the anode as it did in previous sections. It is assumed that the plasma density in the cloud is still substantial enough to dominate the motional electric field so the cloud will be cylindrically symmetric. At even greater distances from the anode, the effects of the orbital motion induced electric field will become important, and the cylindrical symmetry will be broken. In this region the electron velocity will be mostly azimuthal, at the drift velocity

$$v_d = \frac{e}{m_e \omega_{ce}} \frac{\partial \phi}{\partial r} - \frac{1}{m_e \omega_{ce}} \frac{\partial T_e}{\partial r} - \frac{T_e}{m_e \omega_{ce} n_e} \frac{\partial n_e}{\partial r} \tag{3.39}$$

For parameters of interest, this drift velocity is much greater than the radial

flow velocity of the emitted ions, which are effectively unmagnetized since it is assumed that the scale lengths are all much less than an ion Larmor radius. The velocity difference between the electrons and ions will then be nearly in the azimuthal direction. This relative cross-field drift velocity of magnetized electrons and unmagnetized ions can give rise to several instabilities, among them the ion acoustic instability for both $k_\perp \rho_e > 1$ and $k_\perp \rho_e < 1$, the Buneman instability, the electron cyclotron drift instability, the modified two-stream instability, and the lower hybrid drift instability. The instability that dominates depends on such parameters as T_e/T_i, v_d/c_s, v_d/v_the, β, ω_{pe}/ω_{ce}, and v_d/v_A, where v_d is the relative drift velocity, v_{the} is the electron thermal velocity, v_A is the Alfven speed, and β is the plasma/magnetic energy density ratio and all other parameters have been defined previously in this work.

It should be noted here that in Urrutia's and Stenzel's experiments, the ion plasma frequency is seen to drive the two stream instability and the ion acoustic instability. In the event that the contactor electron density and the incoming ambient electron density are comparable and both populations have comparable speeds, a two stream instability could result from this effect. Such a driver for the two stream instability is unlikely, however, since the small number of electrons that exit the plasma contactor should be quite cold in comparison to the ambient electrons which have been accelerated through the Bohm presheath. It is also useful to note that the Buneman instability cannot contribute steady-state anomalous resistivity in a one-dimensional system, so that previous treatments that have relied on this mechanism to achieve the desired level of collisionality within the plasma are in error. Instead, a two-dimensional system should be adopted as in this anisotropic contactor model. Steady-state resistivity is then due to the ion acoustic instability primarily.

These instabilities will give rise to turbulent azimuthal electric fields, which will exert an azimuthal drag force $\nu_e m_e v_d$ on the electrons, giving rise to an inward radial drift at velocity

$$v_r = \frac{\nu_e}{\omega_{ce}} v_d. \tag{3.40}$$

It can be assumed that the potential drop in the plasma cloud is much,

much greater than the ion temperature T_i, which is typically only a few eV. Since, as will be shown later, T_e tends to be only a few times less than ϕ_o, this implies that $T_e/T_i \gg 1$, except perhaps near the edge of the cloud. Also $c_s \ll v_d \ll v_e$. In these circumstances, one expects the $k_\perp \rho_e > 1$ ion acoustic instability to dominate. This is the same as the ion acoustic instability in an unmagnetized plasma. The effective collision frequency ν_e for this instability in its nonlinear saturated state scales with density like ω_{pe}, and is independent of c_s/v_d for $c_s \ll v_d$. But there is some uncertainty as to its dependence on T_e/T_i and v_d/v_e. As a first cut at this problem, it was simply assumed that

$$\nu_e \approx 10^{-2}\omega_{pe}, \tag{3.41}$$

independent of the other parameters. The method to be used to find analytic expressions for $\phi(r,z)$ and the collected electron current may also be applied using more realistic expressions for ν_e.

The divergence of the radial flux of electrons due to ν_e and the radial electric field and temperature and density gradients must be balanced by an inward flux of electrons along the magnetic field, neglecting ionization and recombination,

$$\frac{1}{r}\frac{\partial}{\partial r} r n_e v_r + \frac{\partial}{\partial z} n_e v_z = 0. \tag{3.42}$$

At high densities, with $\omega_{pe} \gg \omega_{ce}$, the mean free path of electrons will be short compared to the length of the contactor cloud, and the velocity v_z along the magnetic field may also be found by balancing the force from the electric field $e\partial\phi/\partial z$ with the drag force $m_e\nu_e v_z$. In this case Eq. 3.42 will generally not be separable in r and z, and it is necessary to solve a fully two-dimensional partial differential equation, as opposed to the one-dimensional differential equation solved by Parker and Murphy in their assumption of an axially symmetric potential function [57]. The boundary conditions will be $v_r = 0$ and $\phi = 0$ at the same surface and the flux of electrons across this particular surface must be equal to the flux of the electron saturation current of the ambient plasma along the magnetic field impinging upon the outside of the surface. The potential $\phi(r,z)$ can be assumed quasineutral everywhere.

Since the position of the $\phi = 0$ surface is not known in advance, this would be

a difficult numerical problem. The ambient plasma in the LEO regime has much lower density, $\omega_{pe} \leq \omega_{ce}$, so that this would also be true throughout most of the area occupied by a space-based contactor cloud, which, as is shown, would extend along the magnetic field to a distance where the cloud density is comparable to the ambient density. In this case, the electrons flow freely along the magnetic field lines and a different model is then needed. If the total potential drop ϕ_o between the anode and the ambient plasma is greater than T_{ec} and T_{ia}, then double layers form at a distance z_o along the magnetic field in both directions, where

$$J_i = \frac{I_i g(z_o)}{2\pi z_o^2} = \left(\frac{m_e}{m_i}\right)^{1/2} J_e^{\infty} \tag{3.43}$$

for thin double layers, just as in the unmagnetized collisionless case. Here $g(z)$ is a factor to take into account that the ions are focussed by the potential $\phi(r,z)$ if it is not spherically symmetric. Although the flow of electrons along the magnetic field is nearly collisionless, it is assumed that there is enough drag to slow down the incoming electrons slightly. They do then not escape out the other end of the contactor cloud, but become trapped in the cloud. Only a small amount of drag is needed for this trapping effect to occur if $\phi_o \gg T_{ea}$. At $z = \pm z_o$, the flux of electrons along the field must then satisfy the boundary condition

$$n_e v_z = \mp J_e^{\infty}/e. \tag{3.44}$$

Because the flow of electrons across the magnetic field is collisional, no double layer exists in the radial direction. For fixed $|z| < z_o$, $\phi(r,z)$ must decrease smoothly to zero at some $r_1(z)$, satisfying quasineutrality along the profile. For fixed r along a given field line, $\phi(r,z)$ will not go to zero for $|z| < z_o$ as long as $\phi(r, z=0) > T_e(r)$. If ϕ_o is at least a few times greater than T_e, then $\phi(r, z=0)$ will be greater than T_e for all r significantly far from $r_1(z=0)$. It follows that r_1 is nearly independent of z. The contours of $\phi(r,z)$ and the flow of ions and electrons, are shown schematically in Figure 3.11.

This means that Eq. 3.42 will be separable in r and z. The boundary conditions in r are

$$\phi(r = r_{anode}, z) = \phi_o + T_e \ln(n_e(z)/n(z=0)) \tag{3.45}$$

$$\phi(r = r_1) = 0 \tag{3.46}$$

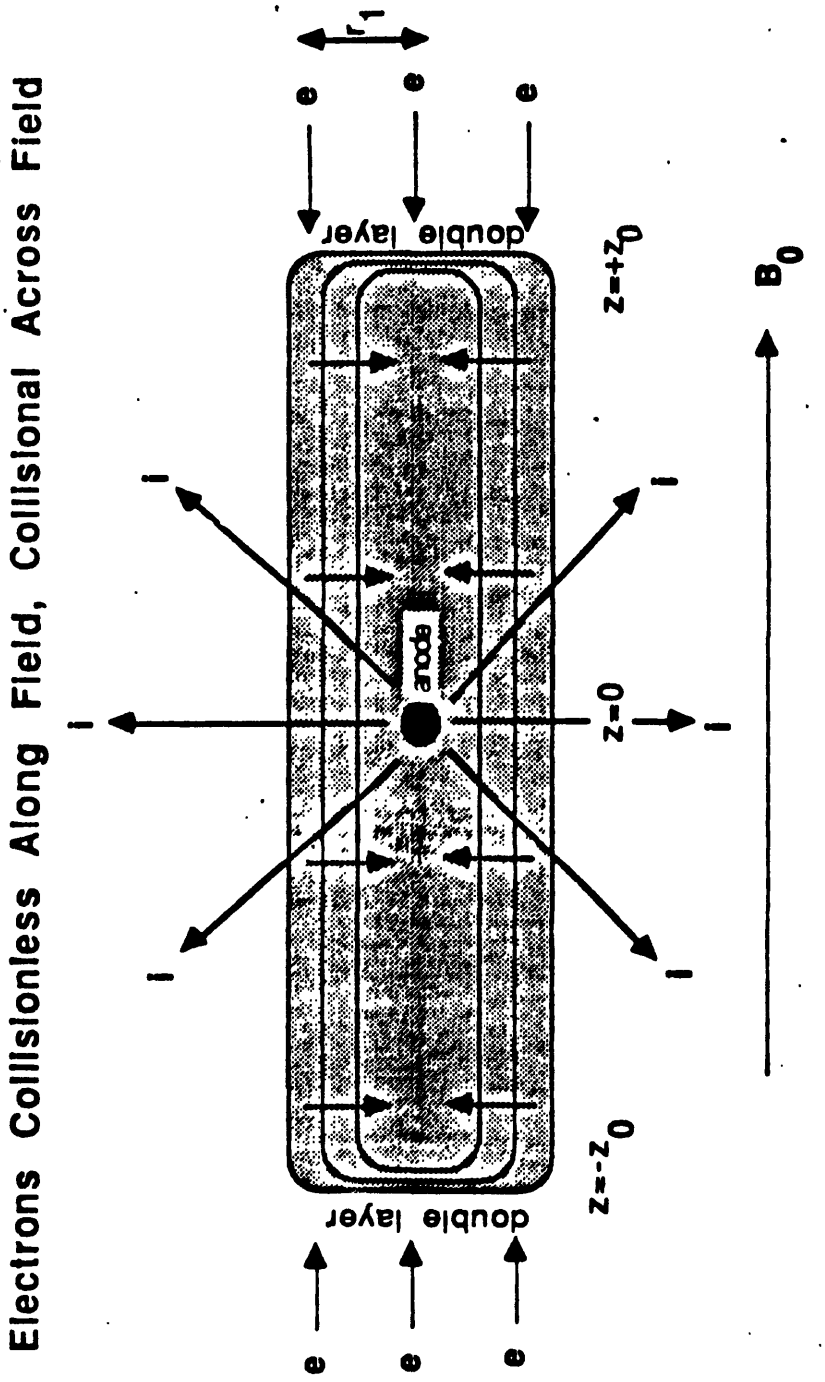

Figure 3.11: Anisotropic Contactor Model, with double layers oriented along the magnetic field

$$\frac{\partial \phi}{\partial r} = \frac{1}{e}\frac{\partial T_e}{\partial r} \tag{3.47}$$

Eq. 3.47 holds true at $r = r_1$, a condition that follows from the facts that $v_r = 0$ outside the contactor cloud, and that there is no source or sink of electrons at $r = r_1$. Therefore, v_r must vanish at r_1 just inside the contactor cloud. Eq. 3.39, with $T_e = 0$, and Eq. 3.40 then yield Eq. 3.47.

3.2.2 Electron Temperature in the Anisotropic Contactor Model

Before proceeding with the calculation of the potential profile $\phi(r)$, it must be considered whether it is justifiable to assume that ϕ_o is at least a few times greater than T_e. The electron temperature profile $T_e(r)$ is determined by the balance between convection, conduction, and ohmic heating. Ionization and line radiation, which should only be important near the anode, and electron heat loss due to boiling out along the magnetic field are all neglected.

$$\frac{-3}{2}v_r\frac{\partial T_e}{\partial r} + \frac{1}{rn_e}\frac{\partial}{\partial r}r\kappa\frac{\partial T_e}{\partial r} + ev_r\frac{\partial \phi}{\partial r} + \frac{J_e^\infty}{n_e z_o}\left(\phi - \frac{T_e}{e}\right) = 0 \tag{3.48}$$

Here κ is the cross-field thermal conductivity term, which is dominated by turbulence, as is the drag term. In general,

$$\kappa = \frac{Cn_eT_e\nu_e}{m_e\omega_{ce}^2}, \tag{3.49}$$

where C is a constant dependent upon the details of the effective collisions causing the heat transport. For electron thermal conductivity across a magnetic field due to Coulomb collisions, $C = 4.7$ for example.

The boundary conditions are

$$T_e = 0 \quad at \quad r = r_1 \tag{3.50}$$

$$\kappa\frac{\partial T_e}{\partial r} = \frac{Q}{4\pi r_{anode} z_o} - n_e v_r T_e \quad at \quad r = r_{anode}, \tag{3.51}$$

where Q is the heat flux entering the anode. This is generally greater than the convective heat flux into the anode, the second term on the right hand

side of Eq. 3.51, because $\langle v_x^3 \rangle$ for a half-Maxwellian is greater than $\langle v_x^2 \rangle \langle v_x \rangle$. Consequently, $\partial T_e / \partial r > 0$ at r_{anode}. Because $T_e = 0$ at $r = r_1$, $\partial T_e / \partial r$ must change sign between r_{anode} and r_1 so that one may estimate that the second term in Eq. 3.48 is of order $-\kappa T_e / n_e r_1^2$. Using Eqs. 3.39, 3.40, and 3.49 one finds,

$$v_r = \frac{\kappa}{n_e T_e C} \left(e \frac{\partial \phi}{\partial r} - \frac{\partial T_e}{\partial r} \right) \tag{3.52}$$

Then the first term in Eq. 3.48 is of order $\pm \kappa e \phi / C n_e r_1^2$, and the third term is of order $+\kappa e^2 \phi^2 / C n_e T_e r_1^2$. From Eqs. 3.42 and 3.44, the fourth term in Eq. 3.48 is comparable to and of like sign to the third term.

If $C \leq 1$, it follows that the second and/or the first term must balance the third and fourth terms, so T_e is of order $e\phi$. If $C \gg 1$, then the second term alone must balance the third and fourth terms, and $T_e \approx e\phi / C^{1/2} \ll e\phi$. The assumption that T_e is at least a few times less than ϕ is thus valid if C is somewhat greater than one. This is true for Coulomb collisions. Whether it is true for ion acoustic turbulence is an open question that is beyond the scope of this present work. If κ is dominated by an energetic tail of the electron distribution, caused perhaps by electrons collected from the ambient plasma which have not yet thermalized, then $C \gg 1$.

3.2.3 Potential Profile and Cloud Radii

To calculate the potential profile, $\phi(r)$, first integrate Eq. 3.42 over z from $-z_o$ to $+z_o$, and use Eq. 3.44 to eliminate v_z, as shown in

$$\int_{-z_o}^{+z_o} dz \frac{1}{r} \frac{\partial}{\partial r} r n_e v_r = 2 J_e^{\infty}. \tag{3.53}$$

To obtain an expression for n_e, which appears explicitly in Eq. 3.53 and also implicitly through the dependence of ν_e on ω_{pe}, use quasineutrality to obtain,

$$n_e = n_i = (4\pi)^{-1} I_i m_i^{1/2} e^{-3/2} (r^2 + z^2)^{-1} g(r,z) (\phi_o - \phi)^{-1/2} \tag{3.54}$$

The expression for n_i in Eq. 3.54 comes from the fact that the ions are unmagnetized and expanding in a spherically symmetric manner from the contactor

anode. The factor $g(r,z)$ takes into account the focussing of the ions by the asymmetric potential profile, $\phi(r,z)$. Using Eq. 3.40 for v_r, Eq. 3.41 for ν_e, Eq. 3.54 for n_e, $B_o = 0.3\,G$, ion atomic weight $\mu = m_i/m_p$, and expressing I_i in amps, J_e^∞ in A/m^2, and ϕ and ϕ_o in volts, Eq. 3.53 becomes,

$$\int_{-z_o}^{+z_o} dz \frac{1}{r}\frac{\partial}{\partial r}\left[r(\phi_o-\phi)^{-3/4}(r^2+z^2)^{-3/2}g(r,z)\frac{\partial\phi}{\partial r}\right] = -12 I_i^{-3/2}\mu^{-3/4}J_e^\infty \quad (3.55)$$

Because $(\phi_o - \phi)$ and $\partial\phi/\partial r$ are fairly independent of z, and the integrand is most strongly weighted near $z = 0$, ϕ and $\partial\phi/\partial r$ are replaced by their values at $z = 0$, so they can be removed from the integral. Similarly, one can set $g(r,z) \approx 1$, since in a self-consistent treatment of this problem, there cannot be a strong focussing effect in the region $z < r$, which happens to be where most of the contribution to the integral is. Then one can perform the integration over z,

$$\frac{\partial}{\partial r}\left[\frac{1}{r}(\phi_o-\phi)^{-3/4}\frac{\partial\phi}{\partial r}\right] = -12 r I_i^{-3/2}\mu^{-3/4}J_e^\infty \quad (3.56)$$

One can integrate Eq. 3.56 over r, using the boundary condition Eq. 3.47 to obtain the integration constant,

$$\frac{1}{r}(\phi_o-\phi)^{-3/4}\frac{\partial\phi}{\partial r} = 6 I_i^{-3/2}\mu^{-3/4}J_e^\infty(r_2^2 - r^2), \quad (3.57)$$

where

$$r_2^2 = r_1^2 + \frac{1}{6}r_1^{-1}\phi_o^{-3/4}e^{-1}\frac{\partial T_e}{\partial r}I_i^{3/2}\mu^{3/4}(J_e^\infty)^{-1}. \quad (3.58)$$

One can integrate over r again, using Eq. 3.45 at $z = 0$ to obtain the integration constant,

$$(\phi_o-\phi)^{1/4} = 0.5 I_i^{-3/2}\mu^{-3/4}J_e^\infty(2r_2^2r^2 - r^4). \quad (3.59)$$

Finally, substituting Eq. 3.46 into Eq. 3.59 to obtain an equation for r_1

$$\phi_o^{1/4} = 0.5 I_i^{-3/2}\mu^{-3/4}J_e^\infty\left[r_1^4 + \frac{1}{3}r_1\phi_o^{-3/4}e^{-1}\frac{\partial T_e}{\partial r}I_i^{3/2}\mu^{3/4}(J_e^\infty)^{-1}\right]. \quad (3.60)$$

If, as has been assumed, $T_e \ll e\phi_o$, then the second term in brackets may be neglected and,

$$r_1 = 1.2\phi_o^{1/16}I_i^{3/8}\mu^{3/16}(J_e^\infty)^{-1/4}. \quad (3.61)$$

Note that r_1 has an extremely weak dependence on ϕ_o. For a given range of ϕ_o values, for example $10\,V < \phi_o < 1000\,V$, an Argon plasma and the average LEO

electron saturation current density, $J_e^\infty = 2\,mA/m^2$,

$$r_1 \approx 15 I_i^{3/8}, \tag{3.62}$$

and

$$I_e = 2\pi r_1^2 J_e^\infty \approx 2 I_i^{3/4}. \tag{3.63}$$

In general the total current $I = I_i + I_e$ is given by,

$$I = I_i + 8(J_e^\infty)^{1/2} I_i^{3/4} \mu^{3/8} \phi_o^{1/8}. \tag{3.64}$$

A substantial ambient electron current can be collected for values of ϕ_o and total current that are of interest for tethers. For 1 A of Argon at $J_e^\infty = 2\,mA/m^2$, for example, a gain is obtained equal to $I/I_i = 3$. As a second example consider $0.5\,A$ of Xenon, at a typical dayside electron saturation current density of $J_e^\infty = 20\,mA/m^2$. For the conditions presented in the second example, $I/I_i = 12$. These gains, although not as large as the gains that were found with a completely collisionless double layer model, can still make a significant contribution to operation of tethers for power generation.

In Figure 3.20, the total current is shown for a fixed ion current of $1\,A$, as a function of electron saturation current, using Eq. 3.64, and is compared to the total current for the quasineutral model discussed in Section 2.3, and for the collisionless double layer model, using an ion current of $0.01\,A$. Note that the current from Eq. 3.64 is much more sensitive to the electron saturation current than in the case of the collisionless double layer model. In Figure 3.21, the current voltage characteristic is shown, from Eq. 3.64, for $J_e^\infty = 2\,mA/m^2$, and compared to the results from the isotropic quasineutral model and the collisionless double layer model for a range of electron saturation currents. For realistic potentials, less than $1000\,V$, the current from Eq. 3.64 is at least an order of magnitude greater than for the collisionless double layer model.

Table 3.4 shows the load power P_{load} against efficiency, using the same ambient plasma and tether parameters as in Table 3.2, but using Eq. 3.64 to relate I and ϕ_{anode}. In this case, the maximum power obtained at $\simeq 80\%$ efficiency is $12\,kW$, much higher than in in Table 3.2. Of course in a comparision with the collisionless double layer results, the energetic cost of producing more ion

Table 3.4: Load power against efficiency of anisotropic contactor

η	$I_i(A)$	ξ	$I(A)$	$P_{load}(kW)$
0.1	1	4.99	4.99	2.64
0.3	1	4.83	4.83	7.65
0.5	1	4.6	4.6	12.1
0.7	1	4.22	4.22	15.4
0.9	1	2.32	2.32	10.6

Table 3.5: Load power against efficiency of emitting an ion beam

η	$I_i(A)$	ξ	$I(A)$	$P_{load}(kW)$
0.1	22.64	1	22.64	12.1
0.3	17.56	1	17.56	28.1
0.5	12.48	1	12.48	33.3
0.7	7.4	1	7.4	27.7
0.9	2.3	1	2.3	11.2

current must be compared to the cost of the high potential associated with the space-charge-limited double layer.

Finally in Table 3.5, the power to the load is shown for a quasineutral model which just emits an ion beam or a double layer with ionization so that a large current flows for very low potential drop, *i.e.* $\Delta\Phi_{contactor} \simeq 0$, $\xi = 1$. At 90% efficiency this configuration, which makes no use of the ambient plasma, can generate only slightly higher power than the anisotropic contactor, and requires substantially higher emitted ion current. This shows that the anisotropic contactor could make a significant contribution to the operation of tethers for power generation.

3.2.4 Validity of Model

Overall, the anisotropic contactor model represents a much needed further step towards understanding the plasma contactor electron collection process. However, there are a few points that should be examined in future work with this model. The neglect of ionization and line radiation will turn out to have a significant impact if the value of r_i turns out to be very close to or equal to the anode. It has been seen through the use of the models in Sections 3.1.3 and 3.1.5 that the value of r_i can indeed be close to or equal to the anode radius. This case should be carefully assessed to determine the validity of assuming $T_e \ll e\phi_o$ when calculating the radius r_1.

Also, it should be considered that the electron-ion instabilities that can arise in this type of plasma could result in the acceleration of ambient electrons to form a high energy component that acts almost as a beam as it enters the double layer. Such accelerations can occur due to local trapping of the electrons in the double layer. This beam-type of instability would be undesirable within the plasma contacting electron collection process since it results in an enhanced mean free path for the streaming electrons, causing them to undergo less collisions [4]. The plasma then becomes less collisional and the electron collection process is hindered.

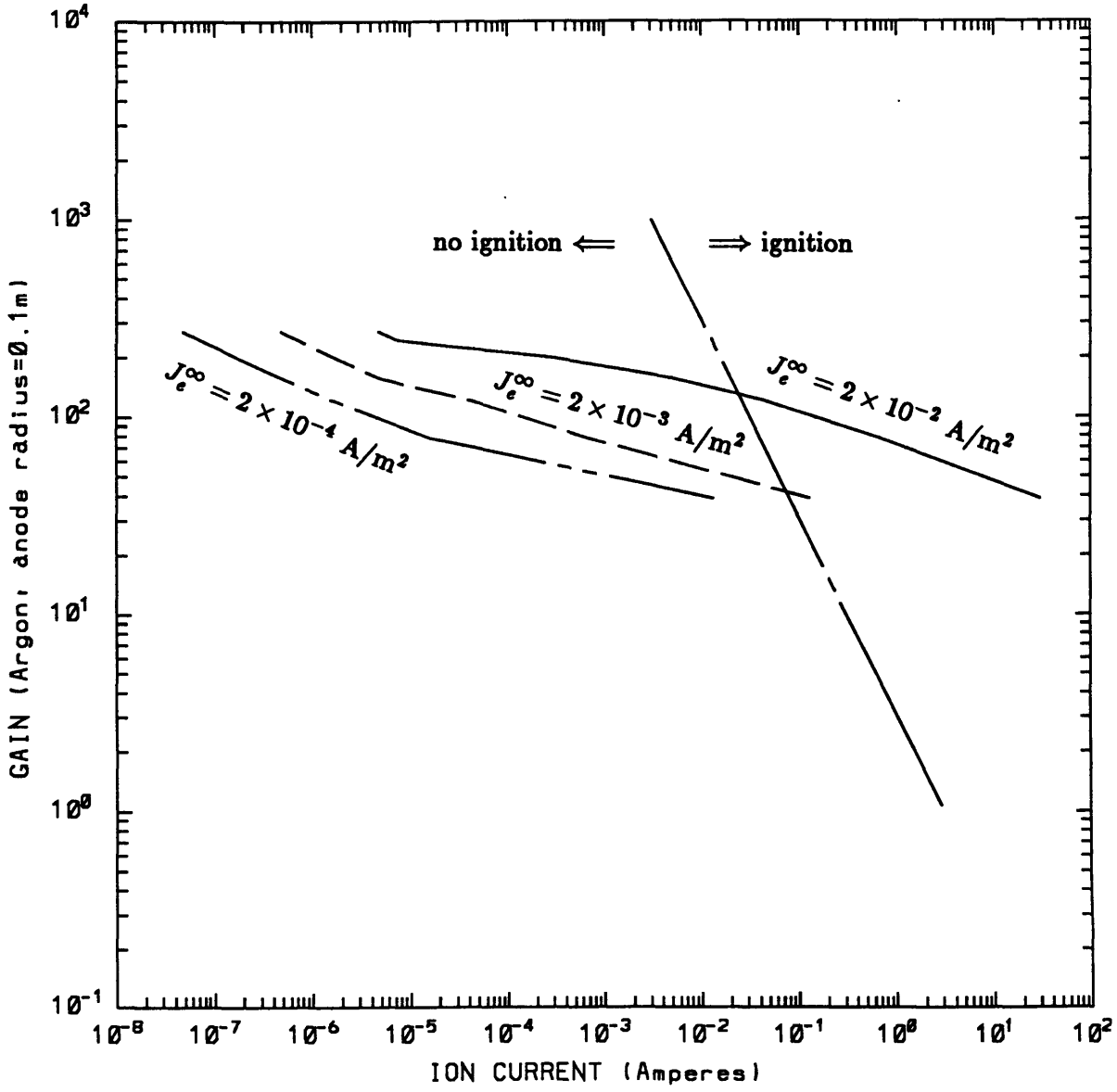

Figure 3.12: Gain vs. Ion Current for Double Layer Model with Gyroradius Condition Imposed on Layer's Outer Edge

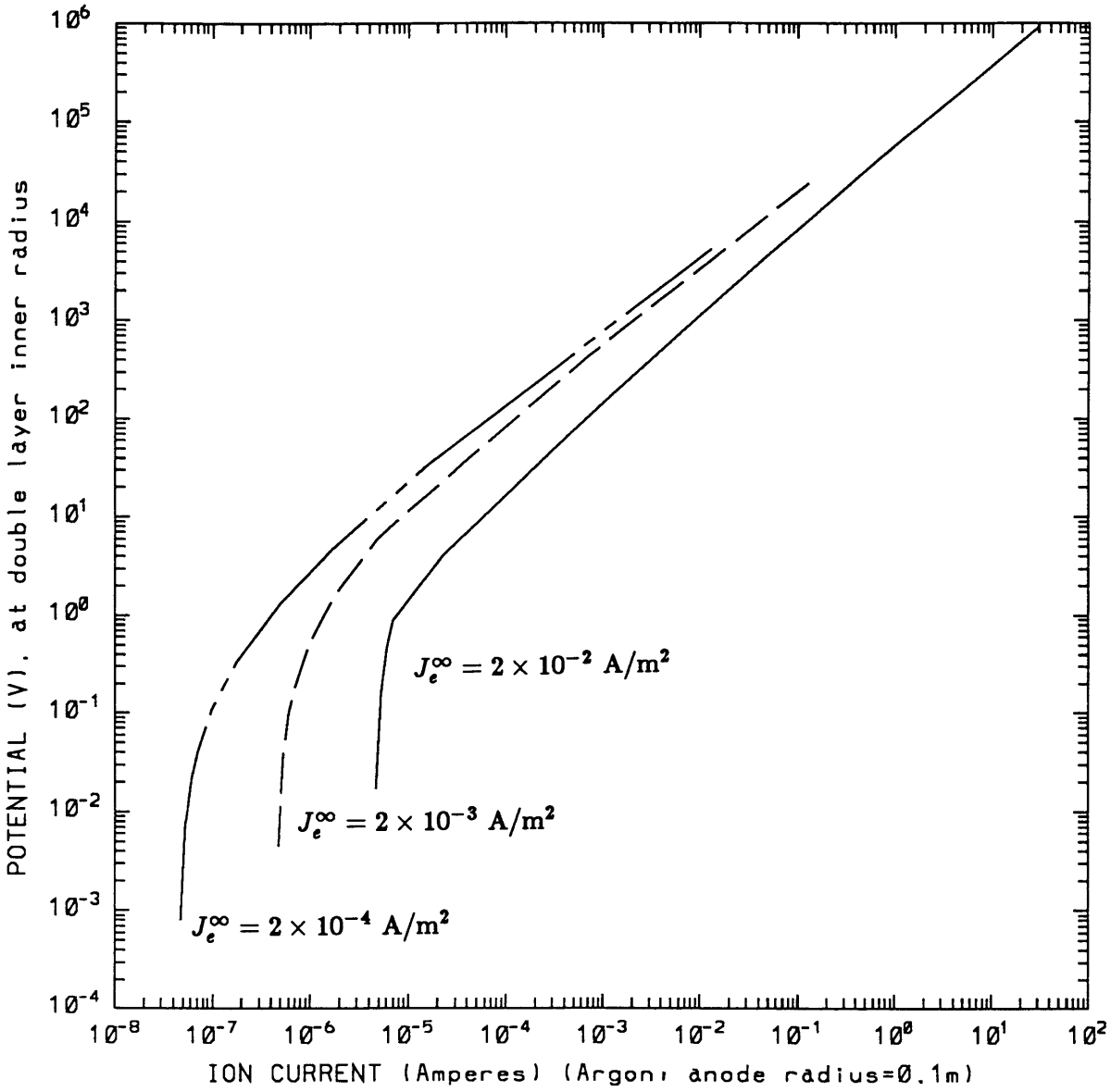

Figure 3.13: Potential Drop vs. Ion Current for Double Layer Model with Gyroradius Condition Imposed on Layer's Outer Edge

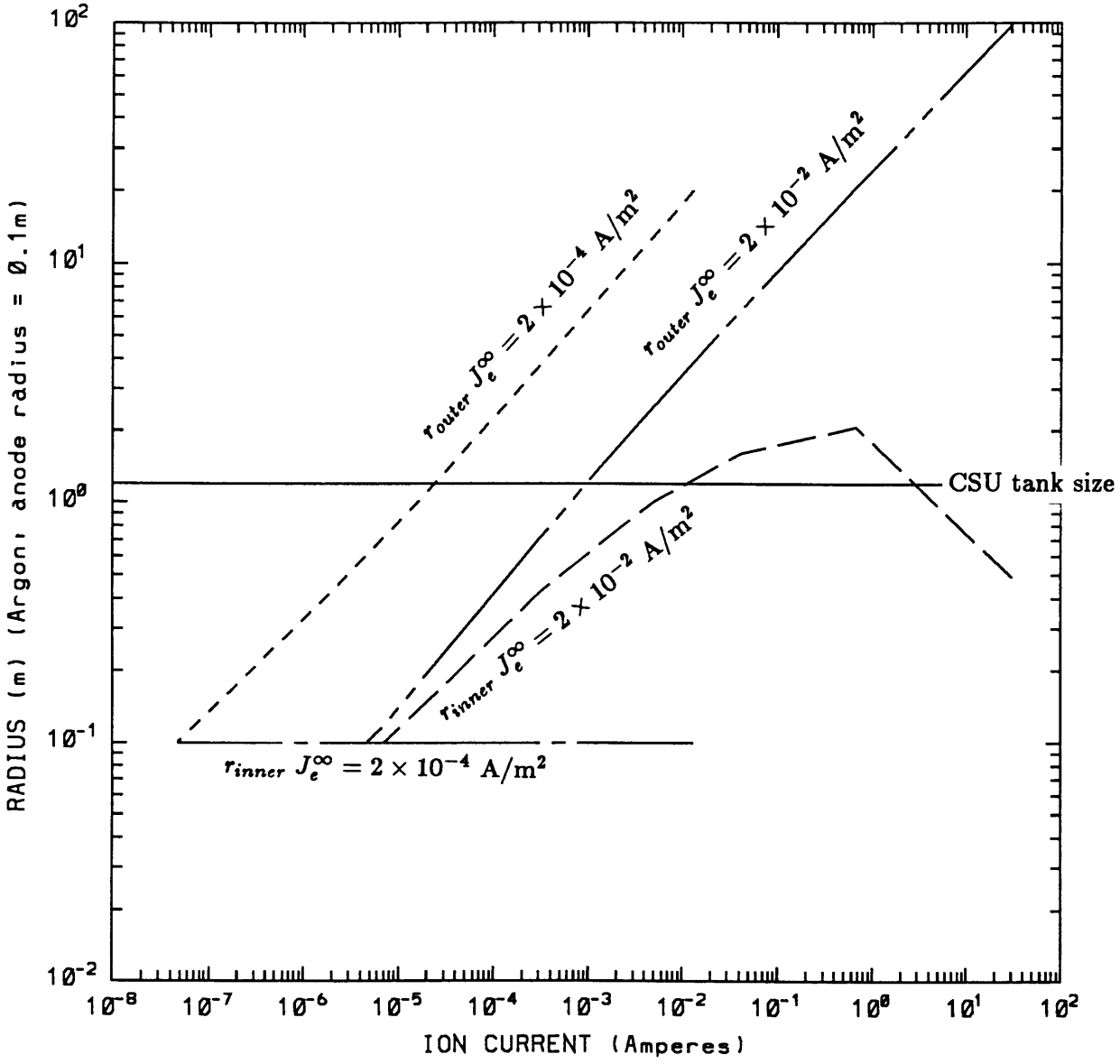

Figure 3.14: Double Layer Radii vs. Ion Current for Double Layer Model with Gyroradius Condition Imposed on Layer's Outer Edge

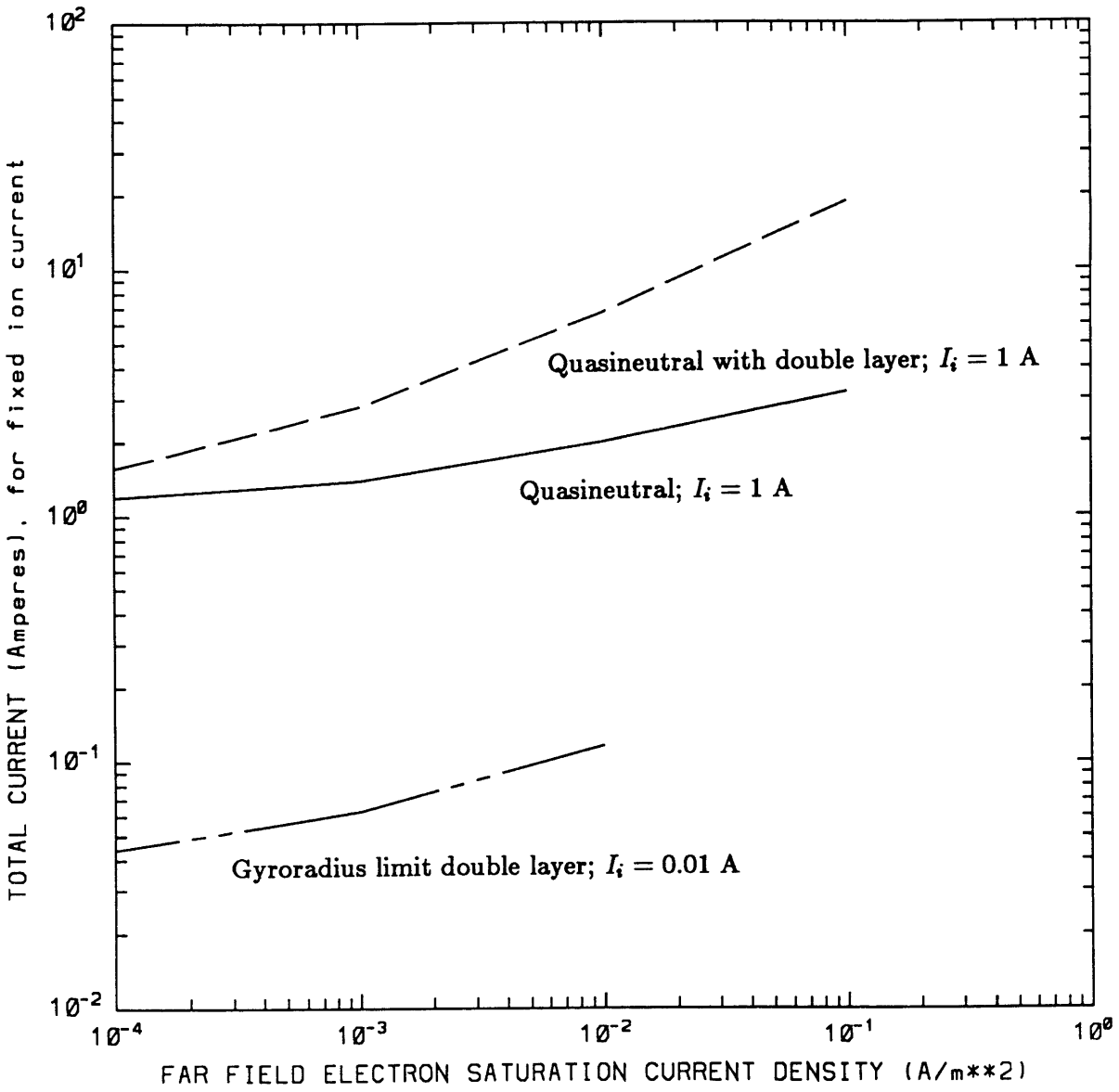

Figure 3.15: Total Collected Current vs. Electron Saturation Current Density for Double Layer (Gyroradius Condition Imposed), Quasineutral, and Anisotropic Models

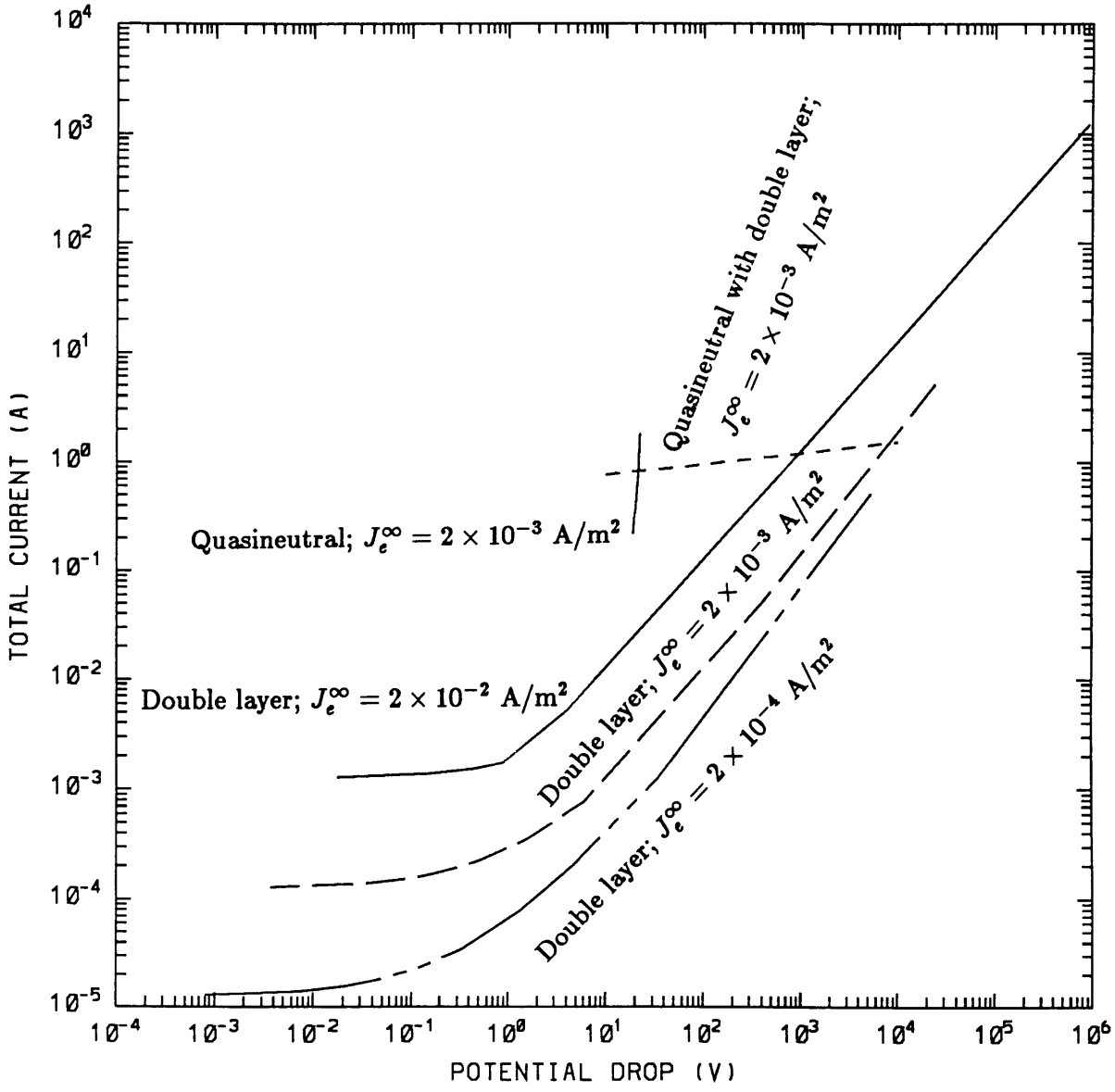

Figure 3.16: Total Current vs. Potential Drop for Double Layer (Gyroradius Condition Imposed), Quasineutral, and Anisotropic Models

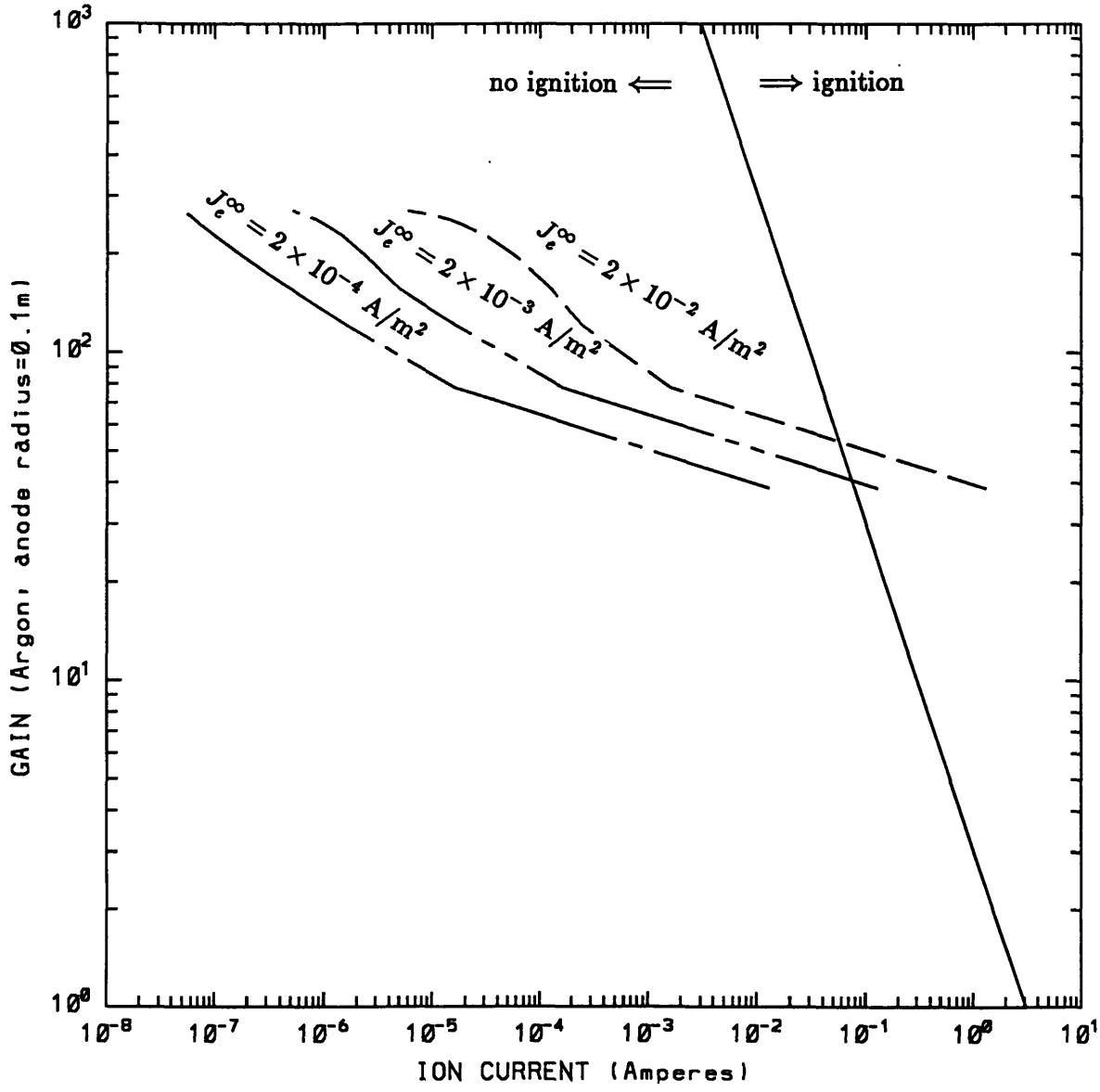

Figure 3.17: Gain vs. Ion Current for Double Layer Model with Parker-Murphy Condition Imposed on Layer's Outer Edge

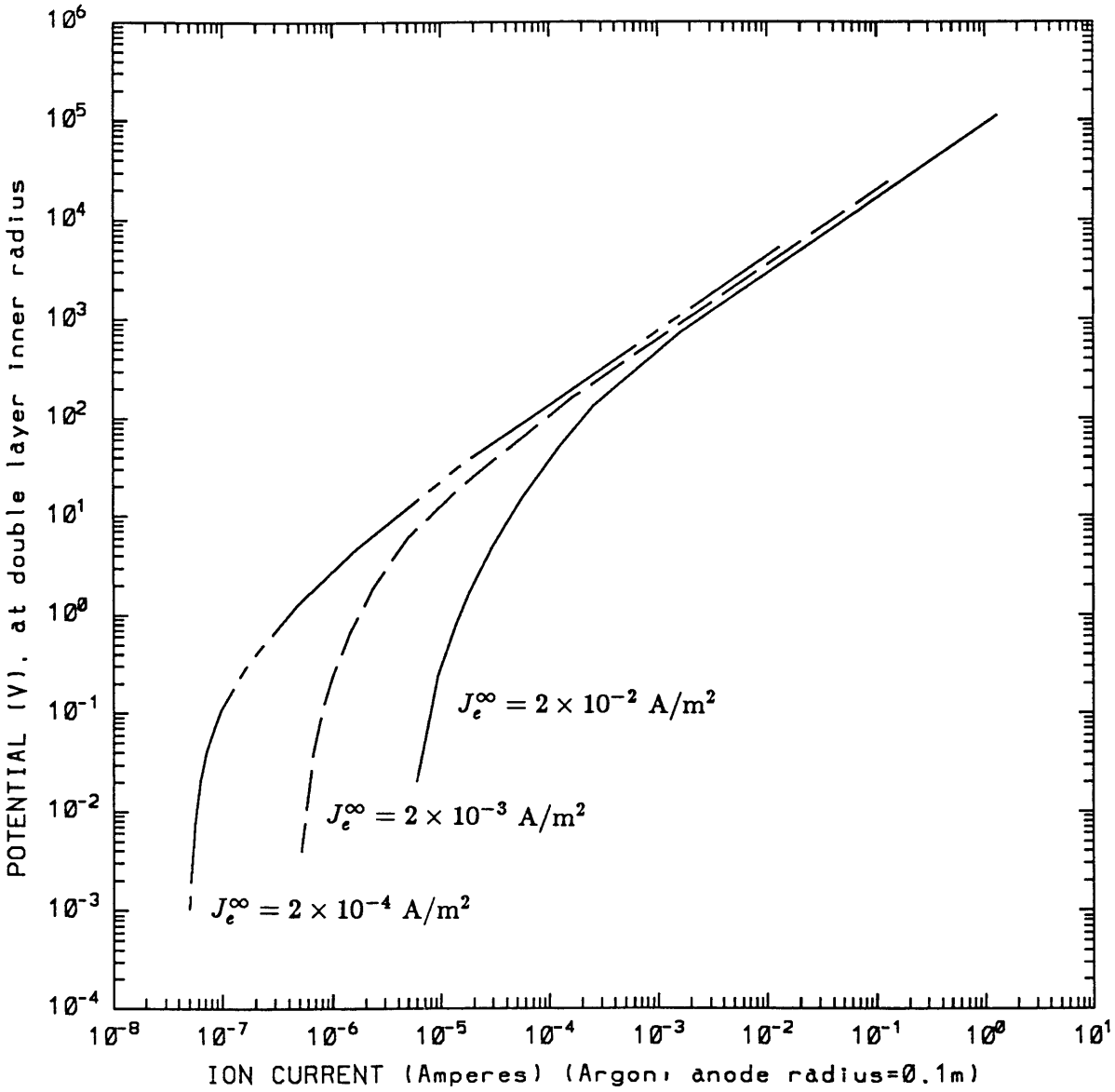

Figure 3.18: Potential Drop vs. Ion Current for Double Layer Model with Parker-Murphy Condition Imposed on Layer's Outer Edge

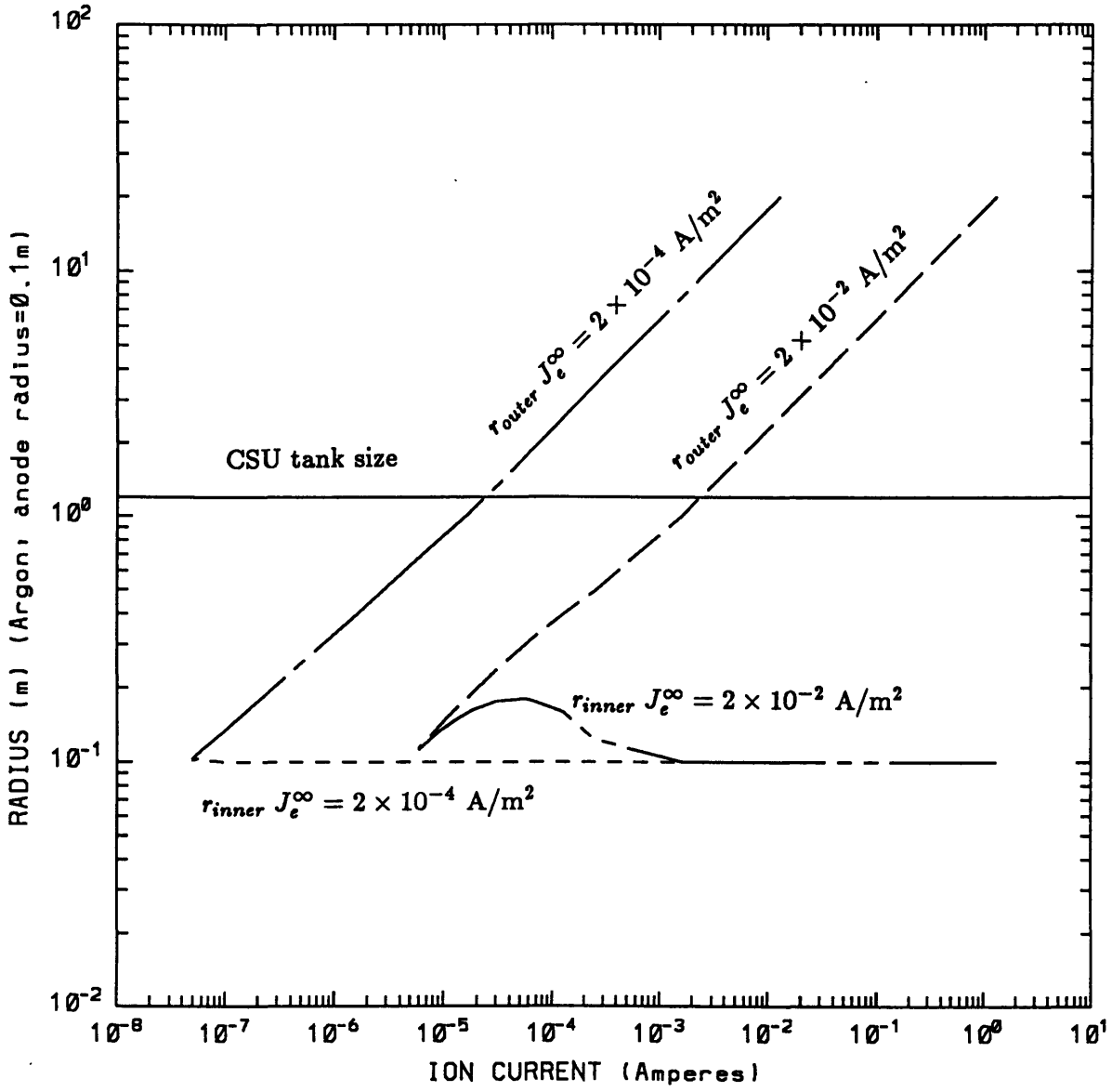

Figure 3.19: Double Layer Radii vs. Ion Current for Double Layer Model with Parker-Murphy Condition Imposed on Layer's Outer Edge

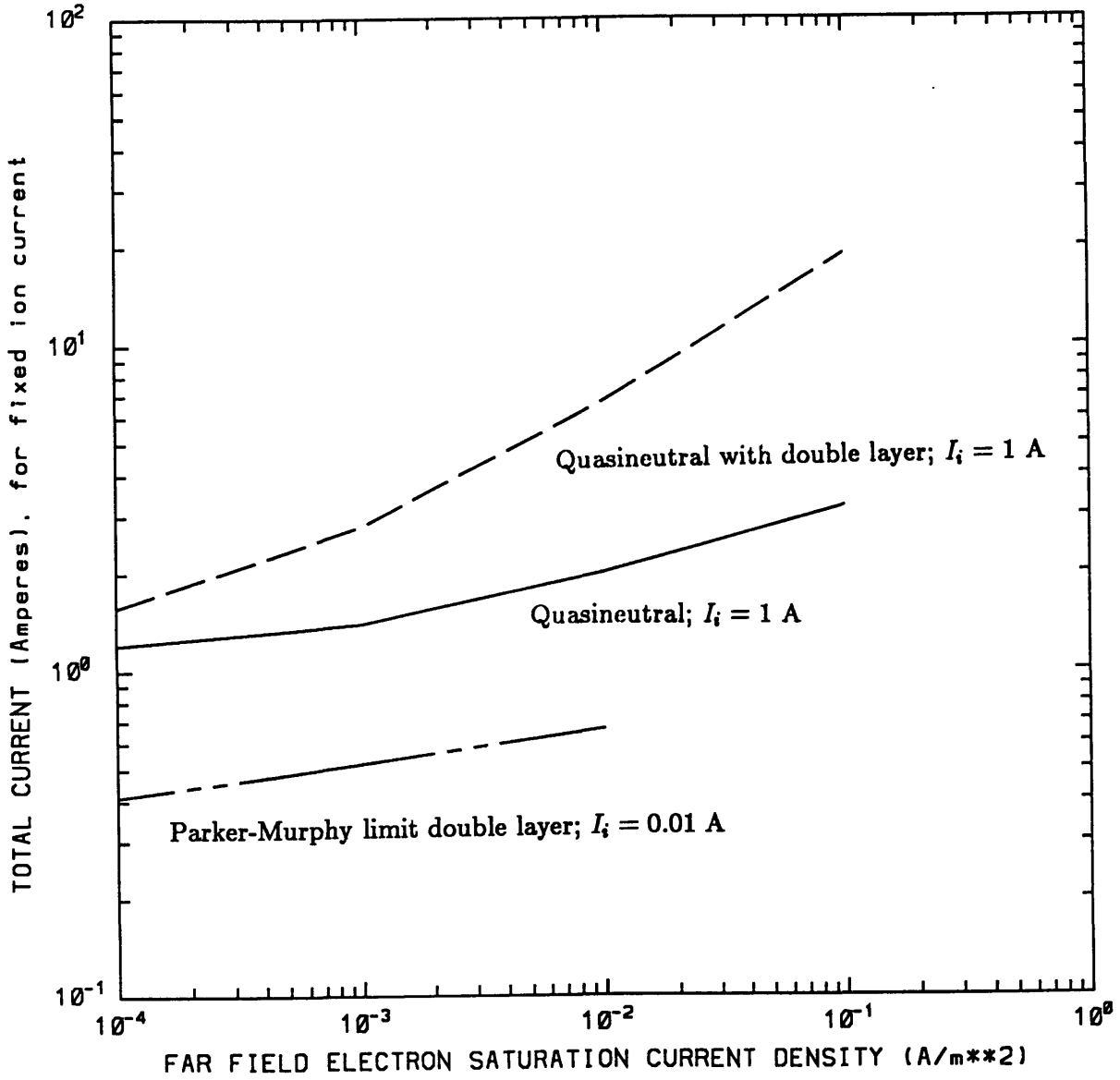

Figure 3.20: Total Collected Current vs. Electron Saturation Current Density for Double Layer (Parker-Murphy Condition Imposed), Quasineutral, and Anisotropic Models

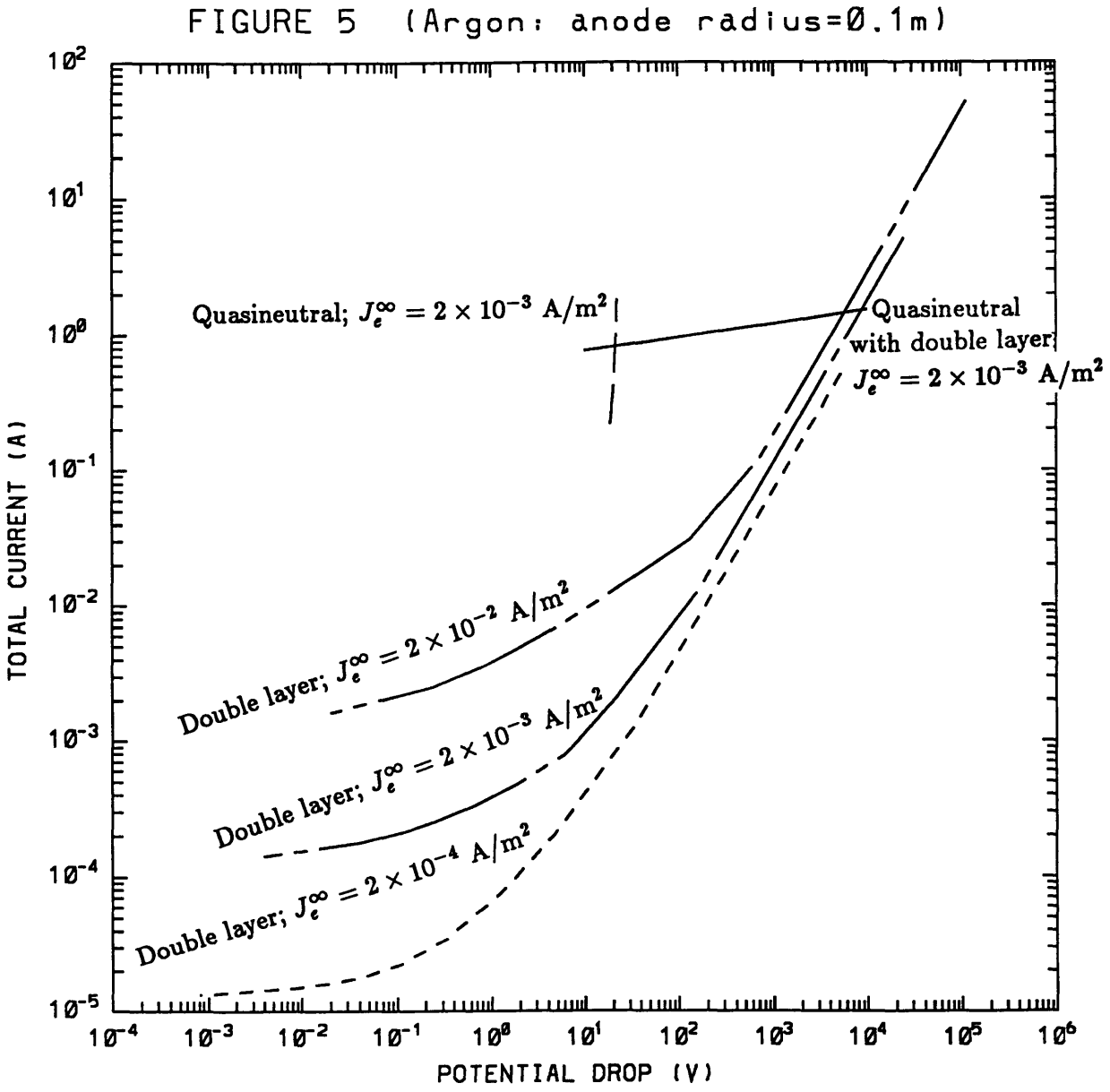

Figure 3.21: Total Current vs. Potential Drop for Double Layer (Parker-Murphy Condition Imposed), Quasineutral, and Anisotropic Models

Chapter 4
Summary and Conclusions

Several models for electron collection by plasma contactors have been examined. Experiments were reviewed in terms of the proposed theoretical models to determine the level of correlation between the two areas. In an effort to determine the efficacy of plasma contactor use in space, new applications of existing models were explored and a new model of the contacting process was proposed. These efforts are summarized below.

The plasma contactor vacuum chamber experiments in which the contactor operated with ion currents below $1\,A$ seem well described by a spherically symmetric double layer model which treats the electrons as collisionless and unmagnetized. In those experiments, the double layer forms approximately at the radius where the plasma reaches the ambient plasma density. This radius is less than or comparable to both the electron Larmor radius and the mean free path of the electrons, if one employs a model including effective collisions due to instabilities. In applications relevant to space power systems, the plasma cloud must have a radius on the order of tens of meters while the ambient electron Larmor radius is only a few centimeters; consequently, neither of these conditions applies.

Still neglecting collisions, but taking into account the finite electron Larmor radius, one finds that ambient electrons can get across the double layer and reach the anode if the Parker-Murphy condition[57] is satisfied. Taking into account the finite anode radius, one must impose that the r_i for space-charge limited current flow in a double-sheath must be greater than r_{anode}. With these requirements, one calculates that a large potential is needed across the double layer in order to draw a reasonably large electron current, so that the available load power for a $20\,km$ long tether is never greater than about $0.5\,kW$, if one

requires an efficiency $\eta > 80\%$.

The maximum power may actually be far less than this, since this power value was found for a configuration with $r_i \ll r_o$, and the Parker-Murphy condition is generally not applicable in that limit. The Parker-Murphy condition becomes impossible to satisfy when dealing double layers of a signficant width since it requires $r_i < r_{anode}$ to remain valid. As stated previously, however, $r_i < r_{anode}$ does not make sense when one is attempting to assess a physical situation. So, there exists a crossover point in the Figures 3.17-3.21 in the collisionless double layer data presented where Eq. 3.5 is not valid. When it is no longer possible to satisfy both the required condition $r_i \geq r_{anode}$ and the Parker-Murphy inequality, this author chooses to maintain physical accuracy by maintaining $r_i \geq r_{anode}$ at the crossover point. In fact, this choice is substantiated by the $3\,cm$ anode data taken by Wilbur [86] in which r_i does in fact move in to meet r_{anode} and if the pressure balance is such that the outer radius moves a great distance away from the anode, the spherical model's validity is lost.

The potential drop across the cloud that is obtained in the manner chosen in extending Wei and Wilbur to space conditions presumably represents the upper limit for the collisionless space-charge-limited contactor. Naturally following from such an upper limit are the values of power available to a system employing this type of a plasma contactor. The potential drop obtained by following the $r_i \geq r_{anode}$ curve after crossover yields an upper limit that is lower than that which would be obtained if the Parker-Murphy condition were followed after crossover. Consequently, this indicates that the available power and efficiency values would be more optimistic when following $r_i \geq r_{anode}$ than when following the Parker-Murphy condition. But to follow the Parker-Murphy condition after crossover causes the inner radius of the double layer to form inside of the anode; the potential drop then calculated based this double layer is a physically unrealistic value. Therefore, the "pessimistic" upper limit, desirable so that one may show that a collisionless double layer does not offer enough for the needs of the space systems planned and that collisional models are really necessary, has no grounding in reality and one should use the $r_i \geq r_{anode}$ condition to make the above point regarding the collisionless models.

Note that when the Parker-Murphy condition is violated, one has presumably moved into a regime where the collisionless assumption is no longer really acceptable, as was pointed out in the earlier discussion of the ignition boundary in Figure 3.17. This makes clear the fact that the collisionless theory has its limitations in space applications. It is then fair to say that at some point past the crossover point deciding on which curve to follow becomes a moot argument. There is a clear need for a self-consistent model that will incorporate the transition from the collisionless to the collisional sheath and also handle the evolution of the sheath from spherical symmetry to cylindrical symmetry to its eventual breakdown at high currents and substantial levels of ionization.

But the collisionless double layer model should be valid in space for a sufficiently low emitted ion current, *i.e.* $I_i < 1\,mA$. The low current is required so that a double layer can form with a potential less than the total tether voltage. A lower contactor potential drop allows electrons to get across the magnetic field to the anode while satisfying $r_i > r_{anode}$. There is a further requirement for validity of the collisionless model in that the electrons must not be deflected from the anode by effective collisions that are the result of instabilities, as they are traversing the contactor plasma. But this additional requirement is easily satisfied in the LEO regime, where the ambient ω_{pe} is on the order of ω_{ce}.

Since a plasma contactor described by the collisionless double layer model cannot generate the power desired for space applications, one must use much higher emitted ion currents. Although the transition from the collisionless double layer model to the collisional quasineutral model is not completely understood, one expects that at sufficiently high ion current that there will be instabilities strong enough to produce a high effective electron collision frequency in the contactor cloud. Such a contactor can be described by a collisional quasineutral fluid model, in which electrons can flow across the magnetic field within a radius r_{core} of the anode.

If r_{core} is defined conservatively as the radius within which the effective electron collision frequency, due to ion acoustic and Buneman instabilities, exceeds the electron cyclotron frequency, then one observes that the contactor plasma cloud has a very low potential drop, but draws very little electron current be-

cause r_{core} is rather small. One must bear in mind that the Buneman instability cannot be relied upon to provide steady-state anomalous resistivity in this one dimensional problem and that the ion acoustic instability is responsible for the bulk of resistivity. The overall system gain then ends up being order 1 with such a model. Even for those cases of higher T_e where a modest gain in current occurs, that gain is due almost entirely to ionization of neutral gas emitted by the contactor, not to collection of electrons from the ambient plasma. In this case, the gas would probably be used more efficiently if it were ionized internally, in an ion source, rather than externally, where much of it can be lost.

Further analysis of the ionization of the neutral gas emitted by the contactor indicates that it does not enhance the performance of the contacting system. Granted, this conclusion is based on a rather rough model, but that model does serve the purpose to show that the primary mode of the plasma contactor should be to draw in ambient electrons from infinity to run efficiently and at high power with low losses. This model requires the use of a collisional and possibly asymmetric transition region to be complete. The results of this analysis do demonstrate that random thermal current collection is the primary factor regulating the gain of a system utilizing a plasma contactor for electron collection.

If one includes the anisotropic part of the contactor cloud where the effective electron collision frequency is less than the electron cyclotron frequency, then electrons can be collected out to a much larger radius. Then an electron current a few times greater than the ion current can be drawn from the ambient plasma, even at fairly low potentials. In contrast to the collisionless double layer model and the quasineutral model based on the more conservative definition of r_{core}, the electron current has a significant dependence on the electron saturation current of the ambient plasma and is substantially higher for a given ion current on the dayside than on the nightside in the LEO regime. Analytic expressions for the potential profile and collected electron current can be obtained when the electron motion along the magnetic field is fairly collisionless, so that a double layer forms in that direction, but the electrons flow collisionally across the magnetic field. This is the regime that is relevant to high current plasma contactors

in LEO. Although the model which is solved analytically in Section 3.2 made the simple approximation that the effective electron collision frequency, due only to ion acoustic turbulence, is equal to $10^{-2}\omega_{pe}$, independent of T_e and the electric field, the same method should be applicable, accounting for the caveats discussed in Section 3.2.4, using more realistic expressions for the effective collision frequency. Another approximation made in the analysis of this model is that there is sufficient electron thermal conductivity across the magnetic field to keep T_e much lower than ϕ_0 in the contactor cloud. The validity of this approximation must be examined using realistic turbulence models. If this approximation is at least marginally valid, then the results presented for this model should at least be qualitatively correct [29].

One important conclusion of analysis is that most of the present ground based experiments have limited relevance to space applications of plasma contactors, since they operate in a regime where the magnetic field and effective collisions are not really felt. This is true of spaceborne contactors only at very low current and power levels. Only the experiments of Urrutia and Stenzel [71] examined a plasma in in which the impact of the chamber wall on the electron motion was avoided and the anomalous transport of electrons in the plasma could be assessed. In their work performed at UCLA, it was found that the contactor anode collected an electron current a few times greater than the saturation current of the flux tube that intersected the anode, even when $\nu_e\omega_{ce}$. The observed cross field electron transport was attributed to ion acoustic instabilities excited by the azimuthal $\vec{E} \times \vec{B}$ drift of the electrons relative to the unmagnetized ions. This drift gave rise to azimuthal wave electric fields that cause radial $\vec{E} \times \vec{B}$ drifts. In this respect the experiment was similar to the anisotropic contactor cloud model considered in Section 3.2. However, this experiment differed in one important respect from the LEO regime that was considered in Section 3.2. In the UCLA experiment, the density was about $2 \times 10^{11}\, cm^{-3}$ and $\omega_{pe}/\omega_{ce} \approx 50$. Those values are much higher than those of found in LEO conditions. As a result, the anomalous parallel resistivity was quite pronounced due to Buneman and ion acoustic instabilities excited by the relative electron and ion flow velocity along the field. The electrons did not flow freely along the magnetic field, but diffused along the field like a collisional fluid so that there were no double

layers along the field.

It would be desirable to perform chamber experiments in the regime where the electrons flow freely along the magnetic field while collisionally across the magnetic field. Such experiments are desirable since the conditions they set up are applicable to high power plasma contactors flown in LEO conditions and would facilitate comparison of the measured $\phi(r,z)$ and collected current to the expressions calculated in Section 3.2, or to similar expressions found with more realistic models for ν_e. Figure 3.19 provides the information with which an experimenter can scale a chamber contactor experiment. Much lower ion currents and plasma densities are required in chamber experiments if the data taken is to be scaled to the LEO environment.

This thesis has demonstrated that an efficient plasma contactor in space achieves modest gains through the collection of ambient electrons and that this process is aided by the collisional mechanisms. An efficient high power contactor cannot be designed for use in space that does not rely on collisions, or effective collisions due to turbulence, to sustain its electron collection. While these results have important implications for power systems relying on electrodynamic tethers in space, it should be clear from the studies presented that much remains to be accomplished. Additional theoretical and experimental studies are needed to answer the remaining questions posed within this work. A synthesis of the work of the theorists and experimentalists is required to advance the state of plasma contactor technology. This thesis was an effort to achieve that sort of synthesis and point the way toward an even greater understanding of plasma processes in space.

Appendix A
Values of Collisionless Spherical Double Layer Radius Ratio Dependent Functions

Spherical Radius Ratio r_r	Normalized Collected Electron Current j_0	Normalized Current Ratio α	Gain for Argon Case ξ
0.00000	0.01687	0.13251	36.043
0.00500	0.01999	0.14241	38.736
0.00678	0.02089	0.14500	39.440
0.01000	0.02318	0.15197	41.336
0.01500	0.02645	0.16122	43.852
0.02000	0.02978	0.17018	46.289
0.02500	0.03349	0.17963	48.859
0.03000	0.03668	0.18733	50.954
0.03500	0.04025	0.19555	53.190
0.04000	0.04389	0.20355	55.366
0.04500	0.04762	0.21136	57.490
0.05000	0.05231	0.22083	60.066
0.05500	0.05533	0.22642	61.586
0.06000	0.05932	0.23370	63.566
0.06500	0.06400	0.24107	65.571
0.07000	0.06757	0.24781	67.404
0.07500	0.07184	0.25465	69.265
0.08000	0.07621	0.26137	71.093
0.08500	0.08068	0.26797	72.888
0.09000	0.08525	0.27445	74.650
0.09500	0.08992	0.28083	76.386
0.10000	0.09471	0.28710	78.091
0.10500	0.09961	0.29328	79.772
0.11000	0.10462	0.29936	81.426

Spherical Radius Ratio r_r	Normalized Collected Electron Current j_0	Normalized Current Ratio α	Gain for Argon Case ξ
0.11500	0.10975	0.30536	83.058
0.12000	0.11500	0.31128	84.668
0.12500	0.12038	0.31711	86.254
0.13000	0.12588	0.32288	87.823
0.13500	0.13152	0.32857	89.371
0.14000	0.13729	0.33419	90.900
0.14500	0.14319	0.33975	92.412
0.15000	0.14748	0.34306	93.312
0.15500	0.15544	0.35069	95.388
0.16000	0.16179	0.35607	96.851
0.16500	0.16829	0.36140	98.301
0.17000	0.17495	0.36668	99.737
0.17500	0.18177	0.37191	101.160
0.18000	0.18876	0.37709	102.568
0.18500	0.19593	0.38223	103.967
0.19000	0.20327	0.38732	105.351
0.19500	0.21079	0.39237	106.725
0.20000	0.21688	0.39621	107.769
0.20500	0.22642	0.40235	109.439
0.21000	0.23452	0.40728	110.780
0.21500	0.24283	0.41218	112.113
0.22000	0.25136	0.41704	113.435
0.22500	0.26010	0.42187	114.749
0.23000	0.26906	0.42667	116.054

Spherical Radius Ratio r_r	Normalized Collected Electron Current j_0	Normalized Current Ratio α	Gain for Argon Case ξ
0.23500	0.27826	0.43144	117.352
0.24000	0.28769	0.43617	118.638
0.24500	0.29737	0.44088	119.919
0.25000	0.30490	0.44400	120.768
0.25500	0.31750	0.45021	122.457
0.26000	0.32796	0.45484	123.716
0.26500	0.33870	0.45944	124.968
0.27000	0.35007	0.46450	126.344
0.27500	0.36105	0.46857	127.451
0.28000	0.37267	0.47309	128.680
0.28500	0.38461	0.47760	129.907
0.29000	0.39687	0.48208	131.126
0.29500	0.40947	0.48655	132.342
0.30000	0.42241	0.49099	133.549
0.30500	0.43571	0.49541	134.752
0.31000	0.44938	0.49982	135.951
0.31500	0.46343	0.50420	137.142
0.32000	0.47787	0.50856	138.328
0.32500	0.49272	0.51291	139.512
0.33000	0.50799	0.51724	140.689
0.33500	0.52370	0.52155	141.862
0.34000	0.53985	0.52585	143.031
0.34500	0.55648	0.53013	144.195
0.35000	0.57943	0.53642	145.906

Spherical Radius Ratio r_r	Normalized Collected Electron Current j_0	Normalized Current Ratio α	Gain for Argon Case ξ
0.35500	0.59118	0.53864	146.510
0.36000	0.60930	0.54287	147.661
0.36500	0.62795	0.54708	148.806
0.37000	0.64715	0.55129	149.951
0.37500	0.66693	0.55547	151.088
0.38000	0.68730	0.55965	152.225
0.38500	0.70829	0.56380	153.354
0.39000	0.72992	0.56795	154.482
0.39500	0.75221	0.57208	155.606
0.40000	0.77901	0.57601	156.675
0.40500	0.79887	0.58031	157.844
0.41000	0.82330	0.58440	158.957
0.41500	0.84850	0.58848	160.067
0.42000	0.87449	0.59255	161.174
0.42500	0.90131	0.59661	162.278
0.43000	0.92899	0.60065	163.377
0.43500	0.95757	0.60469	164.476
0.44000	0.98708	0.60871	165.569
0.44500	1.01755	0.61272	166.660
0.45000	1.06573	0.61908	168.390
0.45500	1.08156	0.62071	168.833
0.46000	1.11518	0.62468	169.913
0.46500	1.14993	0.62865	170.993
0.47000	1.18587	0.63260	172.067
0.47500	1.22303	0.63655	173.142

Spherical Radius Ratio r_r	Normalized Collected Electron Current j_0	Normalized Current Ratio α	Gain for Argon Case ξ
0.48000	1.26148	0.64048	174.211
0.48500	1.30128	0.64441	175.280
0.49000	1.34246	0.64832	176.343
0.49500	1.38511	0.65223	177.407
0.50000	1.44058	0.65641	178.544
0.50500	1.47504	0.66000	179.520
0.51000	1.52246	0.66388	180.575
0.51500	1.57161	0.66774	181.625
0.52000	1.62258	0.67160	182.675
0.52500	1.67545	0.67544	183.720
0.53000	1.73030	0.67928	184.764
0.53500	1.78724	0.68310	185.803
0.54000	1.84635	0.68692	186.842
0.54500	1.90775	0.69073	187.879
0.55000	1.97154	0.69452	188.909
0.55500	2.03783	0.69831	189.940
0.56000	2.10677	0.70209	190.968
0.56500	2.17847	0.70586	191.994
0.57000	2.25307	0.70962	193.017
0.57500	2.33073	0.71337	194.037
0.58000	2.41160	0.71712	195.057
0.58500	2.49584	0.72085	196.071
0.59000	2.58364	0.72458	197.086
0.59500	2.67519	0.72829	198.095

Spherical Radius Ratio r_r	Normalized Collected Electron Current j_0	Normalized Current Ratio α	Gain for Argon Case ξ
0.60000	2.76854	0.73068	198.745
0.60500	2.87033	0.73570	200.110
0.61000	2.97438	0.73939	201.114
0.61500	3.08306	0.74307	202.115
0.62000	3.19664	0.74674	203.113
0.62500	3.31540	0.75040	204.109
0.63000	3.43964	0.75406	205.104
0.63500	3.56968	0.75770	206.094
0.64000	3.70587	0.76134	207.084
0.64500	3.84857	0.76497	208.072
0.65000	3.99818	0.76859	209.056
0.65500	4.15513	0.77220	210.038
0.66000	4.31988	0.77580	211.018
0.66500	4.49293	0.77939	211.994
0.67000	4.67480	0.78298	212.971
0.67500	4.86609	0.78655	213.942
0.68000	5.06740	0.79012	214.913
0.68500	5.27942	0.79368	215.881
0.69000	5.50288	0.79723	216.847
0.69500	5.73857	0.80077	217.809
0.70000	5.98735	0.80430	218.770
0.70500	6.25016	0.80783	219.730
0.71000	6.52802	0.81134	220.684
0.71500	6.82205	0.81485	221.639

Spherical Radius Ratio r_r	Normalized Collected Electron Current j_0	Normalized Current Ratio α	Gain for Argon Case ξ
0.72000	7.13346	0.81835	222.591
0.72500	7.46357	0.82184	223.540
0.73000	7.81385	0.82532	224.487
0.73500	8.18589	0.82879	225.431
0.74000	8.58145	0.83225	226.372
0.74500	9.00246	0.83571	227.313
0.75000	9.45104	0.83915	228.249
0.75500	9.92956	0.84259	229.184
0.76000	10.44062	0.84602	230.117
0.76500	10.98710	0.84944	231.048
0.77000	11.57223	0.85285	231.975
0.77500	12.19956	0.85625	232.900
0.78000	12.87309	0.85965	233.825
0.78500	13.59730	0.86303	234.744
0.79000	14.37718	0.86641	235.664
0.79500	15.21837	0.86977	236.577
0.80000	16.02105	0.87283	237.410
0.80500	17.11090	0.87648	238.403
0.81000	18.17756	0.87982	239.311
0.81500	19.33648	0.88315	240.217
0.82000	20.59821	0.88647	241.120
0.82500	21.97487	0.88979	242.023
0.83000	23.48036	0.89309	242.920
0.83500	25.13077	0.89639	243.818
0.84000	26.94468	0.89967	244.710

Spherical Radius Ratio r_r	Normalized Collected Electron Current j_0	Normalized Current Ratio α	Gain for Argon Case ξ
0.84500	28.94377	0.90295	245.602
0.85000	31.81732	0.90579	246.375
0.85500	33.60309	0.90948	247.379
0.86000	36.32818	0.91273	248.263
0.86500	39.37032	0.91597	249.144
0.87000	42.77926	0.91920	250.022
0.87500	46.61494	0.92243	250.901
0.88000	50.94985	0.92564	251.774
0.88500	55.87240	0.92884	252.644
0.89000	61.49136	0.93204	253.515
0.89500	67.94161	0.93522	254.380
0.90000	75.39313	0.93840	255.245
0.90500	84.05663	0.94157	256.107
0.91000	94.20912	0.94473	256.967
0.91500	106.20465	0.94788	257.823
0.92000	120.51075	0.95101	258.675
0.92500	138.83092	0.95405	259.502
0.93000	158.77971	0.95727	260.377
0.93500	184.77637	0.96038	261.223
0.94000	217.42372	0.96348	262.067
0.94500	259.18759	0.96657	262.907
0.95000	323.76852	0.96956	263.720
0.95500	387.07419	0.97273	264.583
0.96000	488.69275	0.97579	265.415
0.96500	635.52332	0.97884	266.244
0.97000	859.52112	0.98189	267.074
0.97500	1227.87305	0.98492	267.898
0.98000	1905.64880	0.98795	268.722
0.98500	3415.28564	0.99096	269.541
0.99000	8553.58627	0.99397	270.360

Bibliography

[1] H. Alfvén, Keynote Address, *Double Layers in Astrophysics*, NASA-CP-2469, March, 1986

[2] Ya. L. Al'pert, A.V. Gurevich, and L.P. Pitaevskii, *Space Physics with Artificial Satellites*, Consultants Bureau, 1965

[3] R.L. Arnoldy, C. Pollock, and J.R. Winckler, "The Energization of Electrons and Ions by Electron Beams Injected in the Ionosphere," *Journal of Geophysical Research*, 90, p. 5197, 1985

[4] M. Ashour-Abdalla and H. Okuda, "Propagation of Electron Beams in Space," Technical Report submitted July 1986 under Air Force Contract f19628-85-K-0027

[5] P.M. Banks "Electron Beam Experiments and Other Observations from STS-3," *Proceedings of the Air Force Geophysics Laboratory Workshop on Natural Charging of Large Space Structures in Near Earth Polar Orbit: 14-15 September 1982*, AFGL-TR-83-0046, Jan 1983

[6] P.M. Banks, private communication, April, 1988

[7] P.M. Banks, P.R. Williamson, and K.-I. Oyama, "Electrical Behavior of a Shuttle Electrodynamic Tether System (SETS)," *Planetary Space Science*, Vol. 29, pp. 139-147, 1981

[8] I. Bekey, Keynote Address, *Applications of Tethers in Space*, Vol. 1, NASA-CP-2364, 1985

[9] J.A. Bittencourt, *Fundamentals of Plasma Physics*, Pergamon Press, 1986

[10] J.J. Blandino, "A Numerical, Parametric Study of Plasma Contactor Performance," S.M. Thesis, M.I.T., Dec 1988

[11] L.P. Block, "A Double Layer Review," *Astrophysics and Space Science*, Vol 55, 1978, pp. 59-83

[12] L.P. Block, "Double Layers," in *Physics of the Hot Plasma in the Magnetosphere*, Plenum, NY, 1975

[13] L.P. Block, "Potential Double Layers in the Ionosphere," *Cosmic Electrodynamics*, Vol 3, 1972, pp. 349-376

[14] D. Bohm, "Minimum Ion Kinetic Energy for a Stable Sheath," in *The Characteristics of Electrical Discharges in Magnetic Fields*, eds. A. Guthrie and R.K. Wakerling, McGraw-Hill, 1949

[15] S.I. Braginski, "Transport processes in a plasma," *Reviews of Plasma Physics*, Consultants Bureau, 1965

[16] R.L. Burden and J.D. Faires, *Numerical Analysis*, Prindle, Weber, and Schmidt, 3rd edition, 1981

[17] P. Carlqvist, "On the Formation of Double Layers in Plasmas," *Cosmic Electrodynamics*, Vol. 3, 1972, pp.377-388

[18] C. Chan, "Formation Mechanisms of Laboratory Double Layers," *Double Layers in Astrophysics*, NASA-CP-2469, March 1986

[19] C. Chan, N. Hershkowitz, and K.E. Lonngren, "Electron Temperature Differences and Double Layers," *Physics of Fluids*, Vol. 26, No. 6, June 1983

[20] G. Chanteur, J.C. Adam, R. Pellat, and A.S. Volokhitin, "Formation of Ion-Acoustic Double Layers," *Physics of Fluids*, Vol. 26, No. 6, June 1986

[21] C.D. Child, "Discharge from Hot CaO," *Physical Review*, Vol. 32, p. 492, 1911

[22] H.A. Cohen and S. Lai, "Discharging the P78.2 Satellite Using Ions and Electrons," AIAA-82-0266, AIAA 20th Aerospace Sciences Meeting, January 11-14, 1982, Orlando, Florida

[23] D.L. Cooke and I. Katz, "Ionization-Induced Instability in an Electron-Collecting Sheath," *Journal of Spacecraft and Rockets*, Volume 25, Number 2, Mar-Apr 88, pp. 132-138

[24] V.A. Davis, I. Katz, M.J. Mandell, and D.E. Parks, "A Model of Electron Collecting Plasma Contactors," presented at American Institute of Aeronautics and Astronautics Aerospace Sciences Meeting, 12 Jan 1989, Reno, NV

[25] M. Dobrowolny and L. Iess, "Model of the interaction of a hollow cathode with the ionosphere," *Space Tethers for Science in the Space Station Era*, Societá Italiana di Fisica, Conference Proceedings, Vol. 14, 1988

[26] M. Dobrowolny and L. Iess, private communication, June 1988

[27] S.D. Drell, H.M. Foley, and M.A. Ruderman, "Drag and propulsion in the ionosphere: an Alfvén engine in space," *Journal of Geophysical Research*, 70:3131, 1965

[28] N.A. Gatsonis, "Theory and Numerical Analysis of Plasma Clouds Surrounding Space Systems in Low Earth Orbit," S.M. Thesis, M.I.T, Aug 1987

[29] M.J. Gerver, D.E. Hastings, and M.R. Oberhardt, "Theory and Experimental Review of Plasma Contactors," submitted to *Journal of Spacecraft and Rockets*, May 1989

[30] B.E. Gilchrist, P.M. Banks, T. Neubert, P.R. Williamson, N.B. Myers, W.J. Raitt, and S. Sasaki, "Electron Collection Enhancement Arising from Neutral Gas Jets on a Charged Vehicle in the Ionosphere," submitted to *Journal of Geophysical Research*, November 1988

[31] C.K. Goertz and G. Joyce, "Numerical Simulation of the Plasma Double Layer," *Astrophysics and Space Sciencs*, Vol 32, 1975, pp. 165-173

[32] M.D. Grossi, "Tether History and Historiography," *Space Tethers for Science in the Space Station Era*, Societá Italiana di Fisica, Conference Proceedings, Vol. 14, 1988

[33] D.E. Hastings, "Enhanced current flow through a plasma cloud by induction of plasma turbulence," *Journal of Geophysical Research*, Vol. 92, pp. 7716-7722, 1987b

[34] D.E. Hastings, "Theory of Plasma Contactors Used in the Ionosphere," *J. Spacecraft*, 24:250-256, 1987

[35] D.E. Hastings, private communication, May 1989

[36] D.E. Hastings and J. Blandino, "Bounds on Current Collection by Plasma Clouds from the Ionosphere," *Journal of Geophysical Research*, 94:2737-2744, 1989

[37] D.E. Hastings, J. Blandino, and M.R. Oberhardt, "Current Collection to Plasma Contactors in the Ionosphere," presented at American Institute of Aeronautics and Astronautics Aerospace Sciences Meeting, 12 Jan 1989, Reno, NV

[38] D.E. Hastings and N.A. Gatsonis, "Plasma Contactors for Use with Electrodynamic Tethered Satellite Systems," *Acta Astronautica*, Vol. 17, pp. 827-836, 1988

[39] D.E. Hastings, N.A. Gatsonis, and D.A. Rivas, "A Two-dimensional Theory of Plasma Contactor Clouds used in the Ionosphere with an Electrodynamic Tether," *Space Tethers for Science in the Space Station Era*, Societá Italiana di Fisica, Conference Proceedings, Vol. 14, 1988

[40] D.E. Hastings and J. Wang, "The Radiation Impedance of an Electrodynamic Tether with End Connectors," *Geophysical Research Letters*, 14:519-522, 1987

[41] L. Iess, private communication, October 1988

[42] L. Iess and M. Dobrowolny, "A Fluid of Plasma Contactors in the Ionosphere," *Tethers in Space Toward Flight*, AIAA Conference Proceedings, Third International Conference on Tethers in Space, 17-19 May 1989, p. 70-76

[43] O. Ishihara, A. Hirose, and A.B. Langdon, "Nonlinear Evolution of the Buneman Instability," *Physics of Fluids*, Vol. 24, pp.452-464, 1981

[44] I. Katz and V.A. Davis, "A Van der Waals-like Theory of Plasma Double Layers," Unpublished, April, 1989

[45] G. Knorr and C.K. Goertz, "Existence and Stability of Strong Potential Double Layers," *Astrophysics and Space Science*, Vol. 31, 1974, p. 209-223

[46] N.A. Krall and A.W. Trivelpiece, *Principles of Plasma Physics*, McGraw-Hill, 1973.

[47] I. Langmuir, "The Interaction of Electron and Positive Ion Space Charges in Cathode Sheaths," *Physical Review*, Vol 33, p.954, 1929

[48] I. Langmuir and K. B. Blodgett, "Currents Limited by Space Charge between Concentric Spheres," *Physical Review*, Vol. 24, p. 49, 1924

[49] L.M. Linson, "Charge neutralization as studied experimentally and theoretically," *Artificial Particle Beams In Space Plasma Studies*, Plenum Press, 1982

[50] L.M. Linson, "The Importance of Neutrals, Transient Effects, and the Earth's Magnetic Field on Sheath Structure," *Proceedings of the Air Force Geophysics Laboratory Workshop on Natural Charging of Large Space Structures in Near Earth Polar Orbit: 14-15 September 1982*, AFGL-TR-83-0046, Jan 1983

[51] L.R. Lyons, "Conditions for Double Layers in the Earth's Magnetosphere and Perhaps in Other Astrophysical Objects," *Double Layers in Astrophysics*, NASA-CP-2469, March 1986

[52] M. Martinez-Sanchez and D.E. Hastings, "A Systems Study of a 100 kW Tether," *J. of Astronautical Sciences*, Vol. 35, No. 1, Jan-Mar 1987

[53] A.B. Mikhailovskii, *Theory of Plasma Instabilities*, Plenum Publishing Corp., 1974

[54] R.C. Olsen, "Modifications of Spacecraft Potentials by Plasma Emission," *J. Spacecraft*, Vol. 18, No. 5, Sept.-Oct. 1981, pp. 462-467

[55] K. Papadopoulos, "A review of anomalous resistivity for the ionosphere," *Rev. of Geophysics and Space Physics*, 15:113-127, 1977

[56] L.W. Parker and E.G. Holeman, "Sheath Shapes: A 3-D Generalization of the Child-Langmuir Model for Large High-Voltage Space Structures in Dense Plasmas," *Proceedings of the Air Force Geophysics Laboratory Workshop on Natural Charging of Large Space Structures in Near Earth Polar Orbit: 14-15 September 1982*, AFGL-TR-83-0046, Jan 1983

[57] L.W. Parker and B.L. Murphy, "Potential Buildup on an Electron-Emitting Ionospheric Satellite," *Journal of Geophysical Research*, Vol. 72, No. 5, March 1, 1967, p.1631

[58] D. Parks and I. Katz, "Theory of plasma contactors for electrodynamic tethered satellite systems," *Journal of Spacecraft and Rockets*, 24:245-249, 1987

[59] D. Parks, M.J. Mandell, and I. Katz, "Fluid model of plasma outside a hollow cathode neutralizer," *Journal of Spacecraft and Rockets*, 19:354-357, 1982

[60] M.J.M. Parrot, L.R.O. Storey, L.W. Parker, and J.G. Laframboise, "Theory of Cylindrical and Spherical Langmuir Probes in the Limit of Vanishing Debye Number," *Physics of Fluids*, Vol. 25, 1982, p. 2388

[61] M.J. Patterson, "Plasma Contactor Laboratory Characterization", presentation at Electrodynamic Tether Meeting, 18 May 1988

[62] M.J. Patterson and R.S. Aadland, "Ground-Based Plasma Contactor Characterization," NASA-TM-100194, 1988

[63] P.A. Penzo and P.W. Amman, eds. *Tethers in Space Handbook*, 2nd ed., NASA, May 1989

[64] R. Peyret and T.D. Taylor, *Computational Methods for Fluid Flow*, Springer-Verlag, 3rd printing, 1986

[65] W.H. Press, B.P. Flannery, S.A. Teulosky, and W.T. Vetterling, *Numerical Recipes: The Art of Scientific Computing*, Cambridge University Press, 3rd edition, 1988

[66] P.L. Pritchett and R.M. Winglee, "Beam-Plasma Interactions in Space Experiments: A Simulation Study," *J. Geomag. Geoelectr.*, Vol. 40, pp. 1235-1256, 1988

[67] W.J. Raitt, "Space Shuttle Charging Results," *Proceedings of the Air Force Geophysics Laboratory Workshop on Natural Charging of Large Space Structures in Near Earth Polar Orbit: 14-15 September 1982*, AFGL-TR-83-0046, Jan 1983

[68] C.E. Rasmussen and P.M. Banks, "Theory of the Electrodynamic Tether," *Advances in Space Research*, Vol. 8, No. 1, pp.203-211, 1988

[69] D.L. Reasoner, J.L. Burch, and T. Obayashi, "Analysis of Electron Spectra Produced by SEPAC Plasma Interaction," *EOS, Transactions of the American Geophysical Union*, Vol. 65, 1984, p. 1042

[70] R.W. Schunk, "Models of the Ionospheric Environment," *Proceedings of the Air Force Geophysics Laboratory Workshop on Natural Charging of Large Space Structures in Near Earth Polar Orbit: 14-15 September 1982*, AFGL-TR-83-0046, Jan 1983

[71] R.L. Stenzel and J.M. Urrutia, "Labratory model of a tethered balloon-electron beam current system," *Geophysical Research Letters*, 13:797-800, 1986

[72] N. Stone, "Electrodynamic Interactions," *Applications of Tethers in Space*, Vol. 1, NASA-CP-2364, 1985

[73] E.P. Szuszczewicz, "Technical issues in the conduct of large space platform experiments in plasma physics and geoplasma sciences," *Space Technology Plasma Issues in 2001*, Jet Propulsion Laboratory 86-49, California Institute of Technology, Pasadena, California, 1986.

[74] W.B. Thompson, "Passive Current Collection," *Space Tethers for Science in the Space Station Era*, Societá Italiana di Fisica, Conference Proceedings, Vol. 14,1988

[75] L. Tonks and I. Langmuir, "A General Theory of the Plasma of an Arc," *Physical Review*, 34:876, 1929

[76] J.M. Urrutia, "Experimental Study of Time-Varying Current Flow between Electrodes Immersed in a Laboratory Magnetoplasma," Ph.D. Thesis, UCLA Institute for Plasma Physics and Fusion Research Report Number PPG-115, October 1987

[77] J.M. Urrutia and R.L. Stenzel, "Anomalous Currents to a Positive Electrode in a Magnetoplasma," *Phys. Rev. Letters*, Vol. 57, 11 August 1986, pp. 715-718

[78] J.M. Urrutia and R.L. Stenzel, "Waves and Whistlers from Tethers and Electrodes in a Laboratory Plasma," *Tethers in Space Toward Flight*, AIAA Conference Proceedings, Third International Conference on Tethers in Space, 17-19 May 1989, p. 63-69

[79] G. Vannaroni, C.B. Cosmovici, U. Guidoni, L. Iess, and L. Scandurra, "Interaction of a Hollow-Cathode Source with an Ionospheric Plasma," *IFSI-88-10*, July 1988

[80] G. Vannaroni, C.B Cosmovici, J. McCoy, C. Bonifazi, M. Dobrowolny, U. Guidoni, L. Iess, and L. Scandurra, "Experimental Characterization of Hollow-Cathode Plasma Sources at Frascati," *Space Tethers for Science in the Space Station Era*, Societá Italiana di Fisica, Conference Proceedings, Vol. 14, 1988

[81] G. Vannaroni, Presentation at Electrodynamic Workshop at the Third International Conference on Tethers in Space, 16 May 1989

[82] A.D. Verga, G. Chanteur, and R. Pellat, "Current Driven Weak Double Layers Under Linearly Stable Conditions," *Physics of Fluids*, Vol. 31, No. 9, September 1988

[83] R. Wei and P.J. Wilbur, "Space-charge-limited Current Flow in a Spherical Double Sheath," *J. Appl Phys.*, 60 (7), 1 October 86, p. 2280

[84] E.C. Whipple, "Theory of the Spherically Symmetric Photoelectron Sheath: A Thick Sheath Approximation and Comparison with the ATS-6 Observation of a Potential Barrier," *Journal of Geophysical Research*, Vol. 81, No. 4, Feb. 1, 1976 p. 601

[85] P.J. Wilbur, "Space Plasma Contactor Research," NASA-CR-182148, 1987

[86] P.J. Wilbur, private communication, Jan 89

[87] P.J. Wilbur and T.G. Laupa, "Plasma Contactor Design for Electrodynamic Tether Applications," *Advances Space in Research*, Vol. 8, No. 1, p.221, 1988

[88] P.J. Wilbur, R. Wei, and J.D. Williams, private communication, Apr 1989

[89] J.D. Williams, Annual Report, Plasma Contactor Research - 1988, NASA-CR-182283, February 1989

[90] J.D. Williams, private communication, Apr 1989

[91] J.D. Williams and P.J. Wilbur, "Ground-Based Tests of Hollow Cathode Plasma Contactors," *Tethers in Space Toward Flight*, AIAA Conference Proceedings, Third International Conference on Tethers in Space, 17-19 May 1989, p. 77-87

[92] J.D. Williams and P.J. Wilbur, "Plasma Contacting-An Enabling Technology," AIAA-89-0677, presented at American Institute of Aeronautics and Astronautics Aerospace Sciences Meeting, 12 Jan 1989, Reno, NV

[93] J.R. Winckler, et. al., "Echo 7: An Electron Beam Experiment in the Magnetosphere," *EOS*, Vol. 70, No. 25, June 20, 1989

[94] J.R. Winckler, "Electron Beams for Magnetospheric Research," *Reviews of Geophysics and Space Plasmas*, Vol 18, No. 3, p.659-682, August 1980

[95] J.R. Winckler, "Floating Potentials and the Hot Plasma Generated by an Electron-Beam-Emitting Rocket in the Ionosphere," *Proceedings of the Air Force Geophysics Laboratory Workshop on Natural Charging of Large Space Structures in Near Earth Polar Orbit: 14-15 September 1982*, AFGL-TR-83-0046, Jan 1983

[96] L.C. Woods, *Principles of Magnetoplasma Dynamics*, Oxford Science Publications, 1987